4 MEASURING GIRDER PERFORMANCE AND CHARACTERISTICS

4.1 Introduction

Three procedural steps are needed to determine timber bridge girder structural health. The first is to identify a parameter that is indicative of girder structural health. The second is to identify how to measure such a parameter; and the third is to identify how to utilise that parameter to predict future performance. Separate research by RTA (Law *et al.* 1992), Yttrup and Nolan (1996), Lake (2001) and Wilkinson (2008) has enabled the creation of data that represents in-service timber bridge girders, but does not result in the identification of any specific parameter, which can be used to predict their structural health (refer Chapter 2). This limitation has been overcome by analysing these data in a combined pool and MoE determined as a suitable SHM parameter (Chapter 3). In particular, it has been identified that girder MoR and MoE change in synchronism and that a spot measurement of girder MoE can be used to predict current MoR. It has been further identified that an in-service girder MoR-v-MoE vector will remain within the prediction bands identified in Chapter 3 (refer Figure 3-46).

A girder's structural health is dependent upon its MoE and it can be classified into three ranges. Firstly, MoE above 36 GPa is indicative of a girder performing above the S2 limit states. Secondly, substandard performance is indicated by MoE below 14 GPa. In that case, the girder should either be strengthened or replaced. In the intermediate range (14 GPa-36 GPa), SHM techniques can be applied to determine a probability of failure and a safety index. The application of such SHM techniques to timber bridges will be explained in Chapter 5.

One of the objectives of this research is to show that continuous deflection monitoring could be used to assess the probability of failure of each timber bridge to which it was applied. To achieve the objective required a series of experiments to validate the use of deflection as the temporally measured parameter and to identify how to utilise the measured data. As was discussed in Chapter 2, the MoE of bridge girders can be measured both in the laboratory and in-field tests using large and expensive bending frame. However, it was obvious that in-service girder MoE can be measured without such equipment and proof loading. Neither was it found in the reviewed literature how to continuously measure in-service girder MoE nor what level of measurement accuracy was required.

This Chapter sets out the methods and results for each of four experiments:

1. deflection caused by static loading (Section 4.2);
2. deflection caused by traffic loading (Section 4.3);
3. deflection caused by Dynamic loading (Section 4.4); and
4. determination of level of variation in a timber load-v-deflection curve (Section 4.5).

These experiments are not intended to provide highly accurate absolute measurements *per se*; those can easily be achieved with high cost, well known, laboratory style measurement techniques. It was not the intention to validate the in-service measurements with in-service laboratory techniques. Such validation can be examined, if necessary, in future targeted research. There are two primary objectives set for these experiments: (1) to identify low cost methods that can be used to measure in-service girder mid-span deflection; and -(2) to determine how the data gained can be transformed into girder MoE. Further objectives are also set for each experiment as follows:

Experiment 1.

a. To determine that an in-service bridge girder deflects linearly over the required test loading range; and
b. Identify a level of variation that can reasonably be achieved in the measurement of MoE.

Experiment 2.

a. To provide a demonstration that traffic loading can be continuously and economically recorded; and
b. To identify that traffic load distribution can be determined by combining: bridge stiffness data; a static loading test; and a traffic volume distribution.

Experiment 3.

a. To provide a demonstration that highway speed traffic data can be recorded; and
b. To demonstrate that low cost measurement equipment can be used to record complex dynamic activity.

Girder MoE has been regularly determined from load-v-deflection curves. However, it was not identified from the literature what variation in MoE can be expected to be achieved for a single in-service girder. Yet it is necessary to know the measurement error of each sample to

realistically determine if two samples have different MoEs. When the measurement error is greater than the difference between the samples then they cannot be identified as different. Experiment 4 is thus a first step in identifying the accuracy of in-service MoE measurement.

Experiment 4.
The objective set for this experiment is:

(a) To identify the lowest level of variation in MoE that can reasonably be expected to be achieved for a single timber sample in the laboratory: and

(b) Use this lowest level to indicate the lower bound that can be expected to be achieved both for an in-service girder and for an excised sample. The variation of in-service girder MoE will be higher than this lower bound variation but it can be inferred from the difference between any particular in-service variation and this lower bound how much extra effort is required to reduce the in-service variation to an acceptable level.

The DS-6 for excised clear samples is represented by an average of 5 samples for each species and the complete dataset is determined from the testing of over 500 samples. These samples were selected by CSIRO as samples to be used to characterise the upper bound of the species. They would have been chosen to include a minimum of defects.

Experiment 5.
The objective set for this experiment was:

a. to determine how the MoR-v-MoE vector of a sample of White Cypress Pine (*Callitris glaucophylla*) with a defect would compare with the characterised range for the species *C. glaucophylla*.

4.2 Experiment 1: Deflection caused by static loading

4.2.1 Aim

This experiment was set out to examine (1) whether a timber bridge deflects linearly; and (2) whether the variation in the measurement of MoE can be achieved with low cost equipment.

4.2.2 Method

Three bridge spans were evaluated at two different bridges. The first of these spans was Powers Creek Bridge, while the second and third were part of Munsie Bridge. These bridges were introduced in Sections 2.3 and 2.7.4. Both linearity and the variation in MoE were examined by recording load-v-deflection data and statistically examining the results.

Case A: Powers Creek Bridge

Powers Creek Bridge was a single span timber beam bridge as shown in Figure 4-1 and 4-2. The bridge comprised four girders, two central main girders and two kerb girders, mounted on timber headstocks and supporting a deck of timber planking. Each deck plank was not joined directly to each girder, but was joined directly to each spiking plank. All the deck planks were, therefore joined together, but only joined intermittently to the girders at spacings of several metres. The nominal span was 8.6 m and the road width about 5.6 m.

Case A: Measuring System

The mid-span of Powers Creek Bridge was over the stream bed and scaffolding was used to enable a graduated scale to be attached to the mid-span of the main girders. The mid-span deflection was measured using a laser based method with equipment as shown in Figure 4-3. The graduated scale, in millimetre intervals, was printed on paper and mounted at the mid-span of the girder as shown in Figure 4-4. The laser was adjusted so that its quiescent position was in the vicinity of the zero line. As a vehicle crossed the bridge the girder deflected downwards and the position of the laser spot appeared to move up the chart.

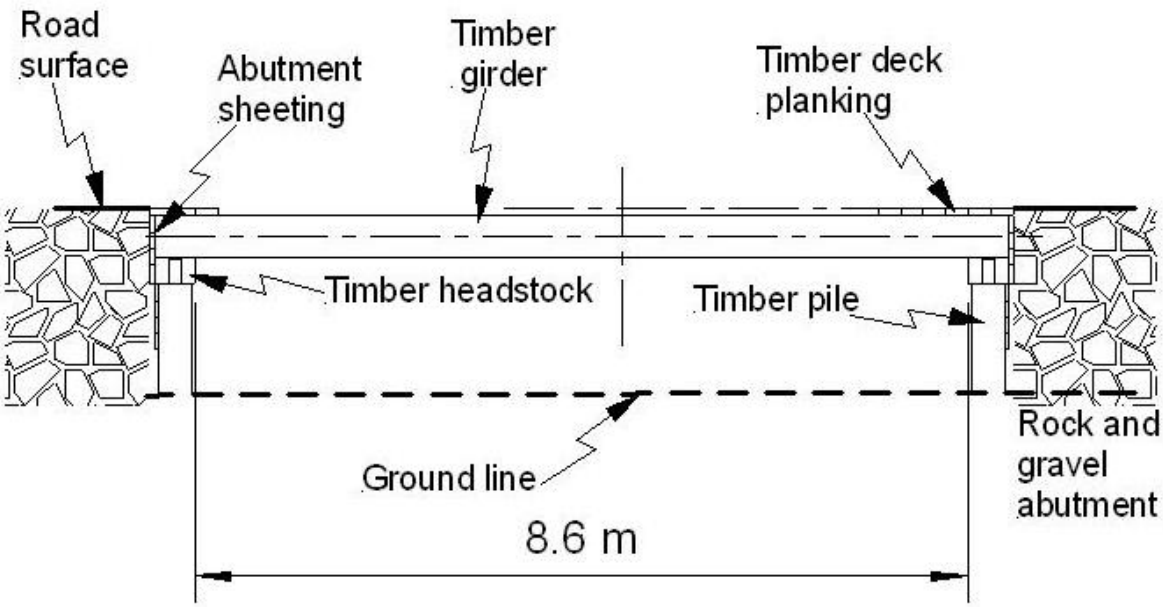

Figure 4-1: Elevation of Powers Creek Bridge

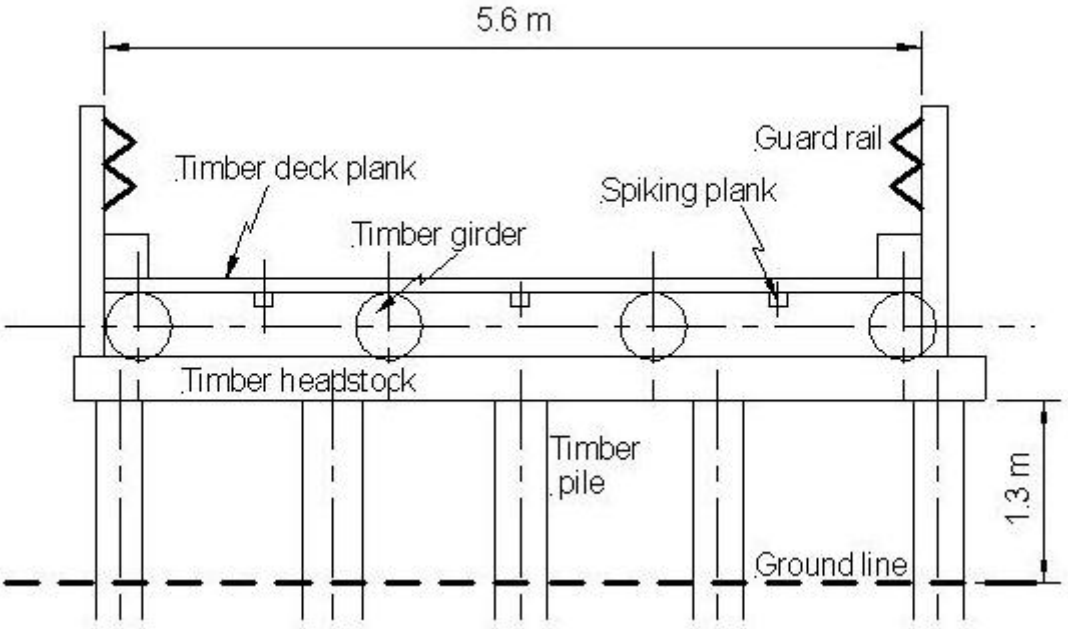

Figure 4-2: End section of Powers Creek Bridge

Figure 4-3: Laser and camera mounted on tripod with graduated scale mounted on girder at mid-span

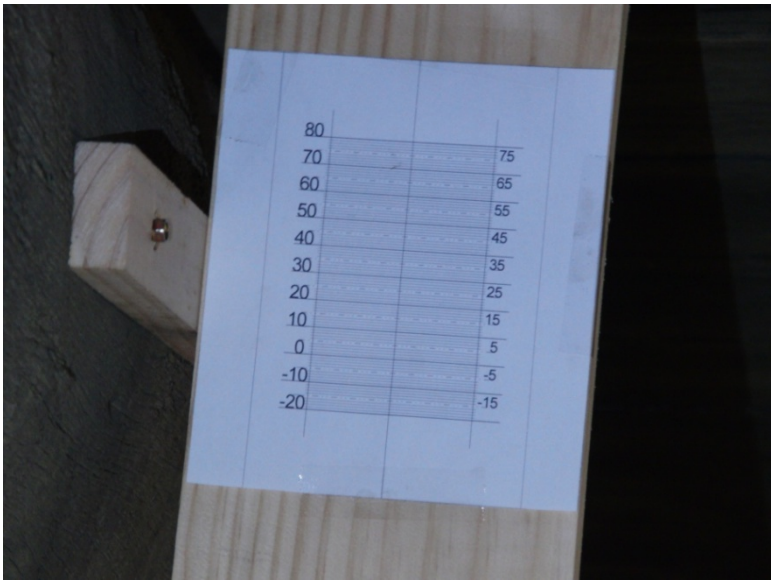

Figure 4-4: Graduated scale attached to mid-span of girder

Five vehicles of different GVM were used to load the bridge (Table 4.1). One test vehicle is shown in Figure 4-5 parked over the mid-span and towards the left side of the bridge. Deflection data were recorded, with a vehicle stationary at the mid-span, by recording the position of the laser on the chart as shown in Figure 4-4. Five independent measurements were made for each case and the data averaged. The vehicle masses were measured on a local licensed weighbridge and the spacing of the axles recorded to enable the effective influence line to be determined. The effective load data were plotted against the average deflection data and the bridge stiffness was evaluated from the slope of the curve.

Figure 4-5: Powers Creek Bridge loaded with vehicle of approximately 4.4.tonne GVM

Case B: Munsie Bridge

The second bridge, Munsie Bridge at Gostwyck, was a six span timber beam bridge as shown in Figure 4-6. Two spans were evaluated: span G-6 and span G-4 both on the eastern side of the creek. Schematics of these two spans are shown in Figures 4-7, 4-8 and 4-9. These spans, as with Powers Creek Bridge, also comprised four girders, two central main girders and two kerb girders, which also supported a deck of timber planking. The girders, however, were supported by concrete piers and a timber capwale. Each girder span was about 10.6 m and the road width about 5.4 m.

Figure 4-6: Munsie Bridge, Gostwyck, spans G-4 and G-6

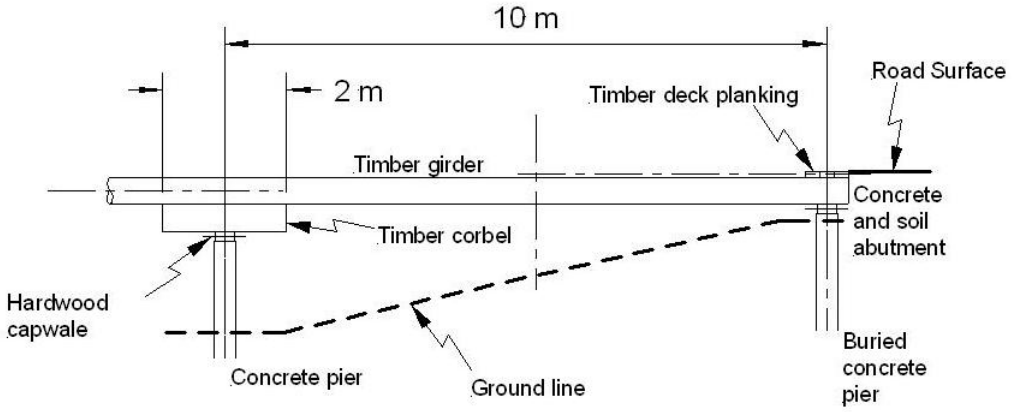

Figure 4-7: Elevation of span G-6, Munsie Bridge

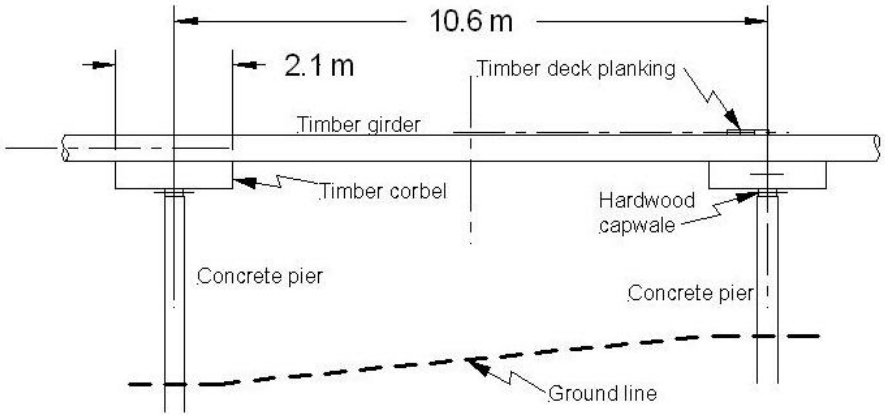

Figure 4-8: Elevation of span G-4, Munsie Bridge

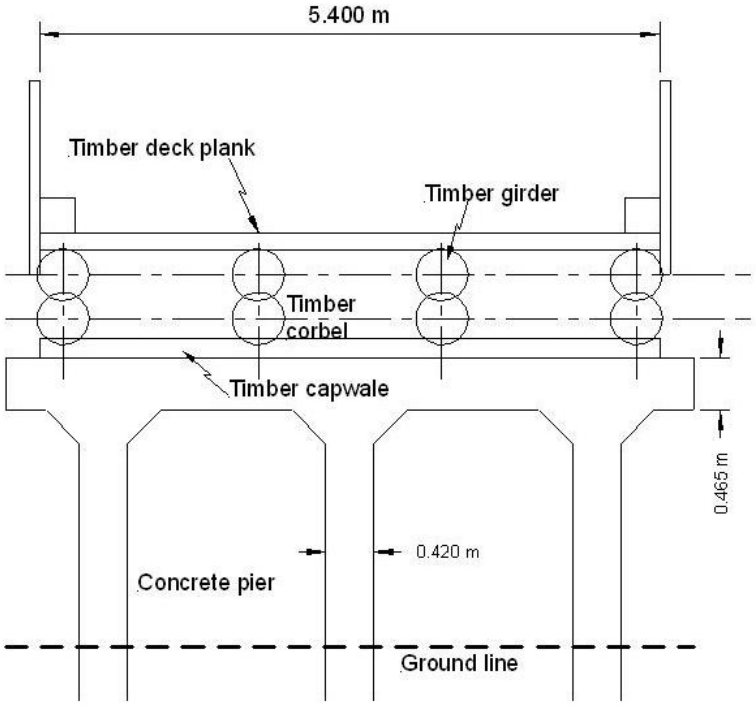

Figure 4-9: End view of spans G-4 and G-6, Munsie Bridge

Case B: Measuring System

The undersides of each span were normally accessible except in times of flooding, although scaffolding was required to access the mid-span of span G-4. The deflection was measured using a vernier together with a graduated scale as shown in Figures 4-10 and 4-11. The vernier scale was attached to a staff that was itself attached to the girder mid-span. The graduated scale was mounted on a section of 100 mm PVC pipe and supported by a tripod. The vernier was read at normal eye level, with the different girder height above ground level accommodated by different length staffs. The initial unloaded quiescent state was recorded, then the bridge loaded with a vehicle of known mass positioned over the girder. The resultant deflection was recorded. This loading was repeated five times for each loading and the data averaged. The vernier was arranged so that movements of less than 0.5 mm could be measured.

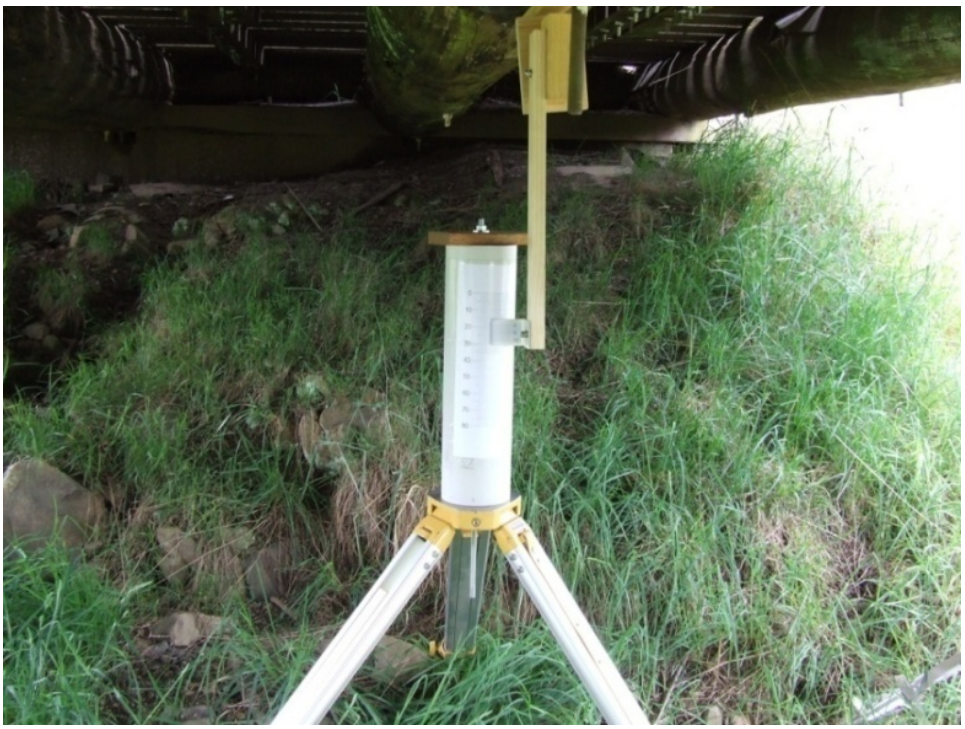

Figure 4-10: Vernier and graduated scale measuring system used at Munsie Bridge

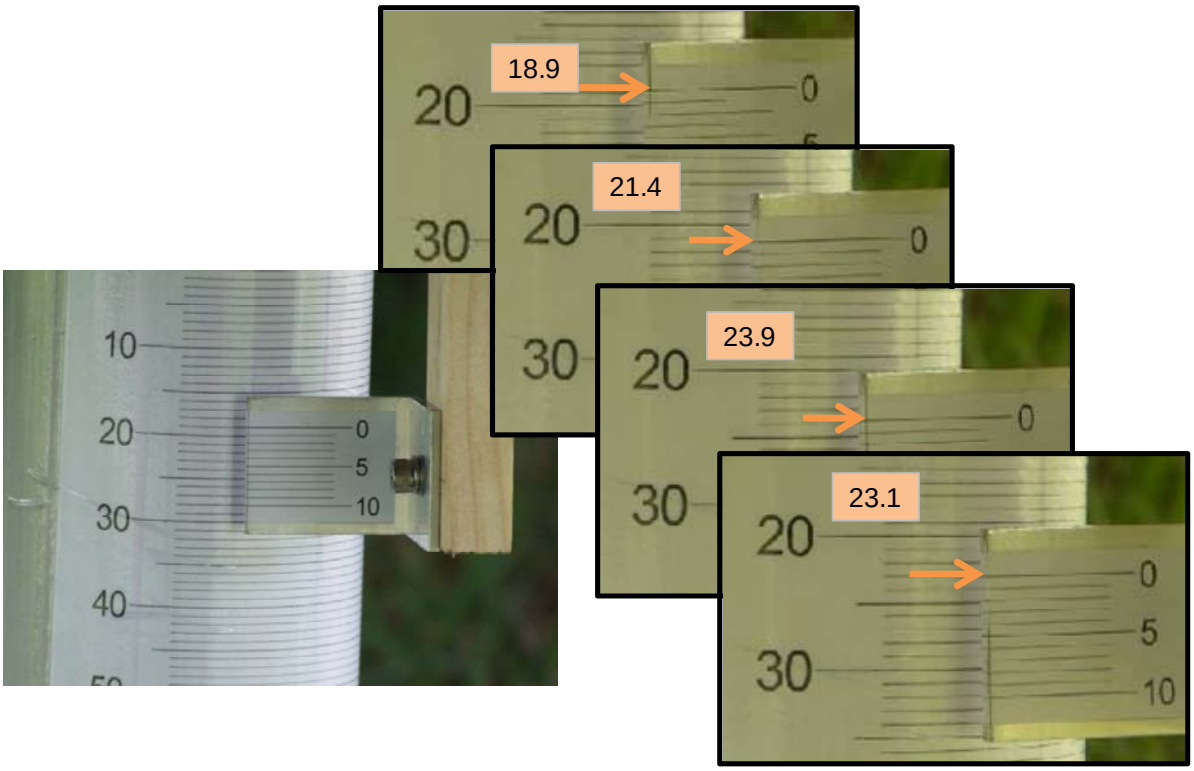

Figure 4-11: Detailed view of vernier and scale

The bridge was loaded with vehicles of known load and axle position with one example shown in Figure 4-12. In particular span G-6 was loaded with a garbage truck of about 10 tonne GVM and span G-4 with a gravel truck of about 21 tonne GVM. Each vehicle's wheelbase dimensions were recorded. The bridge stiffness was again evaluated from the slope of the curve obtained by plotting the effective load data against the average deflection data.

Figure 4-12: Munsie Bridge loaded with test vehicle

4.2.3 Results

Three bridge spans were monitored at two bridges. The first span, Powers Creek Bridge, consisted of a single span timber beam bridge. The effective road width was wide enough to allow two small vehicles to be on the bridge concurrently, but this was not normal. It was observed that normally only one vehicle was on the bridge at a time. Smaller vehicles would cross either over the centre line or slightly to the left side of travel. Larger and heavier vehicles would pass centrally across the bridge. The girder deflections could vary, for the same loading, according to whether the vehicle passed towards one-side or over the centre line, thus sharing load between adjacent girders. The road was relatively straight and level near the bridge and the deck was comparatively even (Figure 4-13). This allowed many light vehicles to cross the bridge at high speed, although some would slow down. Trucks would also cross at speeds above about 40 km hr^{-1}. Because of the approaches of the road and the small discontinuities at the entrance to the bridge, high speed vehicles would appear to bounce as they crossed and this was observed as the bridge reverberated to these high speed vehicles.

Figure 4-13: Powers Creek Bridge, road view to north

The typical loading positions of light and heavy vehicles are shown in Figure 4-14 through to Figure 4-17. Light vehicles had two axle loads present on the bridge at once. Heavy vehicles, with axle spacing longer than half the span (4 m), only had one axle loading the span at any one time, as shown in Figure 4-16. In both cases, light and heavy vehicles, the axle width was such that the load was predominately applied over the central main girders (refer Figures 4-15 and 4-17), but this applied load was distributed to all four girders by the action of the deck planks.

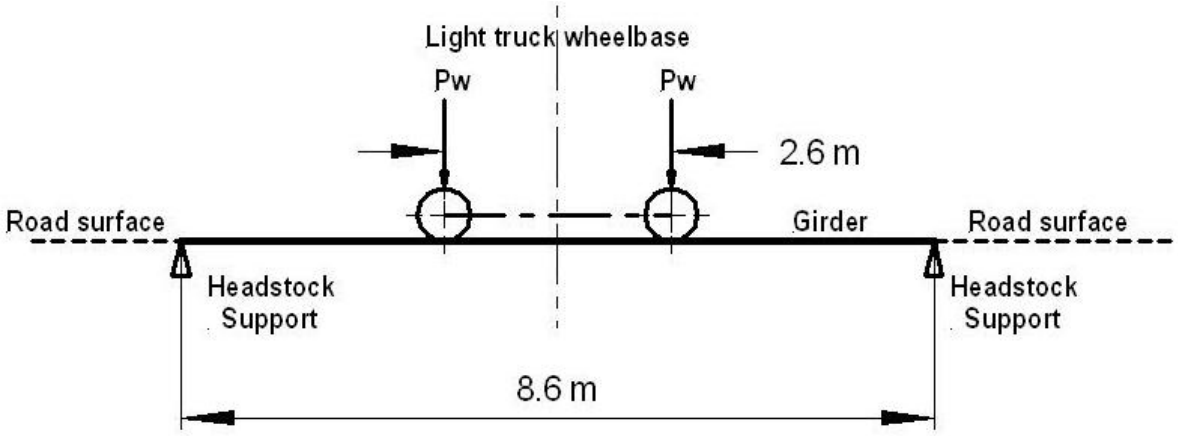

Figure 4-14: Elevation view of Powers Creek Bridge showing loading configuration for light truck

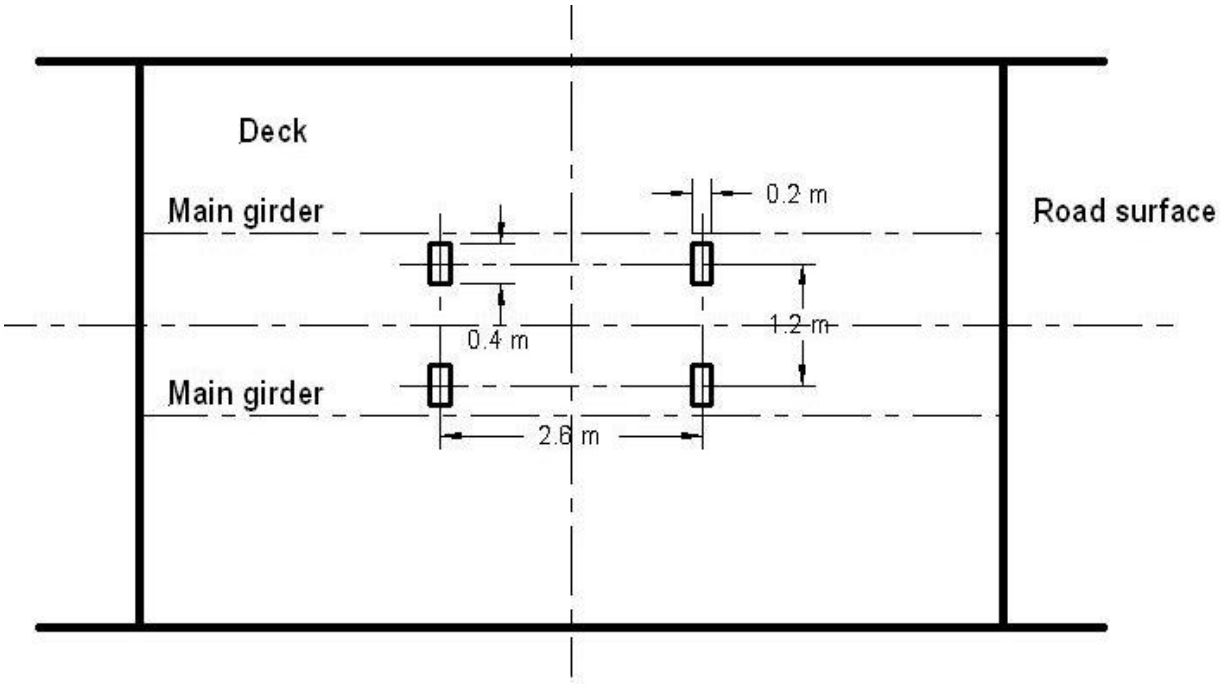

Figure 4-15: Plan view of Powers Creek Bridge with light truck configuration

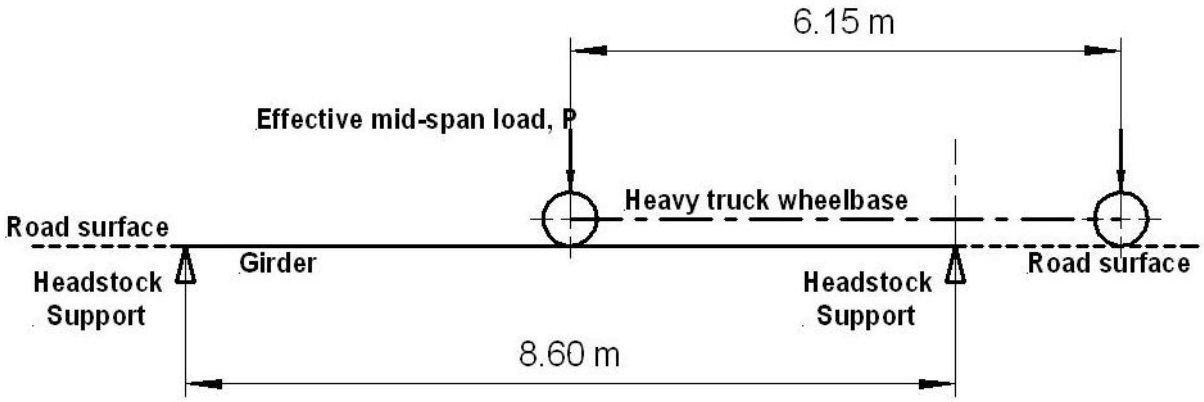

Figure 4-16: Powers Creek Bridge showing loading configuration for heavy truck

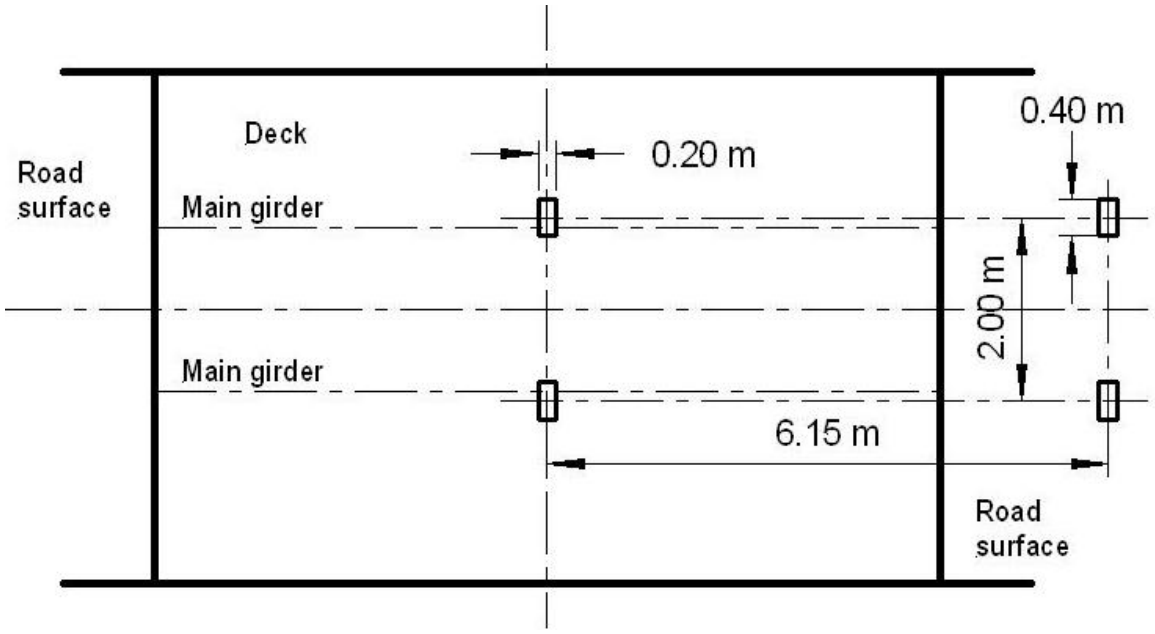

Figure 4-17: Plan of Powers Creek Bridge showing loading configuration for heavy truck

The test vehicle loads, measured on a local licensed weighbridge, together with their measured wheelbases (axle spacings) are as shown in Table 4-1. The measured deflections are shown in Table 4-2. Also shown are the computed effective mid-span deflections taking into account the effect of number of axles and the wheelbase (column 4). The resultant load-v-deflection curve is shown in Figure 4-18.

Table 4-1: Vehicle loads applied to Powers Creek Bridge

Vehicle No.	Vehicle type	Load, P (kN)	Wheelbase (m)
1	Light car	10.0	2.40
2	Light truck	20.6	2.60
3	4 x 4 utility	43.2	3.15
4	Front axle, heavy truck	49.2	6.15
5	Rear axle heavy truck	66.7	6.15

Table 4-2: Vehicle loads applied to Powers Creek Bridge

Vehicle No.	Measured mid-span deflection, δ (mm) [no account made for multiple axles]		Effective single point mid-span load, mid-span deflection, δ (mm) [account made for multiple axles]
	Mean upstream main (UM)	Mean downstream main (DM)	
1	1.0	1.0	1.1
2	2.4	2.0	2.7
3	6.0	5.5	6.6
4	7.4	7.4	7.4
5	11.0	10.0	10.5

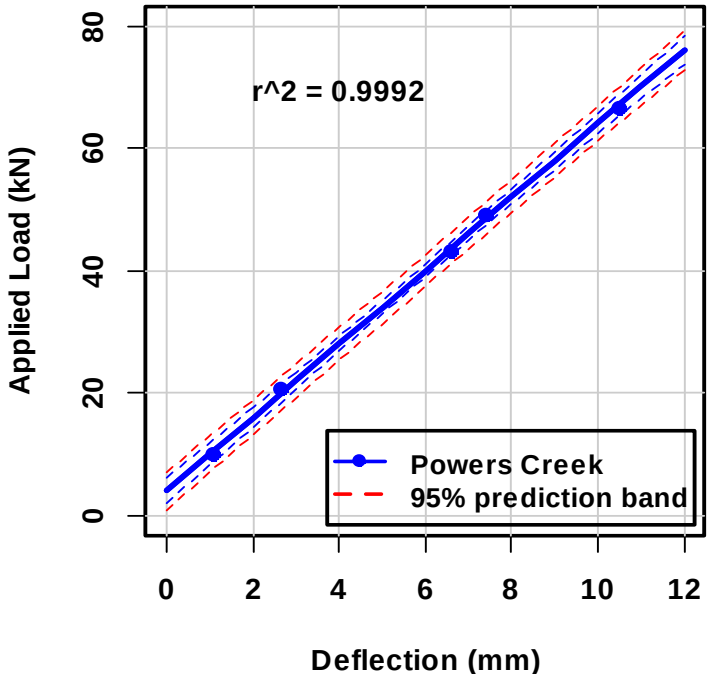

Figure 4-18: Static deflection curve for Powers Creek Bridge [Applied load is effective single point mid-span load]

The results of the statistical analysis of the Powers Creek Bridge data (Figure 4-18) are shown in Table 4-3. The data have a high level of linearity (coefficient of determination of 0.9992) and a variation of the slope of the curve of about 2.5% CV (standard error ÷ mean slope). Results were also recorded for the two spans G-4 and G-6 of Munsie Bridge and the effective stiffness for each of the three spans is shown in Table 4-4.

Table 4-3: The regression coefficients for the data shown in Figure 4-18

Parameter	Value
Intercept	4.1
Slope (stiffness)	6.0 (kN/mm)
Tolerance of slope, 95% confidence	0.31
Coefficient of determination, r^2	0.9992
Model	Load = 4.1 + (6.0 ± 0.3) x Deflection

Table 4-4: Stiffness of the tested bridge spans

Span	Stiffness (tonne/mm)	Span (m)
Powers Creek Bridge	0.61	8.6
Munsie Bridge, Span G-6	0.64	10.6
Munsie Bridge, Span G-4	0.47	10.6

Comparison of in-service load-v-deflection curve with a laboratory curve

This experiment was continued to indicate whether a complete bridge structure behaves in a linear fashion over the range of loading such that the data could be used for the experiments in this research, in similar fashion to the load-v-deflection curves measured in the laboratory for individual girders. As one example, a laboratory measured girder deflection curve is shown in Figure 4-19 is prepared from the data previously shown in Figure 2-27. Since the linear range was not explicitly shown in the original citation by whom (date) it has been analysed here to identify the linearity of the load-v-deflection curve for deflections less than 40 mm. Also shown in Figure 4-19 is the load equal to half the breaking load. The deflections that occurred for half the breaking load, and above, were greater than 40 mm. The non-linear region of this curve begins above the region limited by the half breaking load line (50% Pmax). The coefficient of determination for the linear region was 0.9989.

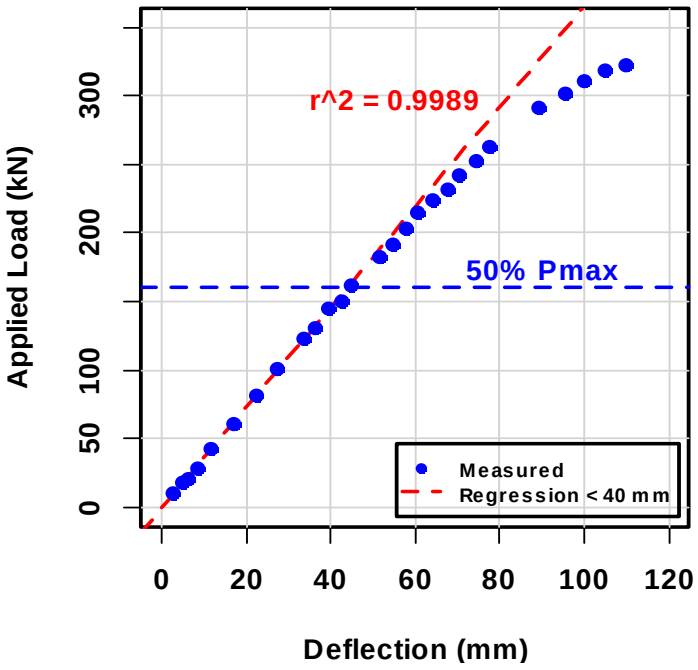

Figure 4-19: Load-v-deflection response for girder #4, DS-4; adapted from Figure 2-27

These two curves, the curve for the Powers Creek Bridge as a complete structure (Figure 4-18) and the redrawn curve for the individual girder (Figure 4-19) cannot be directly compared. However, by using some of the results that are developed in the next chapter they can be realistically compared to demonstrate their similarity in a complete bridge structure. In Chapter 5 both the girder MoE and girder fraction of applied load are determined for the Powers Creek

Bridge using a SAP2000 model and Euler-Bernoulli beam theory (refer Chapter 5 for details). These model data are replicated and extended in Table 4-5 where two cases are shown: Case 1 represents the measured bridge; and Case 2 represents the bridge with the upstream girder replaced in the model with a hypothetical girder of characteristics as indicated in Figure 4-19. In the measured case the upstream girder had a MoE of 20 GPa and the percentage load fraction was 39.4%. The hypothetical girder has a MoE of 27 GPa and supports 49.4% of the applied load.

Table 4-5: Development of fractional load for Powers Creek upstream hypothetical girder (PC-MU)

Case	Parameter	KU	MU	MD	KD
1	Girder MoE (GPa)	12	20	20	14
1	Mid-span deflection for a 4.4 tonne vehicle (mm)	2.8	5.2	4.7	2.7
1	Fraction of total load on each girder	8.8%	39.4%	46.3%	7.0%
2	Girder MoE (GPa)	12	27	20	14
2	Mid-span deflection for a 4.4 tonne vehicle (mm)	2.4	4.6	4.6	2.5
2	Fraction of total load on each girder	6.8%	49.4%	45.2%	6.0%

In Figure 4-20 the regression data (blue line) for the tested bridge span is replicated (refer Figure 4-18) and overlaid with the effective data for the hypothetical girder scaled by the reciprocal of the loading factor (yellow dots). There is reasonable co-incidence between these two cases. The effective experimental static bridge maximum test load was only about 35% of the maximum mid-span legal axle loading, but because of the load sharing that occurs in the bridge structure, the hypothetical girder is only loaded to about 20% of the girder linear range. The maximum girder mid-span deflection that would occur in such a static bridge test is only about 12 mm.

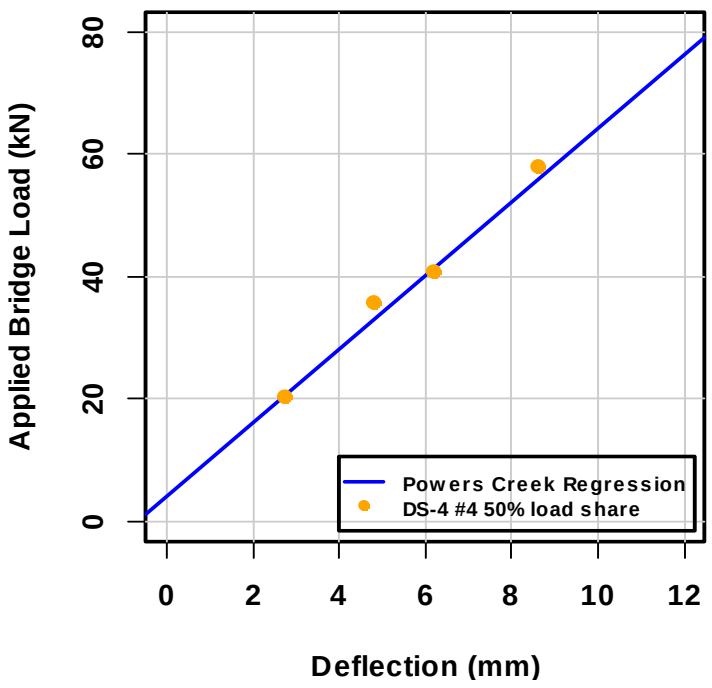

Figure 4-20: Measured deflection for Powers Creek Bridge compared with DS-4 girder #4 modified according to load share

4.3 Experiment 2: Deflection caused by Traffic loading

4.3.1 Aim

This experiment aimed to determine firstly the level of traffic loading applied to Powers Creek Bridge, and spans G-4 and G-6 of Munsie Bridge by using a permanent, unattended recording system. Secondly, these results are combined with static load measurements to determine a traffic load distribution.

4.3.2 Method

A Bridge Deflection Meter (BDM) was applied to a centre girder to record the deflections caused by traffic activity on the bridge. In this experiment the BDM laser source was rigidly attached to the headstock using a purpose-built mounting bracket and the detector attached to the mid-span of the girder with circular support clamps, as shown in Figures 4-21, 4-22 and 4-23. On Powers Creek Bridge, the BDM was mounted on the downstream main girder (PC-MD), on Munsie Bridge span G-6 on the upstream main girder (G6-MU) and on the span G-4 downstream main girder (G4-MD). The peak deflection produced by each vehicle crossing the bridge was logged electronically, together with the time that the deflection occurred. Data were recorded for a period of about three weeks on each of the three spans. Recording on Powers Creek Bridge was

terminated when the local council removed the timber bridge and replaced it with a concrete box culvert structure.

Figure 4-21: Bridge Deflection Meter attached to downstream main girder of Powers Creek Bridge

Figure 4-22: BDM attached to centre girder of span G-6, Munsie Bridge

Figure 4-23: BDM attached to centre girder of span G-4 of Munsie Bridge

4.3.3 Results

The number of vehicles crossing each span was recorded for a period of three weeks and the numbers exceeding each threshold deflection are shown in Table 4-6. These data are compared in Figure 4-24, where the data are shown as a percentage of the total data for each bridge span and the ordinate is logarithmic so that the smaller values can be seen. In the case of Powers Creek Bridge there were only 49 vehicles in 5585 that exceeded Threshold 5 which was less than 1% of the total traffic volume. The G-4 and G-6 spans represent traffic crossing the same bridge, but measured at different times and on different girders, whereas the Powers Creek Bridge span is not on the same road and represents different traffic. Both bridges, Powers Creek Bridge and Munsie Bridge (spans G-4 and G-6) service the same geographically isolated area, but the former connects to Armidale and the latter to Uralla. Vehicles would tend to cross one bridge or the other and not both, although a few vehicles might make the round trip and cross both (given that it is promoted as a tourist drive). The data for Powers Creek Bridge are thus an independent set from the other two sets.

Table 4-6: Number of vehicles crossing each bridge span

Threshold Level (refer Table 2-10)	Powers Creek Bridge (PC)	Munsie Bridge, span 4 (G-4)	Munsie Bridge, span 6 (G-6)
1	4938	2540	5167
2	363	200	353
3	107	51	39
4	128	31	131
5	24	12	30
6	25	13	15
7	0	0	0
8	0	1	5

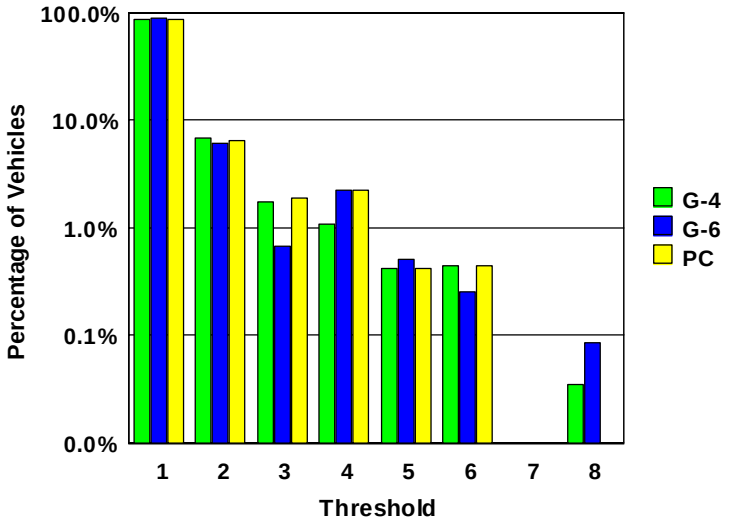

Figure 4-24: Number of vehicles crossing each test bridge span as a percentage of the total for each span-v-Threshold

The number of vehicles that exceed each threshold depends on the stiffness of each bridge span. As an example a 1.1 tonne vehicle did not exceed Threshold 1 for the Powers Creek Bridge span and Munsie Bridge span G-6 but did exceed Threshold 1 for Munsie Bridge span G-4. The numbers of vehicles exceeding Thresholds 1 and 2, together with the ratio of Threshold 2 to Threshold 1 are shown in Table 4-7.

Table 4-7: Ratio of number of vehicles exceeding Level 2 to number exceeding Level 1

Parameter	Powers Creek Bridge (PC)	Munsie Bridge, span 4 (G-4)	Munsie Bridge, span 6 (G-6)
Number of vehicles exceeding Threshold 1	5585	2848	5749
Number of vehicles exceeding Threshold 2	647	308	573
Ratio of Threshold 2 to Threshold 1 (%)	11.6%	10.8%	10.0%

The vehicle distribution was translated to a load distribution by the use of a static load calibration. Each BDM threshold level is equivalent to a specific applied load (refer Table 2-10). By combining the static bridge stiffness data (Table 4-4) with the threshold level (Table 2-10) and the traffic volume distribution (Table 4-6) a traffic load distribution was calculated. The results of this calculation, made assuming that the data were lognormal, are shown in Table 4-8. The resulting distributions are as shown in Figure 4-25. Because the structural detailing on each

span are different they each represent different stress situations and different likelihood of failures. The probability of failure of these spans is discussed in Chapter 5.

Table 4-8: Lognormal traffic load distribution parameters test Bridge span

Bridge Span	Mean load, μ* (kN)	Standard Deviation, σ* (kN)
Powers Creek, PC-MU	3.0	0.42
Munsie Bridge, G6-MU	2.6	0.40
Munsie Bridge, G4-MD	2.3	0.40

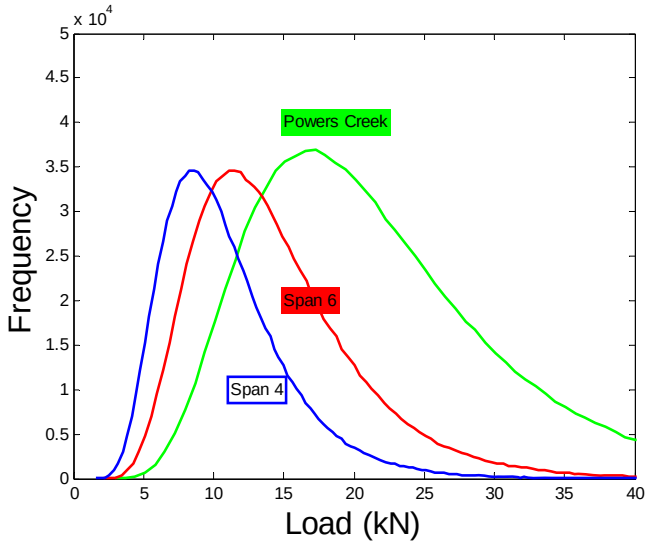

Figure 4-25: Lognormal traffic loading distributions for test Bridge spans

The traffic load distribution for Powers Creek Bridge, as shown in Figure 4-25, is repeated in Figure 4-26a together with the measured traffic data represented as a bar graph. In order to be able to differentiate the data related to heavy vehicles, represented by bars at 182 kN and 277 kN, the graph is repeated as Figure 4-26b with the ordinate chosen a logarithmic scale. The first of these two load groups (182 kN) represents vehicles that cause deflections above Threshold 5 and below Threshold 6. The second group (277 kN) represents vehicles that cause deflections above Threshold 6 and below Threshold 7. The magnitude of the frequency of the lognormal load distribution represented by the blue curve is greater than two orders of magnitude less than that measured for heavy vehicles and does not correctly represent heavy vehicle frequency. However, for the lighter traffic below about 100 kN, the lognormal distribution (lognormal mean, μ*, of 3.0, lognormal standard deviation, σ*, of 4.2) provides a representation of the traffic volumes with a standard error of the mean of 0.006.

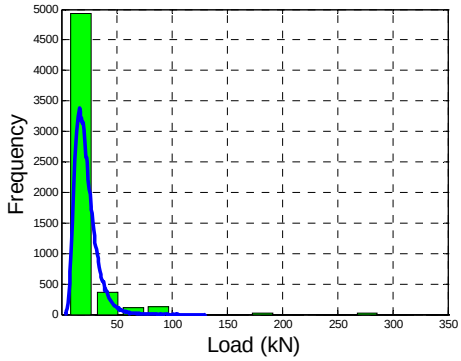

Figure 4-26a: Log normal traffic load (kN) distribution (blue) superimposed on measured traffic data (green) for Powers Creek Bridge

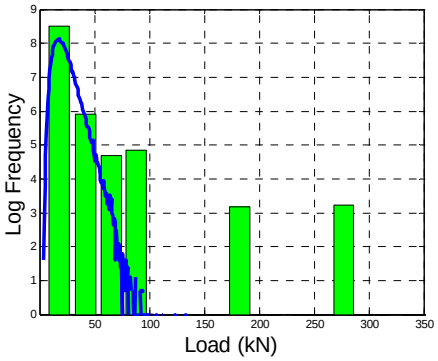

Figure 4-26b: Data as for Figure 4-26a but with log scale ordinate

4.4 Experiment 3: Deflection caused by dynamic loading

4.4.1 Aim

This experiment was used to identify that mid-span deflection data can be gathered that was representative of highway speed traffic and, in particular, that low cost measurement equipment is a valid technology to record complex dynamic activity.

4.4.2 Method

The deflections, caused by vehicles of known mass over the bridge, were achieved using a high speed camera (Casio EX-FH25). This involved, at Powers Creek Bridge, recording the movements of the laser on the graduated scale (Section 4.2, Figures 4-10 and 4-11). The camera was capable of recording at 120 frames per second (fps), 240 fps and 480 fps, with an upper speed of 1000 fps. A speed of 240 fps was used here and was of sufficient frequency. The camera and software were calibrated by comparing recorded images with the moving sweep-hand of a standard clock. The software used was AVS Video Editor 5.2 supplied by Online Media Technologies Ltd, UK.

The recordings from the video camera were used to identify:

Case A. The influence line of a vehicle moving across the bridge at a speed of about 5 km h^{-1};

Case B. The transient response of a truck crossing the bridge at highway speed; and

Case C. A normalised peak deflection versus vehicle speed relationship.

4.4.3 Results

Case A: Influence line

The passage of a 4.4 tonne vehicle with an axle spacing of 2.6 m and a transit speed of about 5 km h^{-1} was driven across the Powers Creek Bridge. A high speed camera at 240 fps was used to record the movement of the graduated scale relative to the laser and the position of the beam inferred by examination of each frame. Over 1000 frames were recorded and examined for each transit which took at least 5 s. Not all the image movements are tabulated, only those showing relative movements of about 0.5 mm. The results are shown in Table 4-9 and the resultant deflection-v-time curve in Figure 4-27.

Table 4-9: Deflection-v-time data for light truck traversing Powers Creek Bridge

Time (sec)	Deflection (mm)	Time (sec)	Deflection (mm)
0.00	0.0	4.00	-4.0
0.30	-0.2	4.79	-4.5
0.91	-0.5	5.10	-5.0
1.06	-1.0	6.13	-5.0
1.50	-1.5	7.54	-4.0
2.36	-2.0	8.39	-3.0
2.78	-2.5	9.17	-2.0
3.22	-3.0	10.26	-1.0
		11.14	0.0

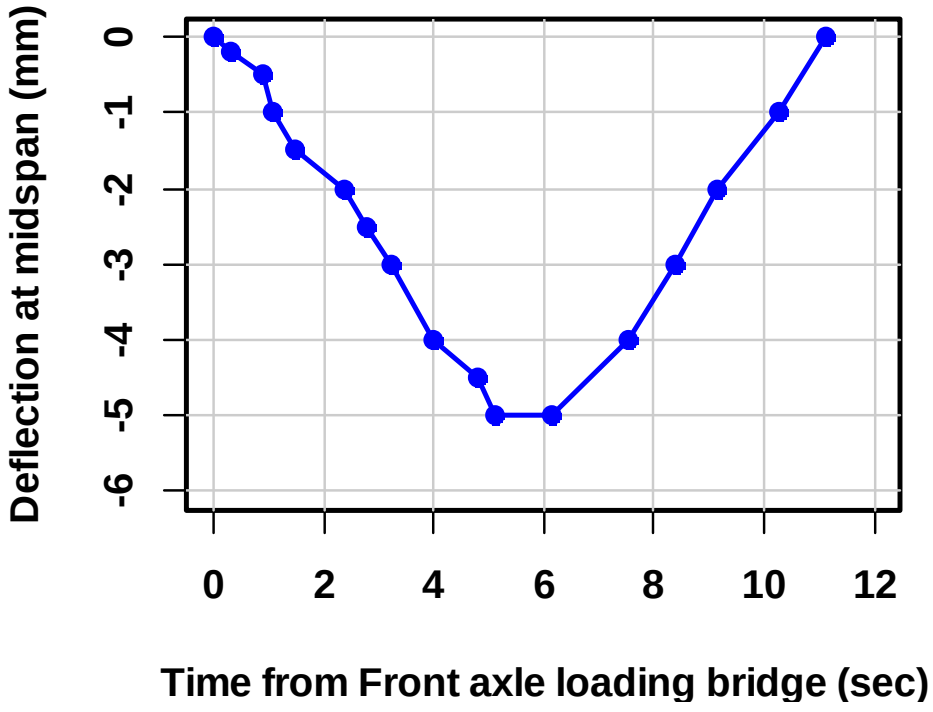

Figure 4-27: Deflection-v-time for light truck traversing Powers Creek Bridge

The effect of the axle loading on the mid-span deflection is determined by transforming the time data into distance data. This is achieved using Equation 4-1 and Equation 4-2:

$$Speed = \frac{(Axle\ spacing + Span)}{T_{transit}}$$

..... Equation 4-1

Where $T_{transit}$ is the time for the vehicle to cross the bridge from the moment of entry of the first axle to the moment of departure of the second axle.

and

$$Distance = Measured\ time\ \times Speed - \frac{Span}{2}$$

..... Equation 4-2

The mid-span deflection is then calculated using the standard equation, Equation 4-3:

$$if(x \leq a)\ \ Deflection, \delta = \frac{P}{6EI} \times \frac{x(L-a)}{L} \times (2aL - a^2 - x^2)$$

$$if(x > a)\ \ Deflection, \delta = \frac{P}{6EI} \times \frac{x(L-a)}{L} \times (2aL - a^2 - x^2) + (x-a)^3$$

..... Equation 4-3

And where the nomenclature for this equation is shown in Figure 4-28.

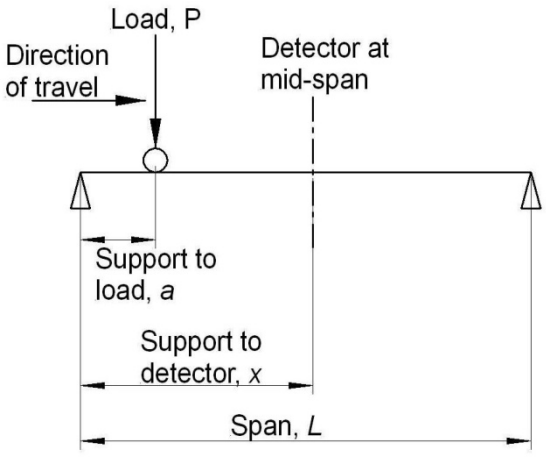

Figure 4-28: Influence line loading schematic

where:

δ	is the mid-span deflection (m)
P	is the applied mid-span load (N)
x	is the distance from the support to the measuring point
L	is the span between supports (m)
a	is the distance from the support to the load
E	is MoE (Pa)
I	is SMA (m^4)

The passage of the vehicle across the bridge is shown schematically in Figure 4-29. The position of the front axle, in the schematic, is defined as follows:

a. The front axle is in line with the entrance of the bridge causes no deflection.

b. The front axle is on the bridge causing a deflection but the rear axle is not.

c. The rear axle is in line with the bridge entrance. This point is coincident with the point of inflection in the combined axle curve (green line, Figure 4-31).

d. Both axles are loading the bridge. This is the loading that causes the peak deflection, with the front axle having proceeded half the axle spacing past the mid-span. From this point the influence of the first axle is declining faster than the rear axle is increasing.

e. The front axle has reached the exit point of the span. The deflection created by this axle has reached zero. This point is coincident with the second inflection point in the combined axle curve.

f. The rear axle has reached the exit point of the span.

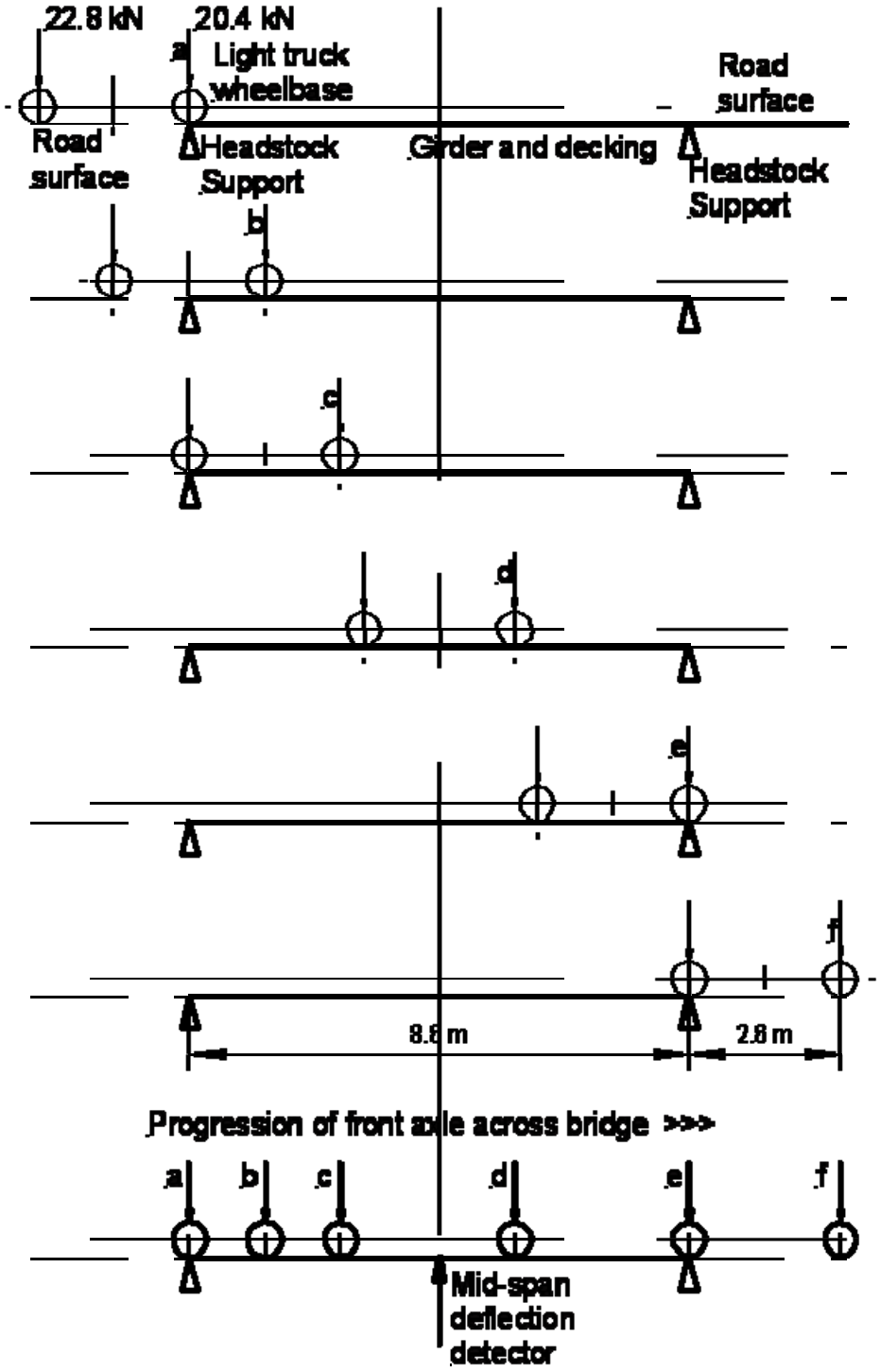

Figure 4-29: Position of light truck on Powers Creek Bridge for influence line test

The progression of a vehicle through these positions, as shown at the bottom of Figure 4-29, is repeated, as Figure 4-30. The data shown in Table 4-9, modified using Equations 4-1 to 4-3, were then combined with the girder data from Experiment 1, shown in Table 4-10, to determine the influence line response shown in Figure 4-31.

The girder data, shown in Table 4-10, are as determined as part of Application 2 (Section 5.3), but modified to suit the current application. In Experiment 2, the girder MoE was increased (refer Table 4-5), whereas in this experiment it is decreased. The situation addressed in Chapter 5 (Application 2), relates to traffic passing nominally centrally across the bridge in both directions. But in this case (Experiment 4) the test load truck was driven across one side of the bridge and centrally across the girder being monitored. The effective MoE of the girder has, therefore, been reduced to reflect the low value of the kerb girder MoE. This MoE value has also been chosen such that the peak calculated deflection is similar to the measured peak deflection. The MoE of the main girder is, therefore, decreased from an initial determination of 20 GPa to 17 GPa, this being justified by the low MoE of the kerb of about 12 GPa (refer Table 4-5).

Table 4-10: Girder parameters used to calculate influence line

Parameter	Value
Girder diameter	0.46 m
Girder effective MoE	17 GPa
Load sharing fraction	39.4%
Front axle load	20.4 kN
Rear axle load	22.8 kN
Axle spacing	2.6 m
Bridge span	8.6 m

The passage of the loaded truck across the bridge is identified in Figure 4-30 and the deflection-v-load curve in Figure 4-31. The data in Figure 4-31 are nominally aligned with the truck positions shown in Figure 4-30. The two vertical black ordinate lines, shown in Figure 4-31, at ± 4.3 m from the detector represent the limits of the girder span and are nominally aligned with the supports shown in Figure 4-30. In Figure 4-31 three curves are shown, one curve for each of the two axles (front and rear) together with the combined load curve which shows the influence line. Also shown overlaid are the data points at which the deflections were monitored.

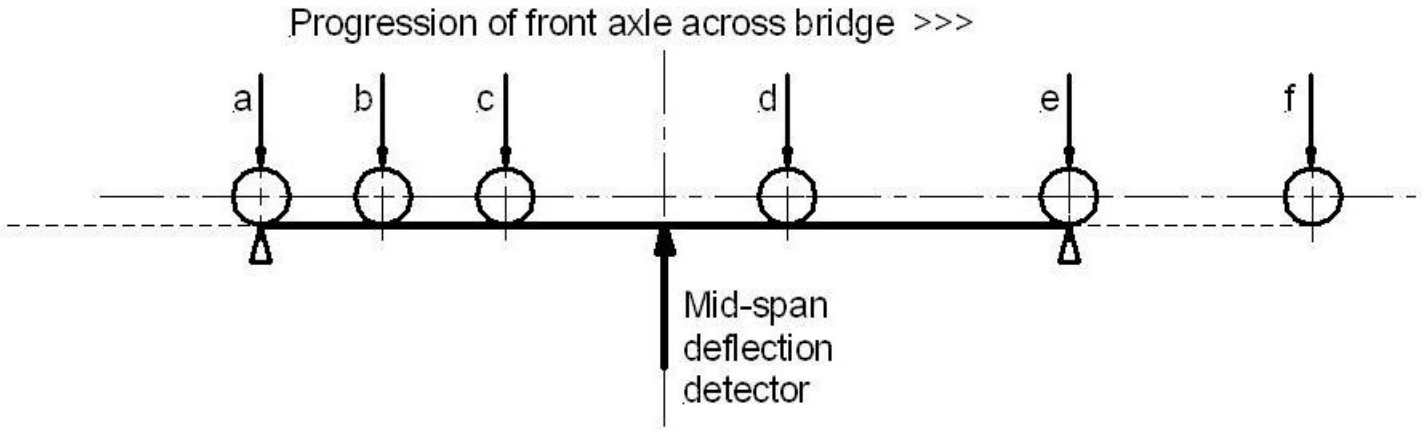

Figure 4-30: Progression of front axle across bridge

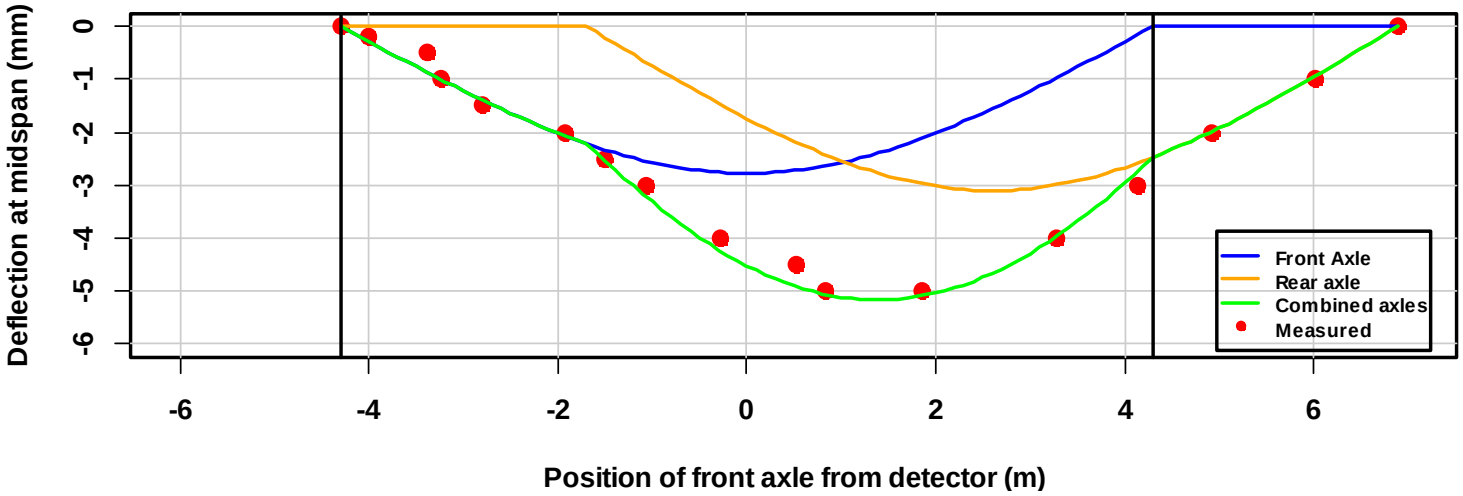

Figure 4-31: Measured influence line of light truck

Case B: Transient response

A recording was made of a heavy test vehicle crossing the Powers Creek Bridge. The data are tabulated in Appendix A and plotted in Figure 4-32 (red line). It is inferred that the first axle of the heavy vehicle, to cross the bridge, is nominally represented by the period from the start of the graph to the point where the deflection returned to zero. The vehicle travelled about 17.2 m sec^{-1} (62 km h^{-1}). The simulated data (Figure 4-32, blue line) comprised natural frequencies at about 8 Hz and 1.3 Hz. A half cycle transient at 1.3 Hz was initiated as the vehicle first entered the bridge, then after about 0.5 s a second impact overcame the first negative transient and produced a second positive 1.3 Hz transient. Both of these transients were coupled with lower amplitude transients at about 8 Hz. These 8 Hz transients continued after the vehicle had left the bridge with no obvious signal decay damping for over two seconds.

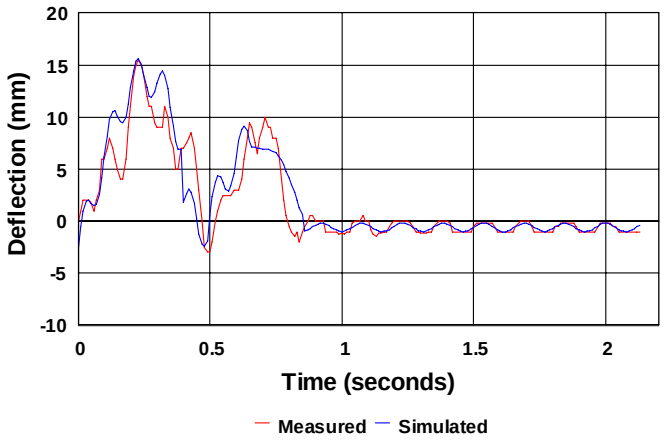

Figure 4-32: Transient behaviour of Powers Creek Bridge with impact load of a heavy vehicle

The transient behaviour evaluated in Case A was for a slow moving vehicle. In the influence line transformation shown in Figure 4-31 there is no significant dynamic behaviour. The measured data deviate little from calculated static influence line data. In case B the dynamic behaviour is significant. The curve in Figure 4-32 contains several different component frequencies. A definitive transformation of these data into an influence line cannot be made because the vehicle mass, speed and axle spacing are unknown. However, a hypothetical transformation was made to demonstrate that dynamic loadings can be interpreted from in-service data recorded with simple equipment. The unknown parameters were estimated as: axle spacing 3 m and axle loading 55 kN. The required parameters are otherwise as specified in Table 4-10. The influence line calculation, that was used to transform the data in Case A is otherwise repeated and the results are shown in Figure 4-34. The calculation is only performed for the first half second and the additional peak dynamic loading can be inferred to be about 25% of the calculated static load.

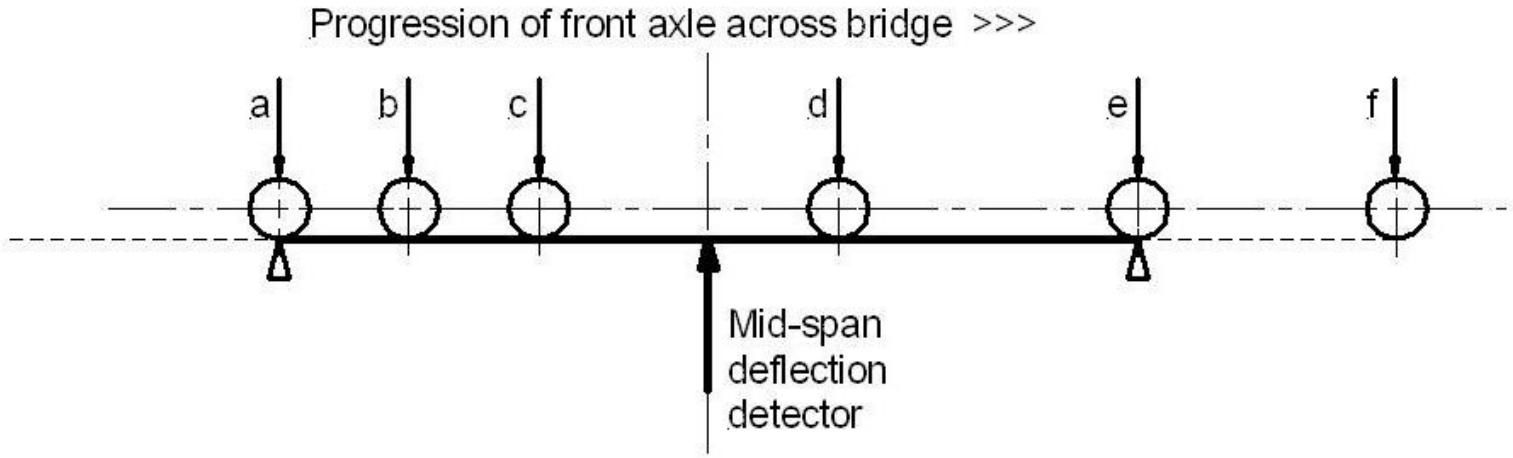

Figure 4-33: Progression of front axle across bridge

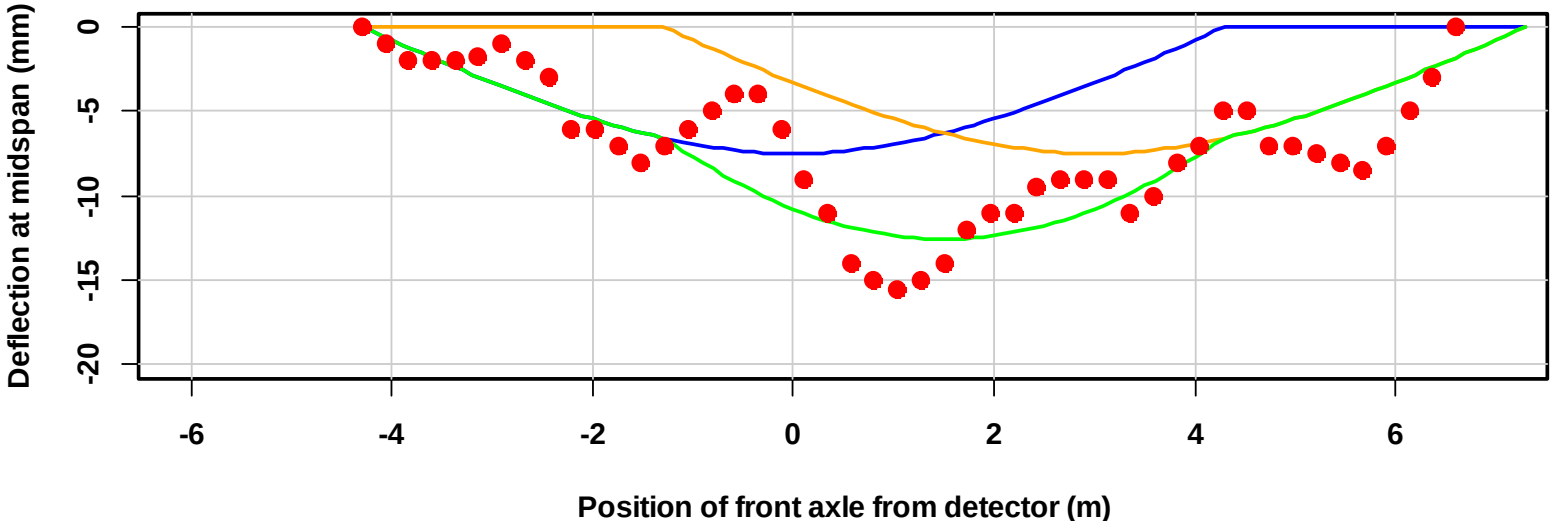

Figure 4-34: Nominal influence line of heavy truck for Powers Creek Bridge

Case C: Influence of speed

A vehicle was driven across span 6 of the Munsie Bridge and the deflections recorded. At speeds of 10 km h^{-1} or less the peak deflections were the same magnitude as those obtained with a static vehicle. At 20 and 40 km h^{-1} the deflections increased. The results shown in Figure 4-35 are normalised by dividing all values by the static value.

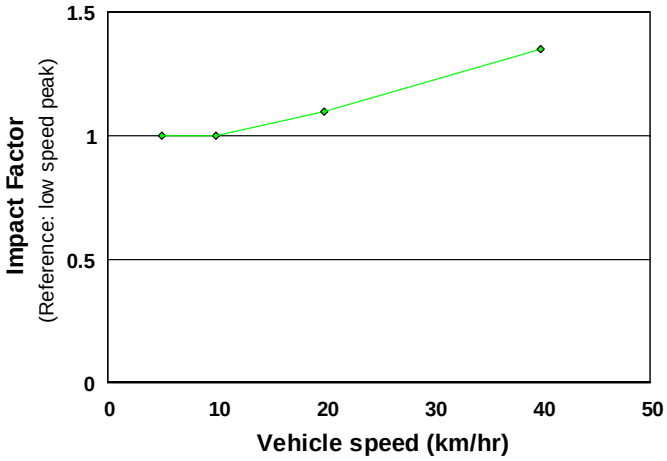

Figure 4-35: Impact factor-v-vehicle speed

4.5 Experiment 4: Determination of level of variation in a timber load-v-deflection curve

4.5.1 Aim

The objective of this experiment was to determine the lowest level of variation in MoE that could be expected to be reasonably achieved for a single timber sample in the laboratory.

4.5.2 Method

The measurements collected for this experiment were used to determine the level of measurement variation that could be expected in a model timber. The material linearity was compared with stainless steel and a table prepared of variation in MoE for measurements made both in ambient conditions and in constant MC conditions. A graph was also prepared indicating the temporal variation of MoE in constant MC conditions.

A sample pine (*P. radiata*)scantling was sawn into six samples of equal width and depth: 25.6 mm wide and 19.2 mm deep (refer Figure 4-36). These samples were two-point loaded in a bending press (refer Figures 4-37 and 4-38) to establish characteristic load-v-deflection curves. Samples were loaded both in the ambient environment and in a controlled moisture environment.

The controlled moisture environment was achieved by placing the samples in a constant humidity chamber of about 50% RH, controlled by salt solution and a fan (Figure 4-39). The MC of the samples was verified to be constant by re-weighing them several times throughout the experiment. While outside the chamber the samples were wrapped in plastic film to ensure that their moisture content did not vary significantly during measurement.

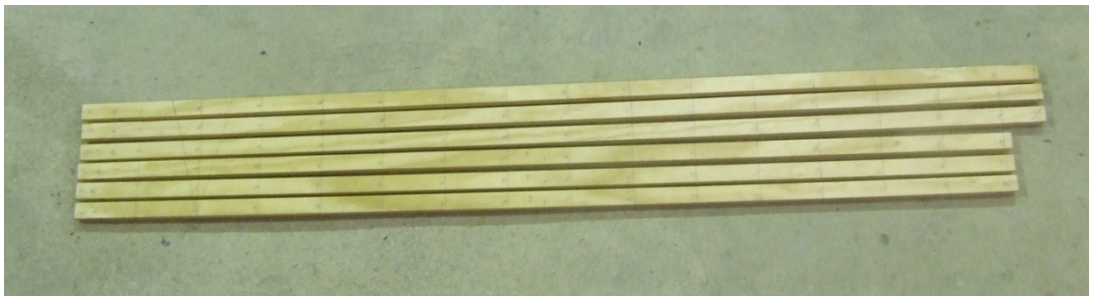

Figure 4-36: Pine samples #1 to #6

Figure 4-37: Bending frame showing sample under load

Figure 4-38: Sample showing yoke and dial gauge for recording deflection

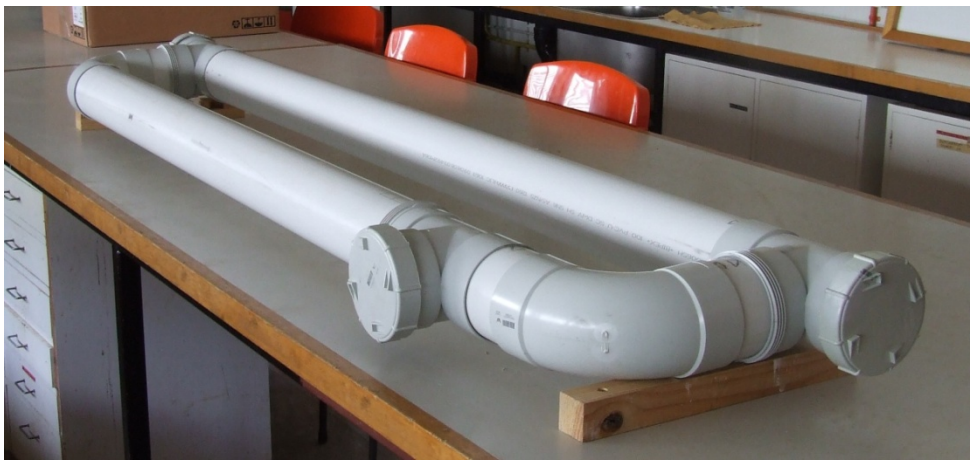

Figure 4-39: Constant humidity chamber

4.5.3 Results

The load-v-deflection curves for two representative samples are shown in Figure 4-40. The first is for a single sample of stainless steel of cross section 12 × 12 mm. The curve is highly linear with a very low level of scatter. The second is for a single sample of *P. radiata*, sample #4. The curve is also highly linear with a low level of scatter. Both of these curves have coefficients of determination above 0.9999.

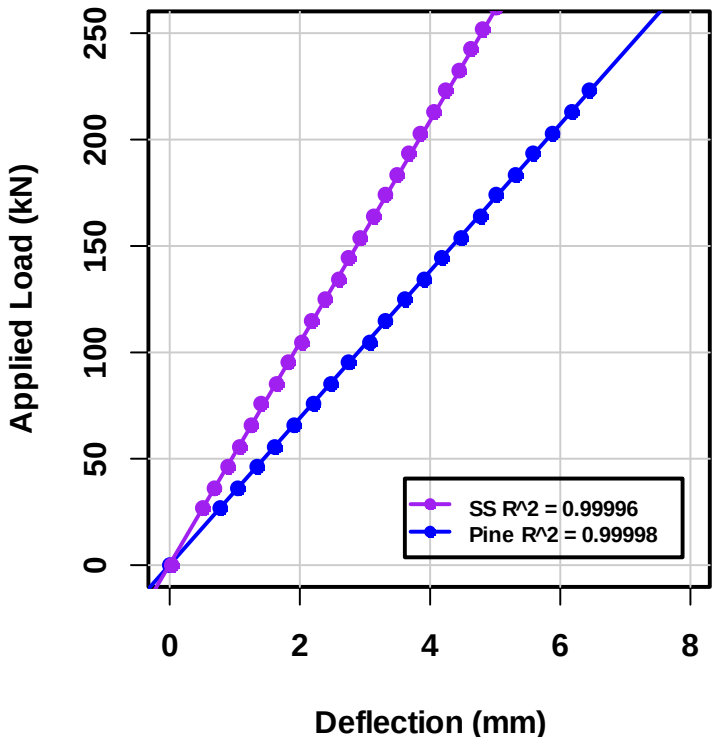

Figure 4-40: Measured load-v-deflection curve for stainless steel and *P. radiata* sample #4

The MoE was calculated from the slope, P/δ, of the load-v-deflection curve using Equation 4-4:

$$MoE = \frac{23}{108} \cdot \frac{L^3}{bd^3} \cdot \frac{P}{\delta}$$

..... Equation 4-4

where:

MoE	is the modulus of elasticity (Pa)
L	is the span between supports (m)
P	is the applied mid-span load (N)
b	is the width of the sample (m)
d	is the depth of the sample (m)
δ	is the mid-span deflection (m)

The measurement data are summarized in Table 4-11. The stainless steel sample was loaded and straightened five times and a CV of about 0.5% was achieved. The six samples of pine loaded in ambient conditions had a combined coefficient of variation of 2.7%. These six samples were all taken from the same clear plank and the CV represented the variation that occurred within one plank. One sample of pine bent in ambient conditions had a CV of 0.94. This pattern of variation between the group and a single sample was repeated when the samples were tested at constant humidity, but a lower level of variation was achieved. The variation of an individual sample, tested at constant humidity, was about 0.5% or less.

Table 4-11: CoV for stainless steel and pine samples

Sample description	Measurement conditions	Mean MoE	CoV%	Number of Determinations
Stainless steel sample	Room temp & humidity	231.4 (GPa)	0.47	5
Pine samples #1 – #6	Room temp & humidity	10.22 (GPa)	2.71	6
Pine sample #1	Room temp & humidity	10.95 (GPa)	0.94	6
Pine samples #4, #5, #6	Room temp & constant humidity	10.45 (GPa)	1.15	9
Pine sample #4	Room temp & constant humidity	10.38 (GPa)	0.22	3
Pine sample #5	Room temp & constant humidity	10.36 (GPa)	0.39	3
Pine sample #6	Room temp & constant humidity	10.61 (GPa)	0.52	3
Mean data for samples #4 – #6	Room temp & constant humidity	10.45 (GPa)	0.38	9

Each independent set of the above measurements was made within a period of several hours. In Figure 4-41 data from a longer period of measurements are shown. The abscissa is the elapsed measurement time and the ordinate range is restricted to enable the variation in MoE to be more clearly seen. The most probable slope of the regression line is zero with the MoE of pine being effectively constant for constant humidity. The variation in MoE was 0.37% CV.

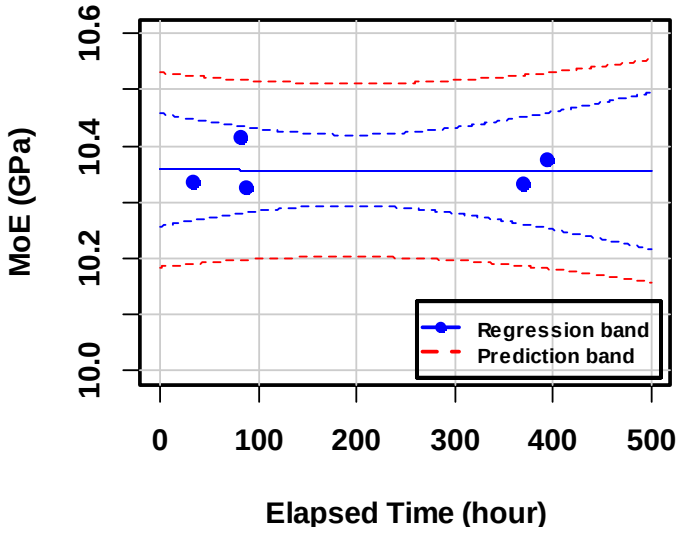

Figure 4-41: MoE of constant MC #4 pine sample-v-time

4.6 Experiment 5: Cypress Pine destructive test

4.6.1 Aim

The objective of this experiment was to determine if a standard sample of timber had a MoR-v-MoE vector consistent with the prediction band developed in Chapter 3.

4.6.2 Method

A sample of cypress pine was obtained from a commercial source. It was tested to bending failure in a laboratory four point bending press as shown in Figure 4-42. The applied load and deflection were recorded and a load-v-deflection curve plotted.

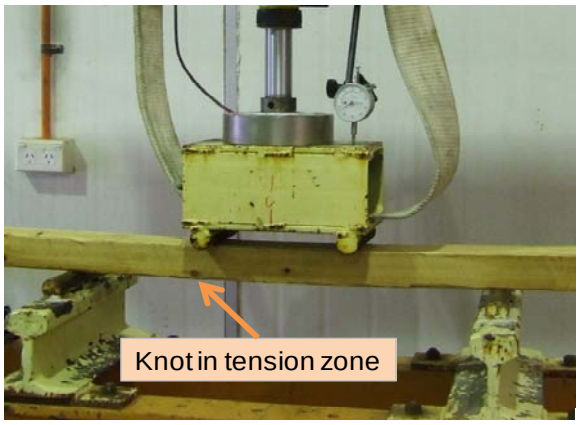

Figure 4-42: Cypress pine sample during bending

4.6.3 Results

The four point bending press had dimensions as shown in Figure 4-43. Loading is applied via a yoke (refer Figure 4-42) and both the combined load, P, (refer Equation 4-5) and the mid-span deflection, δ, measured. The measured deflection data is shown in Table 4-12 and the sample dimensions in Table 4-13.

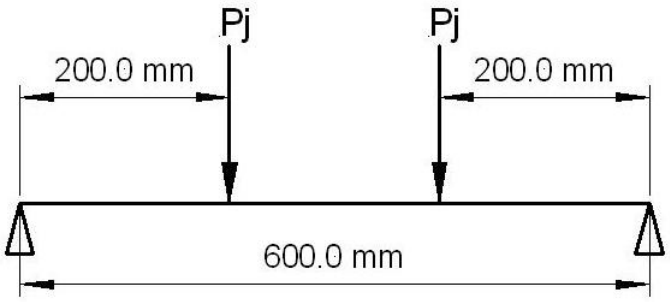

Figure 4-43: four point loading diagram

$$\text{Total applied load } P = 2\ x\ P_j$$

..... Equation 4-5

Table 4-12: Load-v-deflection data, Cypress pine

No.	Total Applied Load, P (kN)	Mid-span deflection, δ (mm)	No.	Total Applied Load, P (kN)	Mid-span deflection, δ (mm)
1	0.4	0.74	13	4.7	9.81
2	1.1	2.06	14	5.2	10.79
3	2.1	4.02	15	5.6	11.77
4	2.3	4.41	16	6.2	12.75
5	2.7	5.3	17	6.7	13.73
6	2.9	5.89	18	7.2	14.72
7	3.2	6.47	19	7.6	15.7
8	3.4	6.87	20	8	16.68
9	3.6	7.36	21	8.5	17.66
10	3.8	7.85	22	8.7	18.15
11	4	8.34	23	8.9	18.64
12	4.2	8.83	24	9.1	19.13
			25	9.5	19.62

Table 4-13: Cypress pine sample size details

Cypress sample parameter	Value
Width, *b*	73 mm
Depth, *d*	50 mm

The sample immediately after failure is shown in Figure 4-44. The failure has been initiated in the vicinity of the knot that is identified in Figure 4-42. The failure was sudden. This is reflected

in the load-v-deflection curve (Figure 4-45) since there was no non-linear region. The linearity of this curve was high with a coefficient of regression of 0.9986.

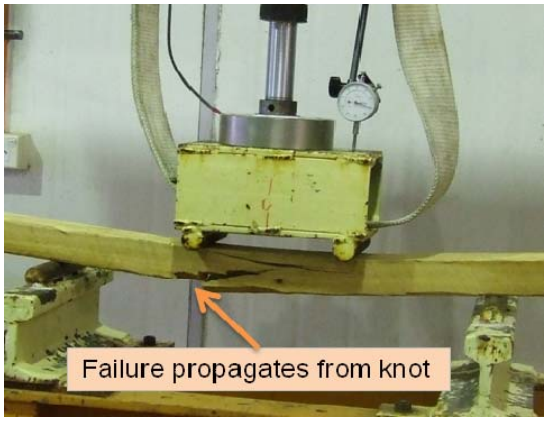

Figure 4-44: Cypress pine sample at failure

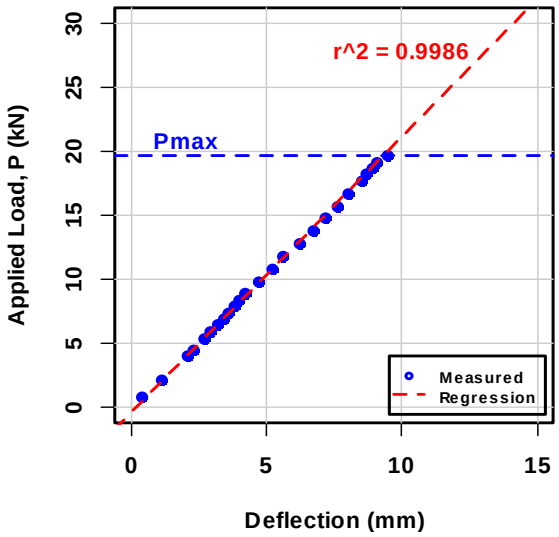

Figure 4-45: Cypress pine load-v-deflection curve

MoE was calculated from the slope, P/δ, of the load-v-deflection curve using Equation 4-4 and MoR was calculated from, *Pmax*, using Equation 4-6.

$$MoR = \frac{P_{max}L}{bd^2}$$

..... **Equation 4-6**

where:

MoR	is the modulus of rupture (Pa)
L	is the span between supports (m)
P_{max}	is the applied mid-span load causing rupture (N)
b	is the width of the sample (m)
d	is the depth of the sample (m)
δ	is the mid-span deflection (m)

The characterisation data for Cypress, as determined by CSIRO, are shown in Table 4-14. Both MoR and MoE maxima and minima data are shown. These data represent both the ranges within which any single sample of Cypress is expected to be found and the range within which the mean values are found to a 95% level of confidence. These data are overlaid on the prediction band data for girders and clears. The wider range for individual samples is shown in Figure 4-46 as a light blue rectangle. The dark blue rectangle represents the range of the characterised mean for the species Cypress. The MoR-v-MoE vector (blue dot) for the measured Cypress sample is also plotted in Figure 4-46. This MoR-v-MoE vector is both in the bottom half of the individual sample range (light blue rectangle) and within the clear prediction band (green dotted lines).

Table 4-14: Characterisation data for Cypress

Parameter	Minimum	Maximum
Sample MoE	5.9 (GPa)	12.0 (GPa)
Mean MoE	8.4 (GPa)	9.57 (GPa)
Sample MoR	46.5 (MPa)	111.1 (MPa)
Mean MoR	72.9 (MPa)	84.7 (MPa)

Note: Source Bolza & Kloot (1963)

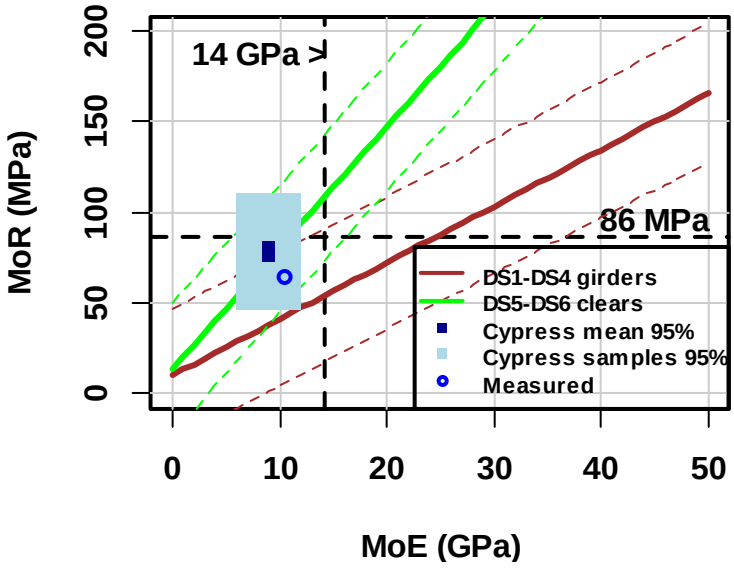

Figure 4-46: Cypress pine measured data overlaid on prediction bands

4.7 Summary

It was inferred by examination of laboratory girder tests that the non-linear region of a girder load-v-deflection curve can start at about 50% of the failure loading. Vehicles with axle loadings up to about 35% of the maximum legal axle loading were used to statically test load a bridge and it was shown that these loadings did not cause the bridge mid-span deflections to exceed about 20%, or less, of the girder linear region. By testing in this lightly loaded linear region, it was

possible to determine bridge stiffness to within about 2.5% with deflection measurements measured to an accuracy of about ± 0.5 mm.

A laser based BDM was used to record the vehicles transits by monitoring mid-span deflection without interfering with traffic flow. Low data volumes were recorded by only capturing the peak deflection of each vehicle, made possible because the test bridges were only single lane structures with traffic volumes about 150 – 300 vpd. Traffic loading distributions were calculated for three test bridge spans. The assumption of a log-normal distribution did not adequately represent both light and heavy traffic.

The dynamic deflections produced by a low speed vehicle were shown to be similar to static case by comparing the influence lines for these two cases. A low speed vehicle, on a timber bridge, was shown to be a vehicle travelling at about 10 km h^{-1} or less, since the deflections caused by vehicles at these speeds were shown to be equivalent to static loading. Examination of the deflections caused by a high speed vehicle enabled it to be shown that dynamic deflection produced by highway speed vehicles could be recorded and interpreted.

Pine timber and stainless steel were used as model comparative materials to enable the investigation of the variation of MoE. The measured variation in the MoE of stainless was found to be about 0.5% and a similar level of variation was found for a single timber sample when tested in constant MC conditions. In normal ambient conditions, with varying MC, the variation can be higher than about 0.5%. Measured variations of about 3% were measured between several samples from one timber plank.

A Cypress pine sample that included a small knot in the mid-span region was destructively tested. It failed with fibre separation propagating from the region of the knot. However, although the MoR-v-MoE vector was below the characterised mean value it was still within the characterised range for individual Cypress samples.

5 APPLICATION OF SHM TO TIMBER BEAM BRIDGE GIRDERS

5.1 Introduction

In this chapter the application of SHM techniques to the determination of girder limit state failure is examined. Three procedural steps are required to determine the structural health of timber-bridge girders. The first is to identify suitable parameter to predict structural health that secondly, can be readily measured on in-service structures. The third step is to utilise that parameter as part of a SHM analysis technique to determine structural health and the probability of failure. The first two of these steps were reported in Chapter 3 and 4.

In Chapter 3 it was shown that girder MoE and condition state can be used to predict girder MoR. The measurement of in-service mid-span deflection data was then examined in Chapter 4, where this data were used to determine in-service bridge stiffness and traffic loading. The third procedural step, examined in this chapter, compares measured in-service girder deflection data for a particular bridge span with data derived from numerical finite element modelling using SAP2000® (refer glossary) of that same span and determine both loading distribution and girder MoE. Because of measurement error and parameter temporal variation, these parameters are not single valued constants but functions with a standard error which are best described as a distribution.

Such distributions are specified with both a mean value and a coefficient of variation. As one example Ironbark has a species mean MoE of 24 GPa and a variation of about 10% for individual results. This variation is the result of both the variation between the measured samples and the measurement error. As another example the measured stiffness of Powers Creek Bridge, with mean value of about 0.6 tonne mm^{-1}, has a 5% CV. Since this measurement is a single determination at one moment in time, the variation is simply the result of measurement variations. Some of these data distributions, such as MoE, can be well described by a normal distribution, whereas others, such as traffic loading, may need more complicated descriptions. The use of lognormal, uniform, multi-modal and other distributions can be required to accurately model these data. Before SHM techniques can be applied, however, the mean values of the material and load distributions need to be determined for each girder. The methods of determining individual girder MoE and the percentage of the applied load are set out in SHM Determination 1.

Three cases of the application of SHM, to limit state failure, are considered. The first case is excess deflection being caused by highway traffic loads, the second case is excess deflection caused by temporal erosion of the girder surface and the third case is girder structural failure. The first case is caused when traffic loading is above the legal limit and the span to deflection limit state is exceeded. The limit state is a single valued constant which is compared with the defection distribution caused by the traffic loading distribution. If the traffic loading causes the deflection to exceed the span to deflection limit state then a failure has occurred. In the second case, if bridge stiffness is reduced by degradation then legally loaded traffic can cause excess deflection. Again the deflection distribution caused by traffic loading is compared with the single valued limit state deflection. The third case is when a girder fails structurally either because of excess loading or because a girder has degraded and is significantly less than its design specification. The third case is that of girder failure; MoR is exceeded. This failure can occur if the girder is significantly degraded (CS-3 or CS-4) and the loading on a particular girder, is significantly above the specified design load. One example of this occurring was cited in Section 2.3 where a cement truck caused a bridge in Singleton to fail. In the case of girder failure the limit state is the distribution that represents the girder MoR. This distribution is then compared with the mid-span stress distribution caused by traffic loading.

To compare a distribution either with another distribution or with a single value requires a Monte Carlo calculation. For example, as shown in SHM Application 1 (Section 5.4) a deflection distribution is determined for the mid-span deflections caused by traffic and a reference value is determined which represents the limit state deflection. A value is then randomly selected from this distribution and compared with the reference value. If the limit state is exceeded then a failure has occurred. The calculation is repeated enough times to determine the probability of failure. As another example, shown in SHM Application 2 (Section 5.5) the mid-span stress distribution caused by traffic is compared with the MoR distribution. In this case, a value is randomly selected, one from each distribution, and the two compared. If the MoR is exceeded than a failure has occurred.

SHM applications involving Monte Carlo comparisons can require significant computer processing power because of the large number of comparisons required. As indicated in Section 2.6.3 structural failure should be calculated to less than 1 in 10^6. To identify if a safety index is varying it should be computed to a rate lower than 1 in 10^6 and this requirement further imposes a limit on the minimum period for which a safety index is calculated. The computation of a failure rate below 1 in 10^7 can require several hours of processing time on a personal computer

(PC), whereas a rate of 1 in 10^5 might only require about 15 seconds. If the computation time is an hour or more, then with current processing techniques, it is only appropriate to calculate a structural failure safety index for an in-service period of more than 24 hours.

To overcome these limitations, a theoretical condition alarm is proposed in SHM Application 4. This is achieved by recording the daily running sums of the peak deflections caused by traffic loads. By comparing the number of vehicles exceeding different deflection thresholds, a real time parameter can be generated that is indicative of bridge stiffness. Significant change in that parameter, at any time, provides a first indication of possible structural change. Application 1 or 2 can then be utilised to determine when any significant structural concern arises.

5.2 SHM Determination 1: Girder MoE and percentage loading

Historically in NSW, the decking of timber beam bridges could comprised cross planking about 100 mm thick (refer Section 2.4.3). These planks were laid across supporting girders and transferred the applied vehicle loads to the girders (Refer Figures 2-1 and 2-7). They deflected according to the load and the girder stiffness. For this reason, girder deflection depends on both the load and the deck stiffness and the manner in which the load is distributed to each girder will be different for each bridge. To understand the full interaction between deck and girder requires a complex model with a large number of descriptive equations. In this determination, a less complex model is evaluated but this still provides an adequate level of detail and reflects real time interactions of an in-service bridge.

5.2.1 Aim

The aim of this determination was to estimate the girder MoE and the percentage of the applied load supported by each girder, by modelling the deflections caused by the static loading of a bridge and comparing them to the measured deflections.

5.2.2 Method

The proposed algorithm used is set out in Figure 5-1. Firstly, the physical dimensions of the test bridge were measured. This enabled the girder lengths, diameters and spacing to be identified which were used to create a SAP2000® finite element model of the bridge using Timoshenko beam theory (refer Glossary). Secondly the bridge was loaded and deflection data experimentally gathered (refer Section 4.3). The finite element model was next loaded with loading identical to the experimental loading and the model girder deflections recorded. The model deflections were then compared to the measured deflections and both the model girder MoE and the decking MoE

adjusted until the model deflection data agreed with the measured data. Girder MoE was the first outcome from this first part of determination 1. Fourthly, a second model of the bridge was created that comprised only the supporting girders and was modelled using Euler-Bernoulli theory. The measured physical girder dimensions and the MoE values determined with the first model were incorporated into this second model. It did not account for the change in deflection caused by shear forces (Timoshenko theory), which were included in the first model, but nevertheless this effect was less than a few percent of the measured girder deflections. The percentage loading of each model girder was then adjusted until the model deflections agreed with the measured deflections. The percentage of the each model girder was then adjusted until the model deflections agreed with the measured deflections. The second outcome of this determination was the percentage of the total mid-span loading effectively applied to each girder.

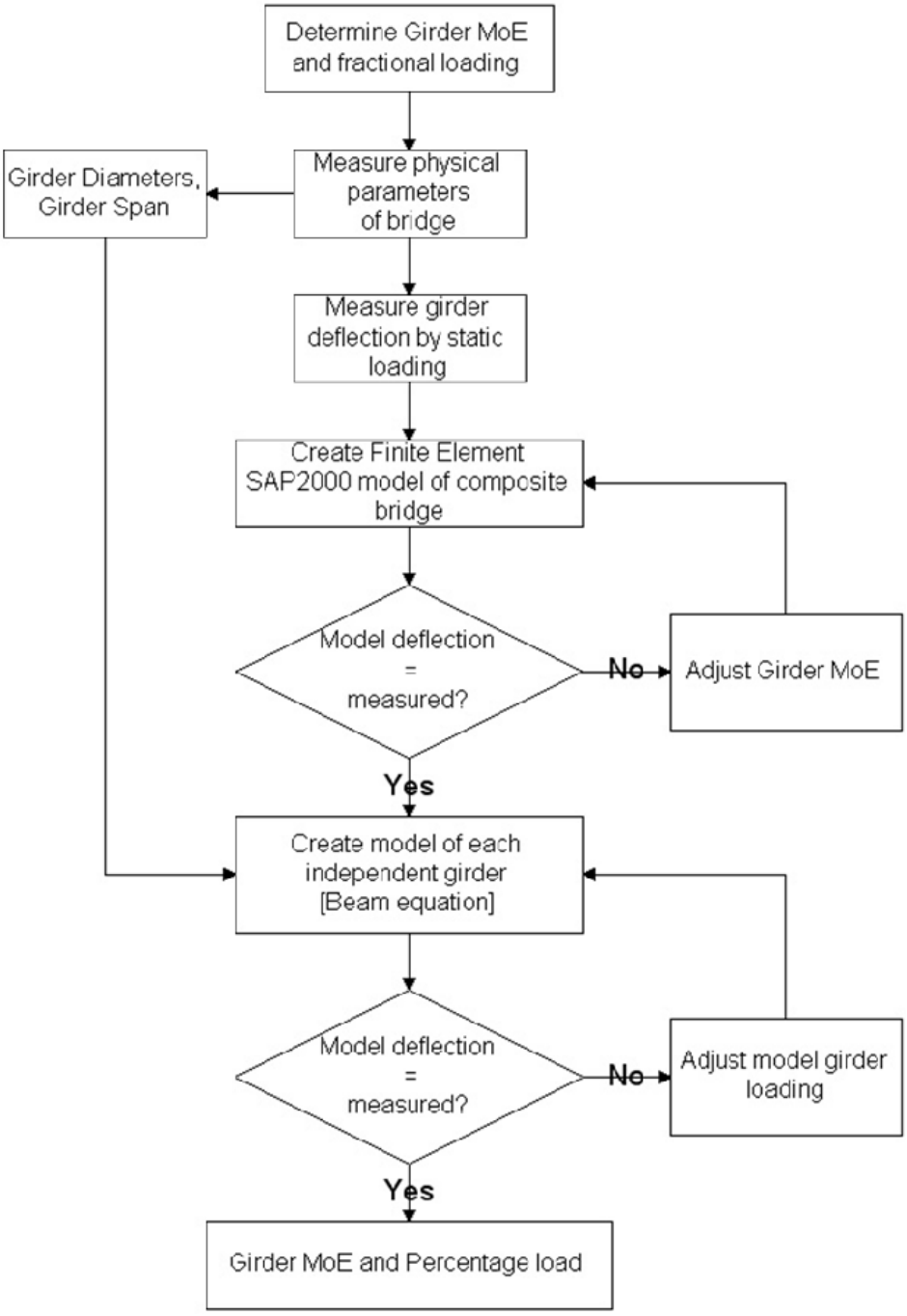

Figure 5-1: Flow chart – Method to determine girder MoE and percentage girder loading

5.2.3 Measured results

The first step was to measure the physical dimensions of the three bridge spans. These are shown in Figures 5-2, 5-3 and 5-4 for the Powers Creek Bridge, Munsie Bridge span G-4 and the Munsie Bridge span G-6 respectively. These dimensions are utilised in the subsequent models and are summarised in Table 5-1. The second step was to load the bridge spans and measure the deflections. These results are shown in Table 5-2.

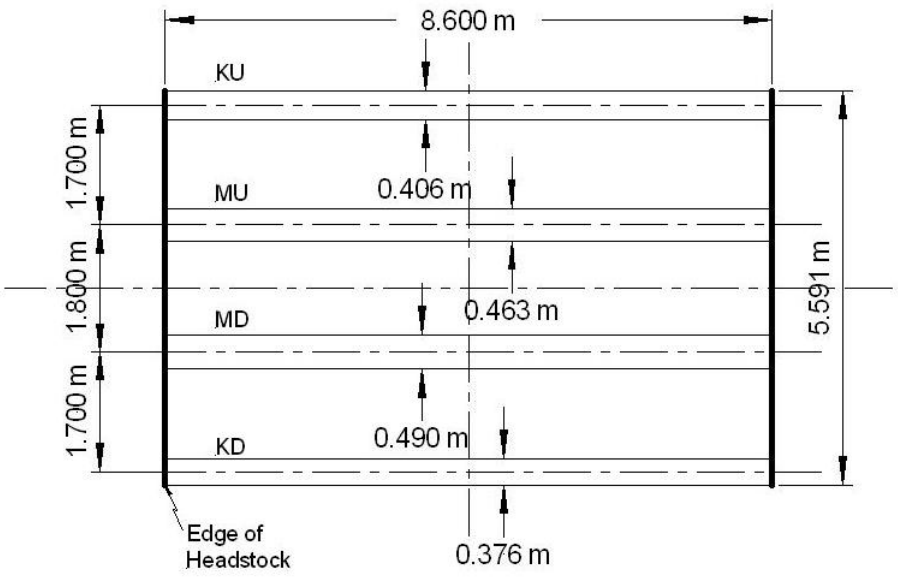

Figure 5-2: Powers Creek Bridge dimensional schematic

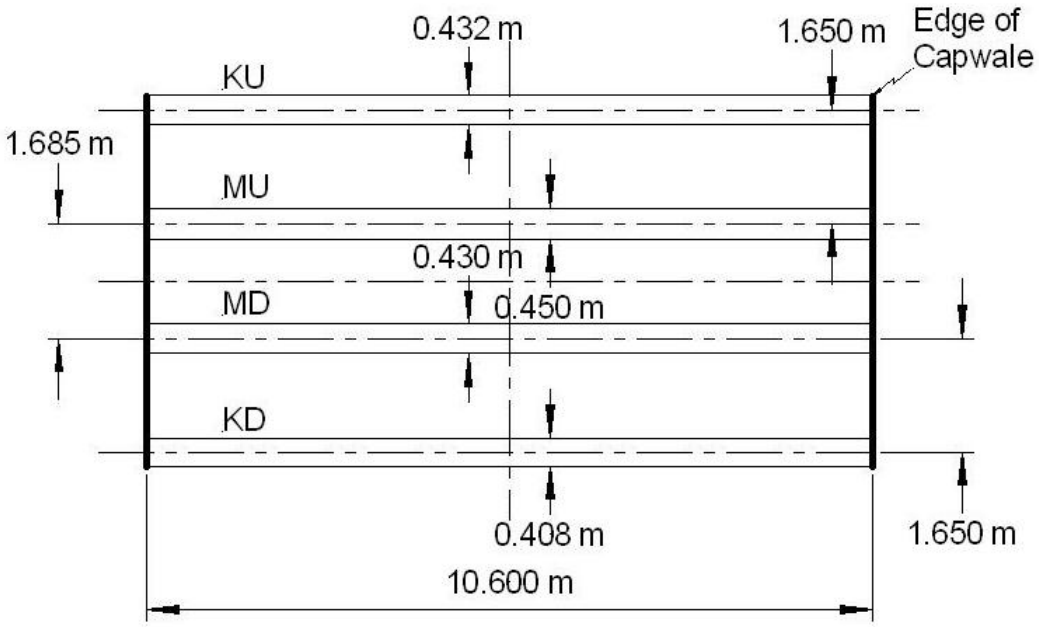

Figure 5-3: Munsie Bridge, Gostwyck Span G-4 dimensional schematic

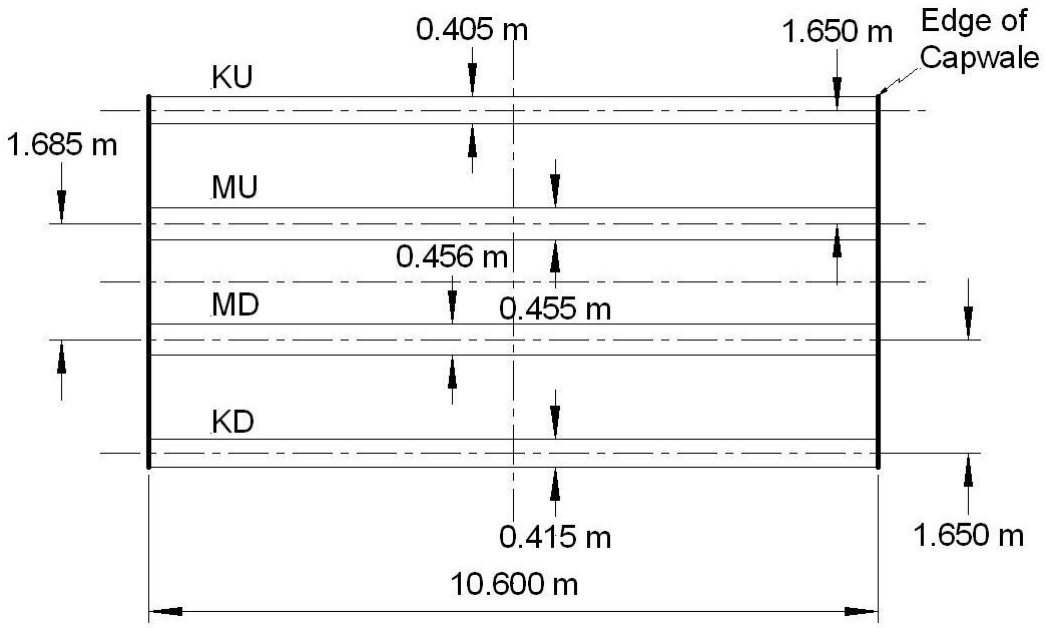

Figure 5-4: Munsie Bridge, Gostwyck Span G-6 dimensional schematic

Table 5-1: Summary of girder dimensions

Span	Girder[1]	Span	Measured Girder depth (mm)	Relative girder position, (m)
Powers Creek	KU	8.6	406	0
	MU	8.6	463	1.70
	MD	8.6	490	3.50
	KD	8.6	376	5.20
Munsie Bridge, Span 4	KU	10.6	432	4.98
	MU	10.6	450	1.65
	MD	10.6	430	3.33
	KD	10.6	408	4.98
Munsie Bridge, Span 6	KU	10.6	405	0
	MU	10.6	455	0
	MD	10.6	456	1.65
	KD	10.6	415	3.33

Note 1, Nomenclature: Kerb = K, Main = M, Upstream = U, Downstream = D

Table 5-2: Measured girder deflections

Parameter	Vehicle loading	Girder deflection (mm)			
		KU	MU	MD	KD
Powers Creek	43 kN	3.2	5.2	4.7	2.9
Gostwyck Span G-4	124 kN	14.8	27.7	26.8	11.2
Gostwyck Span G-6	55 kN	4.7	8.81	9.4	6.2

5.2.4 Calculated results

A SAP2000® model was next used to determine the effect that the deck had in distributing the loads to the girders. This interaction between the deck and the girders is complicated in that a

full analysis would require complicated modelling with a large number of descriptive equations. In this experiment only a simple analysis was attempted with a limited number of descriptive equations describing girder and deck plank bending and not bolted connections.

The MoE values for the decking were iteratively chosen so that the calculated deflections of the model were similar to the actual measured deflections for similar loading conditions. This allowed the model deck to curve in a similar fashion to the true deck and enabled the distribution of the load between the main and kerb girders to be determined. An example of the outline of the model for the Powers Creek Bridge was as shown in Figure 5-5. The models for the two Munsie Bridge spans were similar, but with different physical dimensions as specified in Table 5-1. The MoE determined for each girder is shown in Table 5-3.

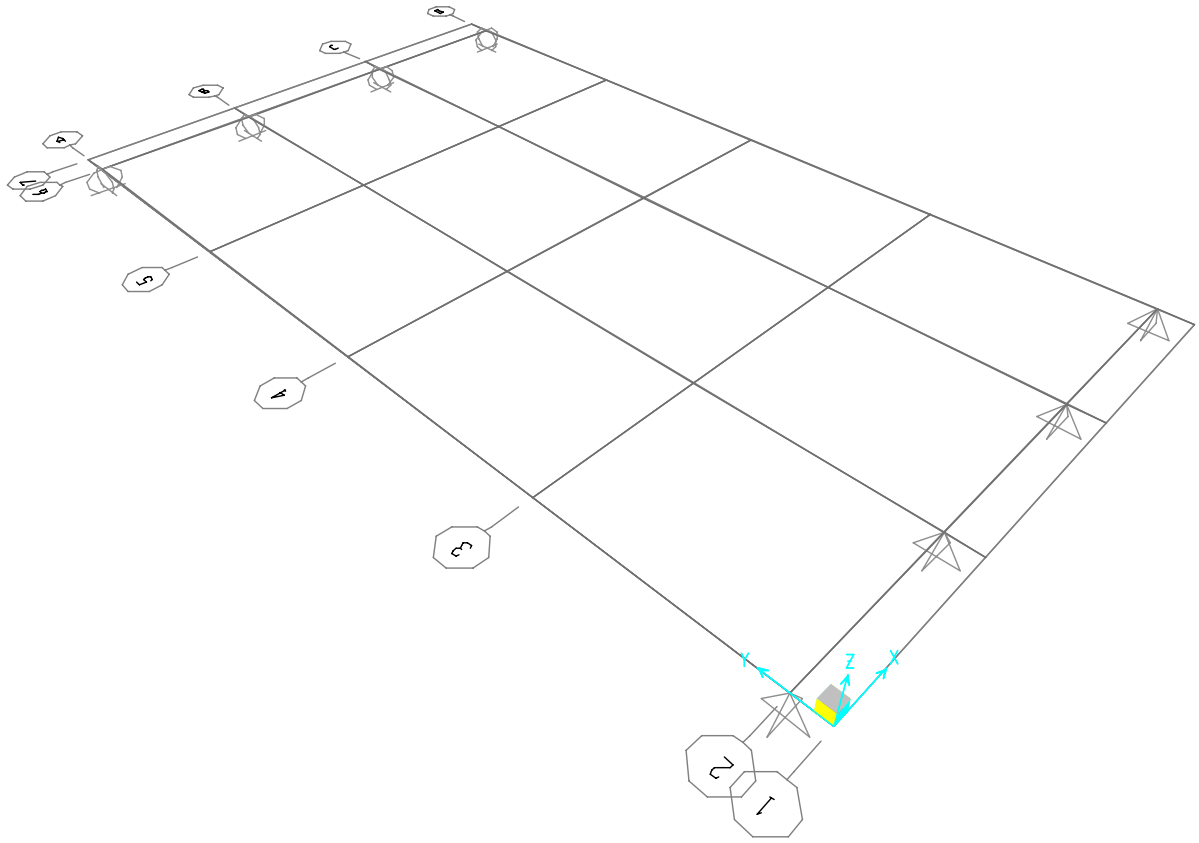

Figure 5-5: Finite element model outline for Powers Creek Bridge

Table 5-3: Calculated MoE for bridge girders

Bridge span	Girder[1]	Span (m)	Measured Girder depth diameter (mm)	Girder MoE (GPa)
Powers Creek	KU	8.6	406	12
	MU	8.6	463	20
	MD	8.6	490	20
	KD	8.6	376	14
Munsie Bridge, Span 6	KU	10.6	405	34
	MU	10.6	455	28
	MD	10.6	456	26
	KD	10.6	415	20
Munsie Bridge, Span 4	KU	10.6	432	28
	MU	10.6	450	19
	MD	10.6	430	22
	KD	10.6	408	24

Note 1, Nomenclature: Kerb = K, Main = M, Upstream = U, Downstream = D

In each case, the total span was set to the actual span and the girder diameters and positions set to fit the measured data. The decking was represented by five wide cross planks joined at the nodes shown (refer Figure 5-5). This layout achieved a representation of the actual deck which was only joined to the girders with bolts widely spaced along the girder. Much of the actual deck was just resting on the girders, not rigidly attached to them, and there was significant freedom for slip to occur between the girders and the deck planks.

The load applied to each girder was next calculated using standard Euler-Bernoulli theory (refer Equation 5-1). The nomenclature used for this equation is shown in Figure 5-6. A summary of the data outcomes are shown in Table 5-4 through to Table 5-7. These results, both girder MoE and girder percentage loading fraction will be used in the next sections to determine bridge safe load limits and probabilities of failure.

$$Applied\ load, P = \frac{3\ \delta\ E\ \pi\ D^4}{4\ L^3}$$

..... Equation 5-1

where:

P is the applied mid-span load (N)

δ is the mid-span deflection (m)

E is the MoE (Pa)

D is the effective girder diameter at mid-span (m)

L is the span between supports (m)

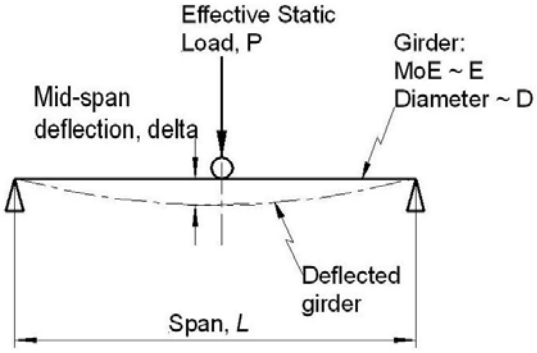

Figure 5-6: Beam equation nomenclature

Table 5-4: Measured deflection and estimated percentage loading, Powers Creek Bridge

Parameter	Girder			
	KU	MU	MD	KD
Measured deflections (mm)	3.2	5.2	4.7	2.9
Estimated girder load (kN)	3.8	17.0	20.0	3.0
Percentage applied load (%)	8.8	39.4	46.3	7.0

Table 5-5: Measured deflection and estimated percentage loading, Gostwyck span G-4

Parameter	Girder			
	KU	MU	MD	KD
Measured deflections (mm)	14.8	27.7	26.8	11.2
Estimated girder load (kN)	28	42	39	14
Percentage applied load (%)	23.0	34.4	32.0	11.8

Table 5-6: Measured deflection and estimated percentage loading, Gostwyck span G-6

Parameter	Girder			
	KU	MU	MD	KD
Measured deflections (mm)	4.7	8.81	9.4	6.2
Estimated girder load (kN)	8.6	20.9	20.8	7.3
Percentage applied load (%)	15.7	38.1	38.0	13.3

Table 5-7: Calculated MoE and Percentage of load for bridge girders

Bridge Span	Girder1	Span (m)	Measured Girder depth (mm)	Girder MoE (GPa)	Percentage of applied load (%)
Powers Creek	KU	8.6	406	12	8.8
	MU	8.6	463	20	39.4
	MD	8.6	490	20	46.3
	KD	8.6	376	14	7.0
Munsie Bridge, G-4	KU	10.6	432	28	23.0
	MU	10.6	450	19	34.4
	MD	10.6	430	22	32.0
	KD	10.6	408	24	11.8
Munsie Bridge, G-6	KU	10.6	405	34	15.7
	MU	10.6	455	28	38.1
	MD	10.6	456	26	38.0
	KD	10.6	415	20	13.3

Note 1, Nomenclature: Kerb = K, Main = M, Upstream = U, Downstream = D

5.3 SHM Determination 2: Bridge load limit

The legal axle loading in NSW is defined by legislation (refer Section 2.2.5) and, for the purposes of vehicle users, is described by the RMS in relation to type of vehicle and both the number of wheels and axles. For the purposes of this determination, the load limit is specified as a single mid-span axle load and for bridges without load limit signage is specified as 20 tonne (refer Section 2.2.5). Thus if a bridge girder can support its percentage loading of 20 tonne to a 95% level of confidence there is no need for load limit signage. If the load that a girder can support, to a confidence level of 95%, is less than 20 tonne then that reduced loading can be used to identify the required bridge load limit. The act of specifying girder MoR to a confidence level of 95% and of specifying the applied load as a single value load limit reduces this determination to a comparison of single valued functions and not the comparison of data distributions.

5.3.1 Aim

This section used previous results to model the individual girder mid-span stress, caused by static loading, and determine the loading that causes a stress equal to the girder MoR.

5.3.2 Method

This determination utilised the results from SHM Determination 1 and a MoR-v-MoE relationship derived in Chapter 3 as identified in the flow chart shown as Figure 5-7. The specific relationship utilised is the lower bound of Equation 3.10. It is repeated here as Equation 5.2 and shown graphically in Figure 5-8. The maximum load is calculated using standard Euler-Bernoulli theory as shown in Equation 5.3.

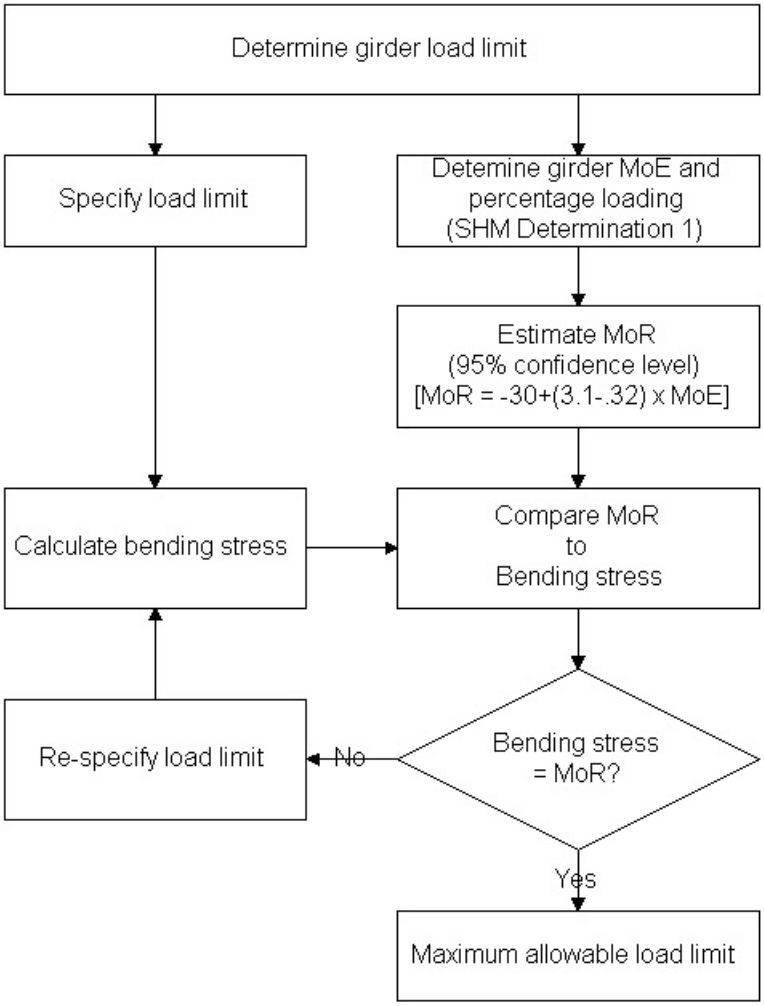

Figure 5-7: Girder maximum load limit flow chart

$$MoR = -30 + (3.1 - 0.32) \times MoE$$

..... Equation 5-2

where:

MoR is the modulus of rupture (MPa)

MoE is the modulus of elasticity (GPa)

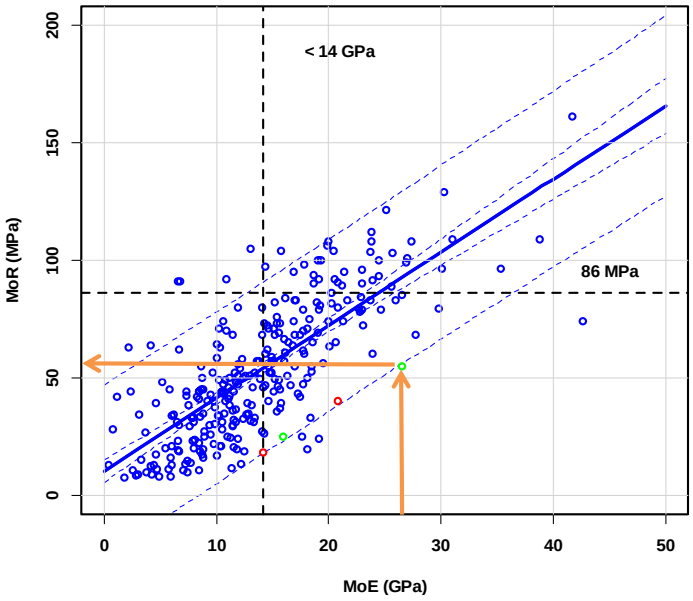

Figure 5-8: Evaluation of MoR from MoE via lowest bound of next prediction band to a confidence level of 95%

$$\text{Maximum load, } P = \frac{MoR\ \pi\ (D)^3}{8\ L\ f_l}\frac{10^3}{9.81}$$

..... Equation 5-3

where:

P	is the applied mid-span load (tonne)
MoR	is the modulus of rupture (MPa)
D	is the effective girder diameter at mid-span (m)
L	is the span between supports (m)
f_l	is the percentage loading

5.3.3 Calculated results

The results from SHM Determination 1 (Table 5-7) are repeated in Table 5-8, but with the 95% confidence level MoR value and not the mean value. Only data for the main girders are shown. Equation 5-4 is shown as one example calculation and the data are summarised in Table 5-9 and Figure 5-9.

Table 5-8: Calculated MoE, MoR and Percentage of load for bridge girders

Span	Girder[1]	Span	Measured Girder depth (mm)	Girder MoE (GPa)	Girder MoR (MPa) (-30+3.1MoE)	Percentage of load (%) f_l
Powers Creek	MU	8.6	463	20	32	39.4
	MD	8.6	490	20	32	46.3
Munsie Bridge, Span 6	MU	10.6	455	28	56.8	38.1
	MD	10.6	456	26	50.6	38.0
Munsie Bridge, Span 4	MU	10.6	450	19	28.9	34.4
	MD	10.6	430	22	38.2	32.0

Note 1, Nomenclature: Kerb = K, Main = M, Upstream = U, Downstream = D

$$\text{Maximum load, } P = \frac{32\,\pi\,(0.463)^3}{8\,\times\,8.6\,\times\,0.394}\,\frac{10^3}{9.81}\;tonne$$

..... Equation 5-4

Hence, for Powers Creek Bridge: $P = 37.5\;tonne$

Table 5-9: Bridge loading to cause girder MoR to be exceeded

Girder	Load to cause MoR to be exceeded to a 95% confidence level (tonne)	Load to cause MoR to be exceeded to a 5% confidence level (tonne)
Main upstream, Powers Creek (PC-MU)	37.7	124.6
Main downstream, Powers Creek (PC-MD)	38.1	125.6
Main upstream, Munsies Bridge span 6 (G6-MU)	53.0	122.6
Main downstream, Munsies Bridge span 6 (G6-MD)	47.7	117.8
Main upstream, Munsies Bridge span 4 (G4-MU)	22.6	106.8
Main downstream, Munsies Bridge span 4 (G4-MD)	36.0	105.6

In Table 5-9 and Figure 5-9 only the loads for each main girder are shown, since under normal loading conditions, these are more highly stressed than the kerb girders. As an example, the main upstream (MU) girder of the Powers Creek bridge was capable of supporting a mid-span load of about 38 tonnes to a confidence level of 95%, whereas the upstream kerb (KU) girder, because of the lower load distribution factor, was capable of supporting about 100 tonnes (data not shown). This is of course only true if the load is centrally applied and this analysis can be repeated to determine the loading levels for non-central loads. The confidence level of 95% is a result of the variation shown in the data (refer Figure 5-8). The load that each girder may be capable of supporting is shown in the right most column of Table 5-9 but only to a confidence level of 5%.

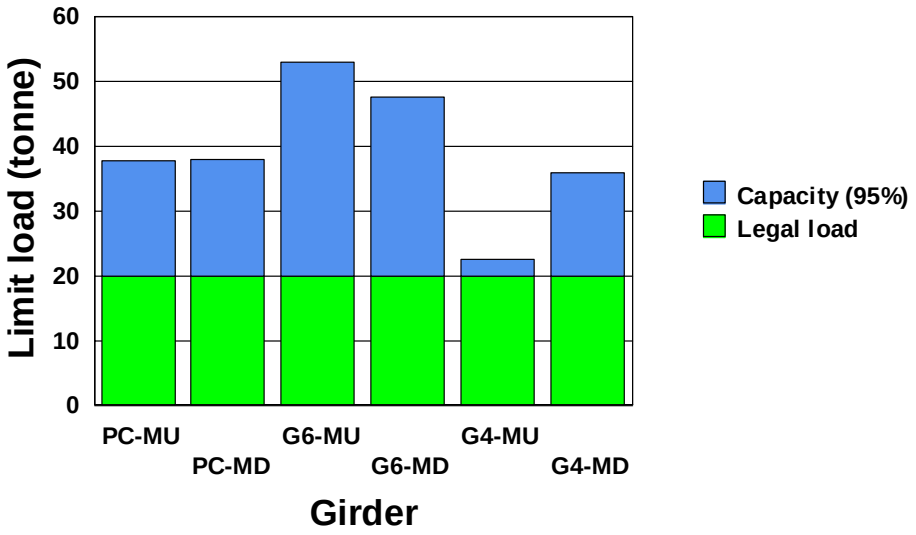

Figure 5-9: Girder maximum loading, 95% confidence level

The girder of most concern was the upstream girder of Munsie Bridge span 4 (G4-MU). This girder would support a load of 22.6 tonnes and be unlikely to fail to a confidence level of 95%. This rating was unexpected since the bridge owners had, before the measurements were made, identified that the downstream girder contained a pipe but had not identified any concerns about the upstream girder. The 95% confidence level data, shown in Table 5-9, represent the lower limit of the data distribution. Also shown are the data values for the higher limit, which are only known to a confidence level of 5%. The actual data will be somewhere between these two limits but for bridge load rating purposes the lower level must be used.

The main upstream girder of Munsie Bridge (G4-MU) was initially thought to be sound. But after closer inspection, it was realised that it was decayed below the outer surface. This decay, shown in Figure 5-10, was probably only present in the outer sapwood, but may have been causing the effective diameter to be lower than the measured outer diameter. If the effective diameter is estimated as 450 mm instead of 470 mm, to allow for this decay, then the effective MoE is 19 GPa and not 16 GPa. Thus a 4% reduction in diameter results in about a 16% reduction of MoE. To account for this variation SHM Determination 1 was repeated with the reduced diameter of 450 mm.

Figure 5-10: Evidence of decay in the main upstream girder, Munsie Bridge Span 4, at mid-span

Applying this increased value of MoE and recalculating the load limit, produces the data as shown in Figure 5-11. This modification cannot be made to all girders since they do not all have a layer of degraded sapwood; the main downstream girder (G4-MD) of the same span is an example of one without sapwood. The result, shown in Figure 5-11, is the slightly wider, probably more realistic, operating band (blue band) for G4-MU. To determine the accuracy and confidence level that should be attributed to these measurements ongoing temporal measurements will be required. Also shown in Figure 5-11, are the upper limits of the data distribution, as the peak of the red bands with a confidence level of 5%. Each girder is thus likely to withstand the load at the peak of the red bar to a confidence level of 5% and at the bottom of the red bar to a confidence level of 95%.

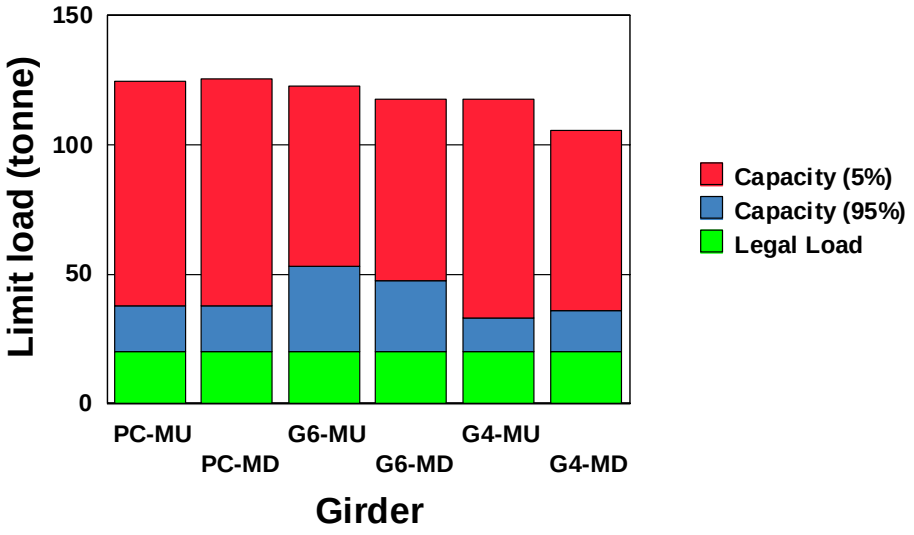

Figure 5-11: Girder maximum loading with modified value of MoE for G4-MU

5.4 SHM Application 1: Probability of failure of the Span to Deflection Limit state

Bridges built to standards of the 21st century are constructed to a higher level of stiffness than they were in the early 20th century (refer Section 2.3). Since there are many extant timber-bridges in NSW that were built in the early 20th century there is a need to identify whether they should be upgraded to current standards or left in their current state. A detailed determination of the failure of the span to deflection limit state would require the parameter distributions to be known. The girder second moment of area, the variation of material strength across the section, the MoE, the level of defects and how the load is applied are all contributing parameters. To reduce the complexity of this analysis only the distributions of the applied traffic load and MoE are considered.

5.4.1 Experiment aim

To determine the probability that the mid-span deflections produced by traffic would exceed the specified span to deflection limit state. The failure probability for each of the main girders for each of the three test spans are determined.

5.4.2 Experiment method

The algorithm used is set out in Figure 5-12. The first steps to identify girder MoE and the percentage loading were as identified in SHM determination 1. The traffic loading distributions were determined from the data gained in Experiment 2. These loads, together with the girder MoE values, were used to determine the mid-span deflection distributions. The deflection distributions were used in a Monte Carlo analysis using MatLab® to generate both a probability of failure and a safety index. This analysis was run 10^6 times to determine the number of times the applied load caused the mid-span deflection to exceed the limit state as set by *Australian Standard AS 5100.*

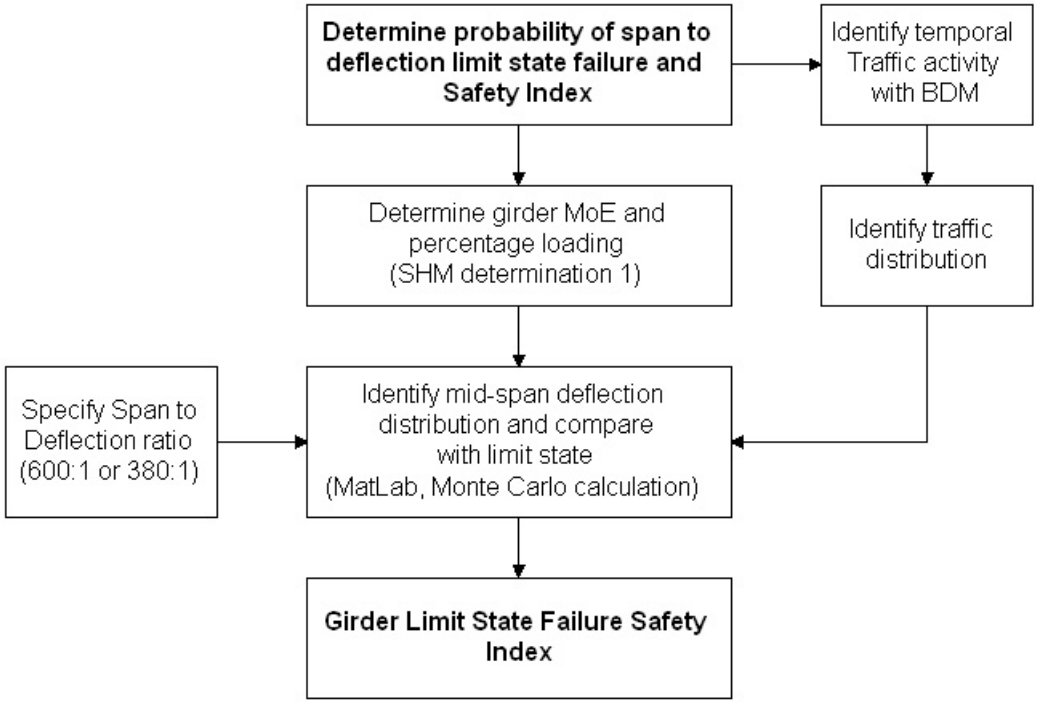

Figure 5-12: Flow chart: Determine the probability of Span to Deflection limit state failure

5.4.3 Probability of Failure of the Span to Deflection limit state

A requirement of modern bridges is that they do not deflect excessively under load. The limit state is defined as the span to deflection limit for any particular bridge span (refer Section 2.3). The limit states for the test case bridge spans are given in Table 5-10.

Table 5-10: Span to deflection limit state maximum deflections for test case bridge spans

Bridge	Span (m)	Limit state	Limit State deflection (mm)
Powers Creek Bridge	8.6	600:1	14.3
Powers Creek Bridge	8.6	380:1	22.6
Munsies Bridge, G-4 and G-6	10.6	600:1	17.7
Munsies Bridge, G-4 and G-6	10.6	380:1	27.9

The applied loads distributions were determined in Experiment 2 (refer Table 4-8). The maximum deflection calculated and the values computed for the probability of failure are as shown in Table 5-11. A safety index of magnitude greater than 4.75 indicates that no failure resulted from the comparison; equivalent to a failure rate less than 1 in 10^6 (refer Section 2.6.3 and Glossary). These calculated deflection distributions are shown in Figures 5-13 and 5-14, grouped according to a common bridge. The distributions for the two main girders (PC-MU and PC-MD) of Powers Creek Bridge are shown in Figure 5-13 and those for Munsie Bridge (G4-MU, G4-MD, G6-MU and G6-MD) in Figure 5-14. A significant feature of these curves is that

the maximum calculated mid-span deflection is not more than 60% of the limit state (refer Table 5-10).

Table 5-11: Computed Safety Index, β, for the Span to Deflection limit state failure of the main bridge girders

Bridge girder	Maximum deflection (mm)	Safety Index
Main upstream, Powers Creek (PC-MU)	6.4	> 4.9
Main downstream, Powers Creek (PC-MD)	7.3	> 4.9
Main upstream, Munsies Bridge span 4 (G4-MU)	10.7	> 4.9
Main downstream, Munsies Bridge span 4 (G4-MD)	6.8	> 4.9
Main upstream, Munsies Bridge span 6 (G6-MU)	8.1	> 4.9
Main downstream, Munsies Bridge span 6 (G6-MD)	7.5	> 4.9

Note: A safety Index of 4.9 is equivalent to a rate of 5 in 10^7; the measured rates were less than 5 in 10^7

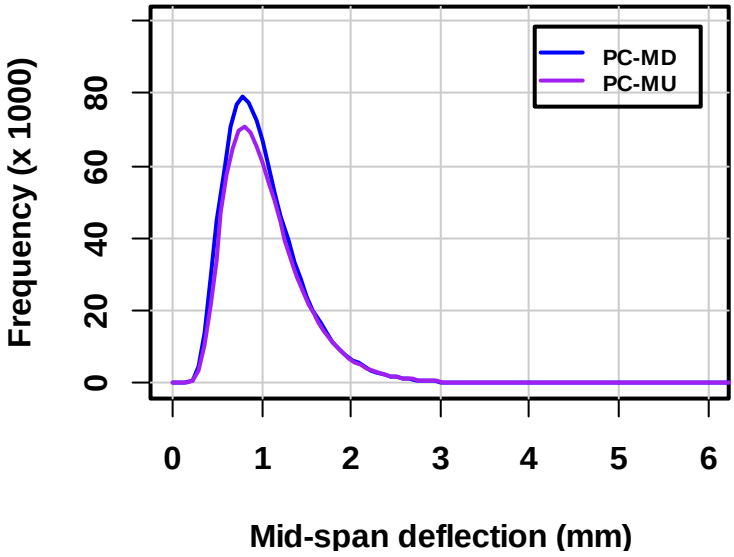

Figure 5-13: Deflection distributions caused by traffic, Powers Creek Bridge

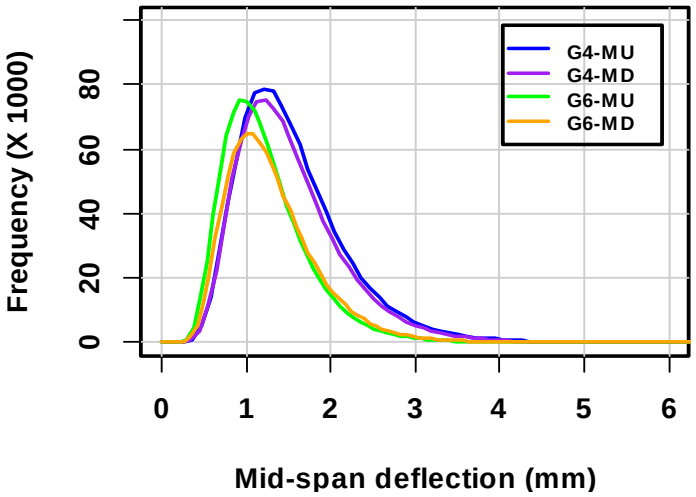

Figure 5-14: Deflection distributions caused by traffic, Munsie Bridge Gostwyck

The reason that the lognormal applied load did not cause deflections above 60% of the limit state was identified in relation to Figure 4-26 (Refer Section 4.3.3). The lognormal load distributions represent the light traffic but do not provide a good representation of the heavy traffic. As one hypothetical example to demonstrate the effect of an alternative load distribution, a distribution was chosen to better represent the heavier vehicles. A lognormal mean was specified as 4.0 with a lognormal standard deviation of 0.6 and applied to the G6-MD span. This modified distribution included about 46 vehicles in the range 100 to 200 kN and about 48 in the range 100 to 500 kN. This is in contrast to the distribution employed to create the data in Figure 5-14 which only included 8.6×10^{-5} of a vehicle in the range 100 kN to 500 kN.

The results utilising this modified distribution are shown in Figure 5-15 and 5-16. The deflection distribution is centred about 2 mm with only the upper tail exceeding the limit state of 17.7 mm. This limit state was exceeded 155 times. The calculated failure rate is, therefore, 0.15 in 10^3 (155 in 10^6) which would be acceptable for a situation not involving loss of life. The maximum deflection calculated was 37.6 mm which was over twice the limit state. This calculation only accounted for variation of load and it is important that a calculation for an in-service girder should also account for the variation in both girder MoE and second moment of area. Inclusion of these extra parameters is, however, not straight forward since a change to the second moment of area causes a change to the MoE which must then be accounted for in SHM Determination 1.

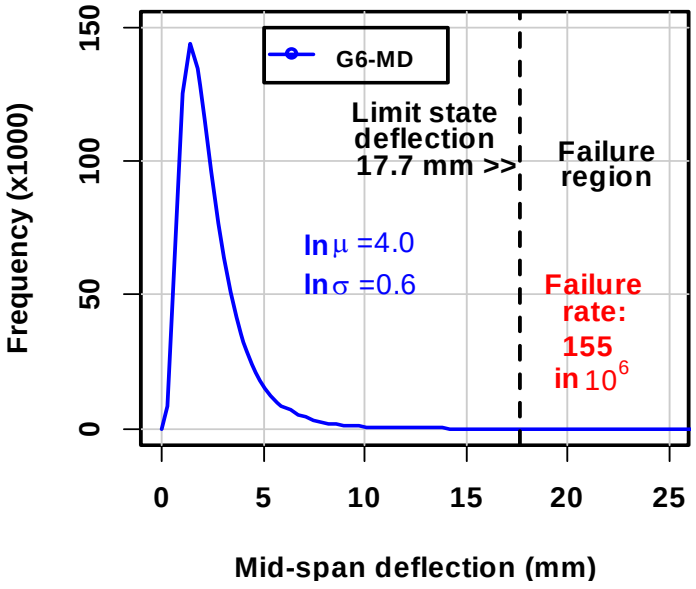

Figure 5-15: Modified traffic deflection distribution, Munsie Bridge G6-MD

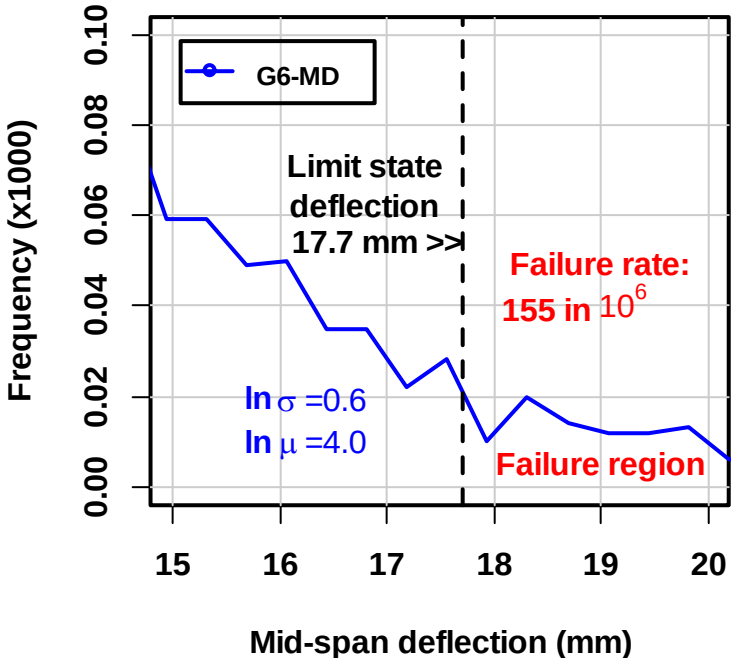

Figure 5-16: Expanded scale, modified traffic deflection distribution, Munsie Bridge G6-MD

5.5 SHM Application 2: Probability of Girder Structural Failure

This section used the results from both SHM Determination 1 and the girder MoR-v-MoE prediction band data inferred in Chapter 3 to determine the probability that the span to deflection limit state would be exceeded. The failure probability were determined for each of the main girders and for each of the three test spans.

5.5.1 Experiment aim

This calculation is set out to determine the probability of structural failure of a girder when the applied load caused the MoR to be exceeded, this probability was then converted to a safety index.

5.5.2 Experiment method

The algorithm employed is shown in Figure 5-17. Again, the first steps in this process were as identified in SHM determination 1, resulting in values of MoE for each girder together with the percentage girder loading (shared loads). The next step used the values of MoE to estimate the mean and the variation of MoR of each girder using Equation 3-10 as shown in Figure 5-18. This step enabled the creation of a MoR distribution. The traffic loading distribution was determined from the data gained in Experiment 2. The traffic load was used to determine the bending stress

and thereby create a bending stress distribution. The MoR distribution and the bending stress distribution were compared, in a Monte Carlo analysis, to determine the probability of structural failure. The outcome of this analysis, the probability of structural failure, was converted to a safety index for each main girder for each of the three spans.

In SHM determination 2 a single value load was determined which required a singled value of MoE that had high level of confidence as shown in Figure 5-8. In this determination the complete distributions are compared and this is achieved by first determining their mean values and the standard deviations. In an extensive analysis the mean MoE is determined complete with its standard deviation. In this analysis the mean MoE was determined from current measurements and treated as a single valued function; it had a standard deviation of zero. The mean MoR was determined and also the standard deviation (refer Figure 5-18). The required standard deviation is equivalent to the standard deviation of the prediction bands which numerically is equivalent to half the distance between the regression line and the out prediction band limit. This is because the outer prediction band limits are two standard deviations from the regression line.

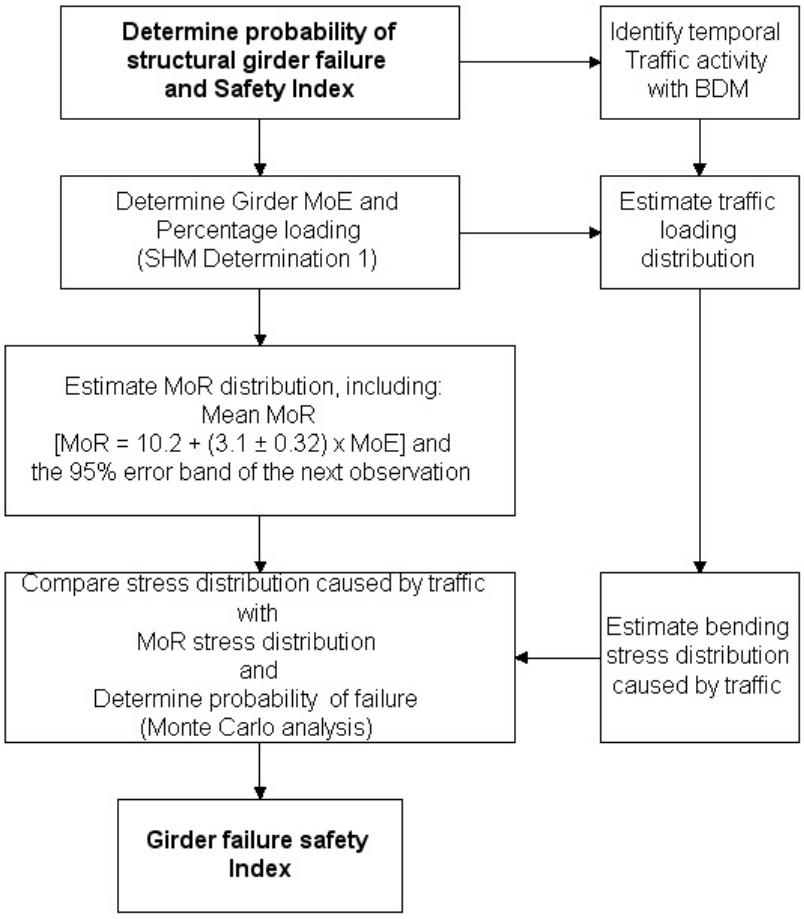

Figure 5-17: Flow chart: Determination of the probability of structural girder failure

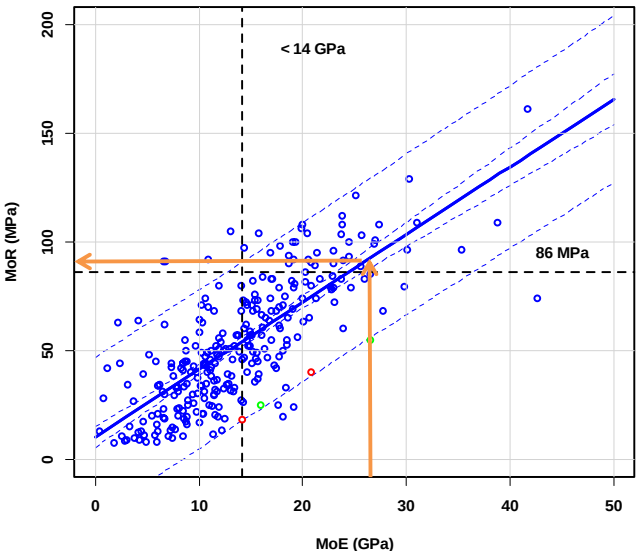

Figure 5-18: Evaluation of mean MoR from MoE via a regression model
MoR-v-MoE relationship

5.5.3 Probability of girder structural failure

The load on the main girders in each span was dependent on traffic loading particular to each case. The loading distribution was identified as a lognormal distribution as shown in Table 4-8. The proportion of this load that was applied to each girder, together with the mean values of MoE, MoR, diameter and span that pertained in each case are shown in Table 5-12. The MoR stress distribution comprised the mean value identified in Table 5-12 and the standard deviation (18.5 MPa) identified from Figure 5-18. The mid-span bending stress produced by the traffic load compared with the MoR stress distribution, were combined in a Monte Carlo calculation to determine the probability of failure. This probability was then converted to a Safety Index, β, which is also shown in Table 5-12. Safety Indices for life threatening situations are expected to be about 4.75 or higher (refer Section 2.6.3 and Glossary). A Safety Index of 4.75 being equivalent to a failure probability of one failure in 10^6 situations. The G6-MU girder would thus be the only girder with a Safety Index above this figure.

Table 5-12: Safety Index for weakest main girder

Bridge Girder evaluated	MoE (GPa)	MoR (MPa)	Diameter (mm)	Span (m)	Safety Index, β	Percentage of applied load (%)
Main upstream, Powers Creek (PC-MU)	20	72.2	463	8.6	3.80	39.4
Main upstream, Powers Creek (PC-MD)	20	72.2	490	8.6	3.78	46.3
Main upstream, Munsies Bridge span 4 (G4-MU)	19	69.1	450	10.6	3.6	34.4
Main upstream, Munsies Bridge span 4 (G4-MD)	22	78.4	430	10.6	4.2	32.0
Main downstream, Munsies Bridge span 6 (G6-MU)	28	97.0	455	10.6	5.1	38.1
Main downstream, Munsies Bridge span 6 (G6-MD)	26	90.8	456	10.6	4.6	38.0

A summary of the failure data for each girder is shown in Table 5-13. The calculated distributions, for each girder are shown in Figure 5-19 through to Figure 5-30. In each case a figure of the full distribution is first shown, followed by an expanded scale figure, to show the detail of the failure region where the applied stress can exceed the girder MoR. In each case the failure rate and the maximum stress, Fmax, are shown together with the ordinate axis adjusted to suit the particular girder failure rate data. Two contrasting cases are girder G6-MU and girder G4-MU. The failure rate of the former is low at 2 in 10^7 and that of the latter high at 1157 in 10^7. In the former it is only the tail of the distributions that are overlapping whereas in the latter there is more significant overlap.

Table 5-13: Summary of Failure data

Girder	Maximum applied stress, Fmax (MPa)	Number of failures in 10^7	Safety index	Stress distribution figure	Expanded stress distribution figure
PC-MU	16.4	742	−3.8	5-19	5-20
PC-MD	16.3	762	−3.8	5-21	5-22
G4-MU	8.6	1157	−3.7	5-23	5-24
G4-MD	10.6	161	−4.2	5-25	5-26
G6-MU	11.6	2	−5.1	5-27	5-28
G6-MD	11.3	8	−4.8	5-29	5-30

In Figure 5-19 two distributions are shown. The first is the narrow applied stress distribution (blue curve) caused by the applied loads crossing the bridge. The second is the broad MoR capability distribution (purple curve) of the PC-MU girder. Most of the stresses caused by the applied loads are well below the material capability distribution and in the figure the level of overlap is not evident. To show the overlap an expanded scale is used as shown in Figure 5-20 with the scale selected according to the failure rate. This overlap is shown in the case of a very low failure rate with a more expanded scale and in the case of a high failure rate a less expanded scale. The failure region shown in Figure 5-20 is the region where it is possible for the applied stress caused by a random load to exceed the random capability. Not all of the applied stresses in

the failure region will exceed the MoR capability, only some of them. Also shown is the probability of failure at 742 in 10^7 which is equivalent to a failure rate of 0.000074 and a safety index of −3.79 (refer glossary for conversion method between failure rate and safety index). The calculated maximum stress F_{max} (16.4 MPa) was recorded and is also shown in Figure 5-20. The probability of failure is not related to maximum stress value but it is related to the number of times that a high stress might occur. The details for the other girders are then shown in the figures as listed in Table 5-13.

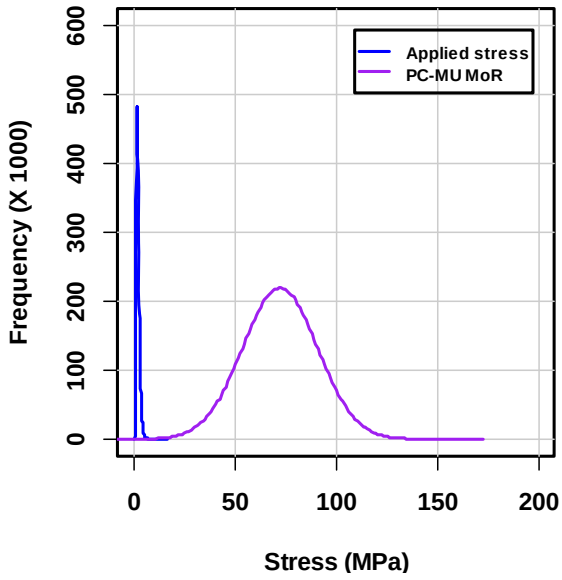

Figure 5-19: Stress distributions for girder PC-MU when under normal traffic loading.

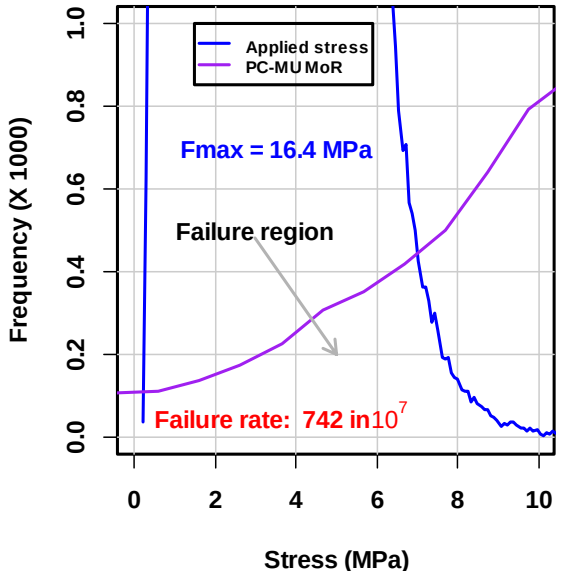

Figure 5-20: Stress distributions for girder PC-MU when under normal traffic loading (amplified ordinate scale)

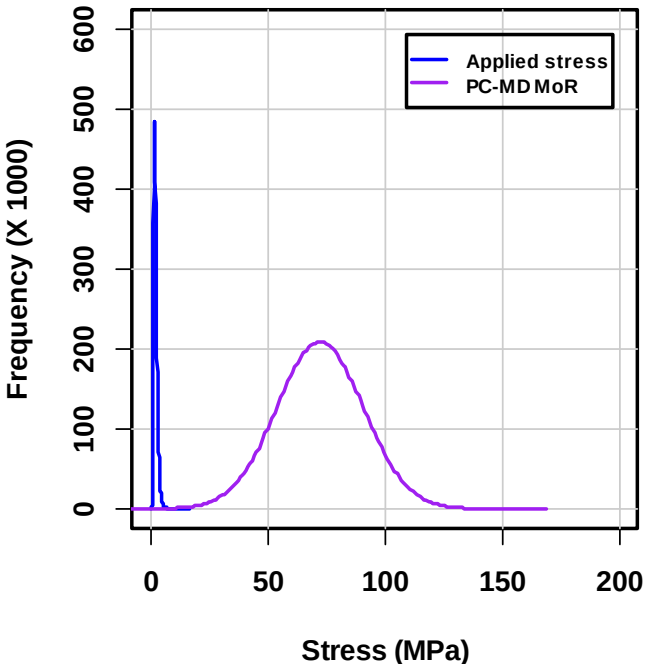

Figure 5-21: Stress distributions for girder PC-MD when under normal traffic loading

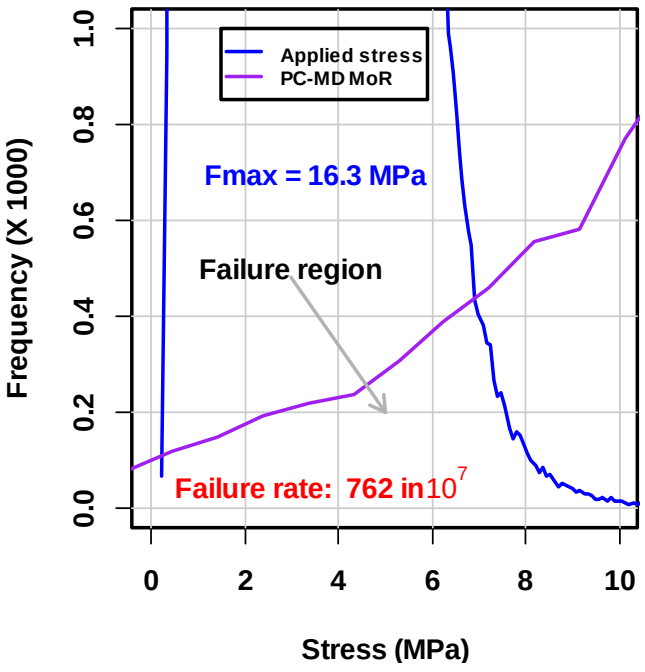

Figure 5-22: Stress distributions for girder PC-MU when under normal traffic loading (amplified ordinate scale)

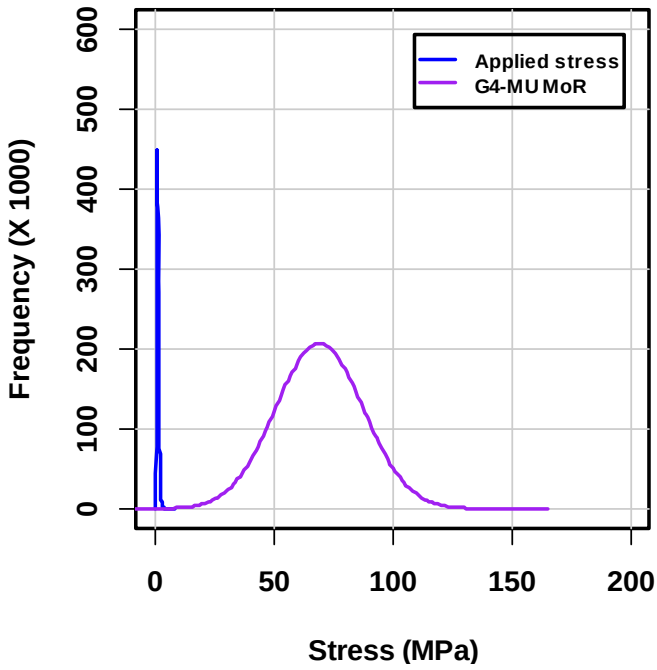

Figure 5-23: Stress distributions for girder G4-MU when under normal traffic loading

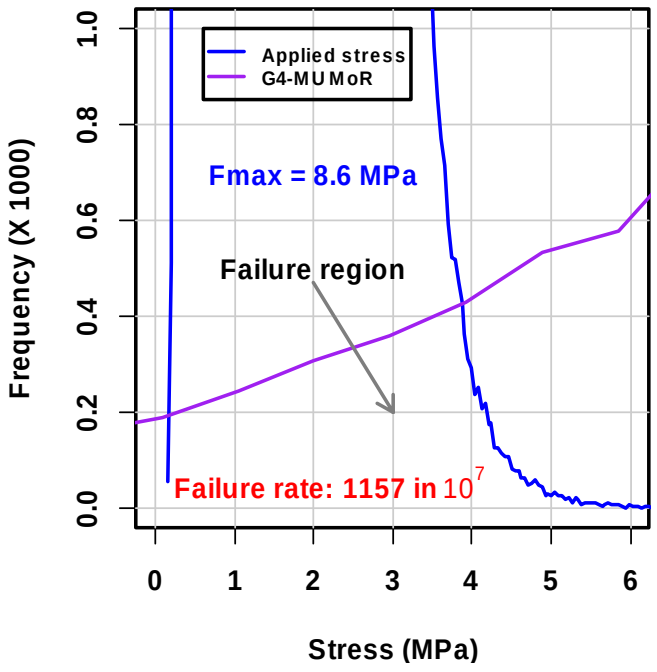

Figure 5-24: Stress distributions for girder PC-MU when under normal traffic loading (amplified ordinate scale)

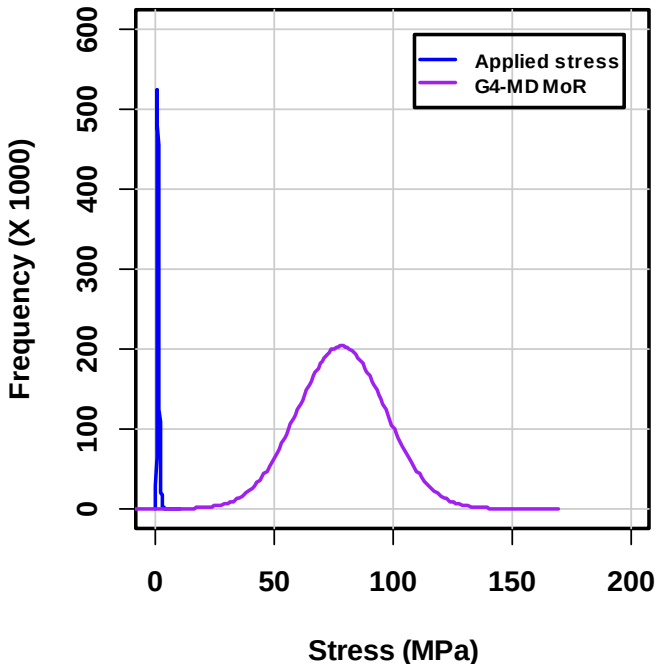

Figure 5-25: Stress distributions for girder G4-MD when under normal traffic loading

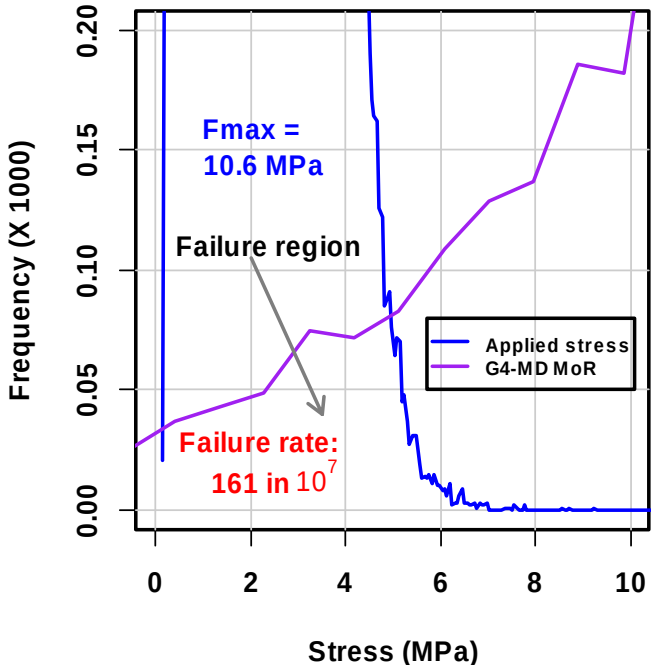

Figure 5-26: Stress distributions for girder PC-MU when under normal traffic loading (amplified ordinate scale)

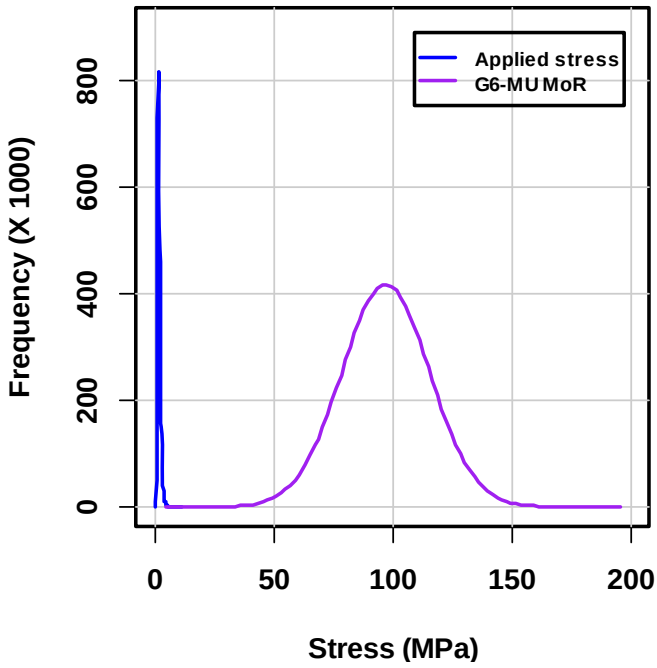

Figure 5-27: Stress distributions for girder G6-MU when under normal traffic loading

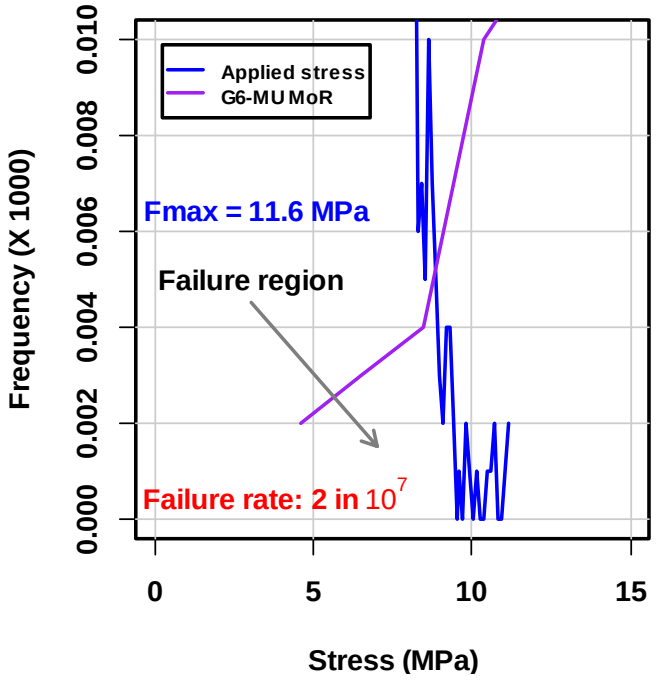

Figure 5-28: Stress distributions for girder PC-MU when under normal traffic loading (amplified ordinate scale)

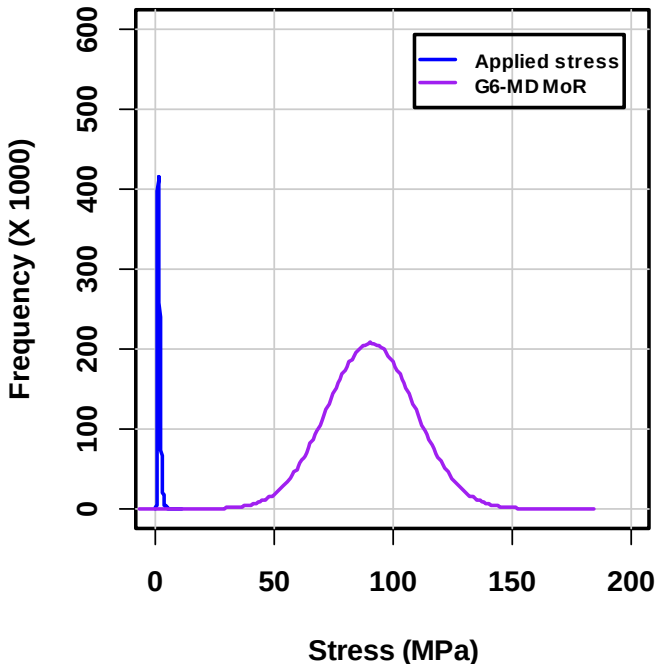

Figure 5-29: Stress distributions for girder G6-MD when under normal traffic loading

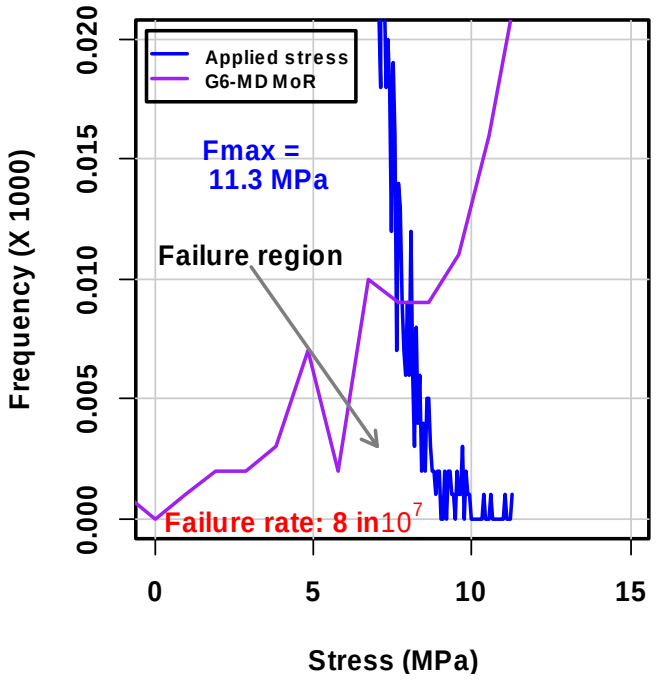

Figure 5-30: Stress distributions for girder PC-MU when under normal traffic loading (amplified ordinate scale)

5.6 SHM Application 3: Calculation of temporal safety index variation caused by surface erosion

The condition state of an in-service bridge girder is assessed visually to determine the moment in time when it has degraded from CS-1 or CS-2 to CS-3 or CS-4. At such time the girder may require strengthening and the bridge could be load limited for a period, thereby reducing its level of service. To determine the load limit a full engineering assessment involving proof loading might be carried out. Such engineering assessments are often in response to an unexpected report indicating structural concern. These assessments are often not planned well in advance. The reason for this is because the degradation rate is not quantified; hence it is not possible to reliably predict future performance. To overcome such unplanned surprises there is a need to provide a remote temporally quantified assessment procedure.

The surface of a girder will start to deteriorate as soon as it is commissioned. Although this rate may be slow, if it is quantified then a maintenance plan can be developed. In SHM Applications 1 and 2, methods were presented that enabled the determination of a safety index. Although these methods can be expanded to determine the temporal changes in safety index it needs to be demonstrated that small changes in deflection can be related to identifiable changes in safety index.

5.6.1 Experiment aim

This section undertook a theoretical examination of the level of change of the span to deflection ratio safety index that occurs as the surface of a girder erodes. The objective of was to determine if the level of change that is caused by a low rate of surface erosion can be used to predict failure.

5.6.2 Experiment method

In this method, equations are developed that related the surface erosion rate to a change in second moment of area. This development involved the use of a temporal equation based upon the temporal loss of surface timber. These equations were used in a Monte Carlo analysis to calculate the temporal mid-span deflection as the girder eroded at 0.2 mm year^{-1} for a specified nominal applied mid-span loading distribution. This model was repeated 10^5 times for each of several elapsed years. The mid-span deflection values were compared with a critical deflection to identify the probability that the calculated mid-span deflection exceeded the critical deflection. Two critical values were specified.

The vehicle load distribution was specified as shown in Figure 5-31 as normal with a mean value of 40 kN and a standard deviation of 10 kN. This distribution was chosen to represent traffic in the range 10kN to 70 kN. It is equivalent to the range of vehicles that exceed Threshold 3 but not Threshold 4 of the BDM utilised in Experiment 2 (Section 4.3). These vehicles comprised over 95% of the test bridge traffic.

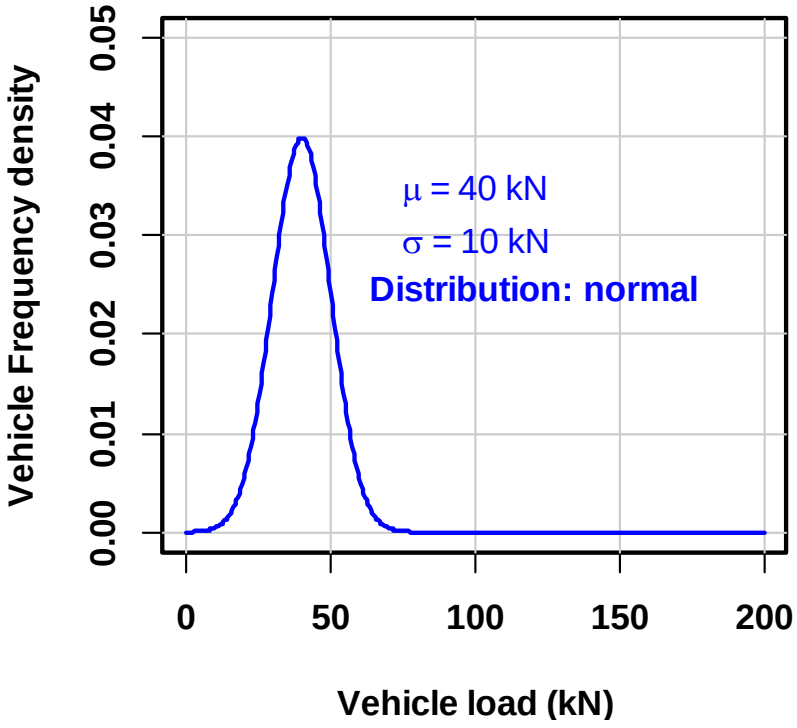

Figure 5-31: Vehicle load distribution applied to hypothetical bridge

5.6.3 Calculation of temporal safety index variation caused by surface erosion

The loss of surface material is a complicated process and only a simple model is examined for the purpose of this experiment. Actual surface material loss will be irregular and occurs in some parts of a girder more than in other parts, as shown in Figures 5-32 and 5-33. The model surface erosion rate, α_d, is specified as 0.2 mm year^{-1} and the number of years calculated for the span to deflection ratio to exceed the span to deflection limit state. Two limit states are considered. The first is 600:1 as required by the current Australian standards (refer Section 2.3) and the second is 380:1, which is indicative of the design standard for many extant timber beam bridges (refer Section 2.3). Since the applied bridge load is vehicular traffic, the load is considered as a distribution and the calculated outcome the safety index, β. The safety index limit state is specified as −3.1 which is representative of a failure rate of 1 in 10^3 (refer Section 2.6.3).

Figure 5-32: Girder checking, low incidence with occasional 3 mm checks

Figure 5-33: Girder checking, high incidence of 10 – 15 mm depth checks

Two new terms are introduced both representing the temporal change of a parameter. The first is the temporal MoE factor, k_E. The second is the temporal SMA factor, k_I. These factors are introduced into the girder deflection equation (refer Equation 2-8) as shown in Equation 5-5:

$$\delta = \frac{P(n)L^3}{48k_E E k_I I}$$

..... Equation 5-5

The value α_d represents the loss of surface material and k_I represents the change in the second moment of area which is given by:

$$k_I = \left(\frac{1}{2} - \frac{\alpha_d n}{D}\right)^4$$

..... Equation 5-6

Where:

δ	is the mid-span deflection (m)
P	is the applied mid-span load (N)
n	Number of elapsed years
L	Span between supports, 8.6 m
k_E	MoE, temporal coefficient = 1
E	MoE, 24 GPa
k_I	Second moment of area temporal coefficient
I	Second moment of area
α_d	Surface material loss rate, 0.2 mm year^{-1}
D	Initial un-eroded girder diameter = 500 mm

and the critical limit state deflections for the specified span to deflection limits are evaluated for a bridge span of 8600 mm as shown in Table 5-14:

Table 5-14: Span to deflection limit state deflections specified for hypothetical bridge

Span to deflection ratio	Limit state deflection, δ_{crit}
600:1	14.3 mm
380:1	22.6 mm

As one example, the mid-span deflection distribution for the un-eroded girder is shown in Figure 5-34. The upper tail of the distribution crosses the 14.3 mm limit state twice and the related safety index, β, is −4.1. These data are tabulated in Table 5-15, with additional calculated data plotted in Figure 5-35. As the girder diameter temporally decreases, the probability that the mid-span deflection will exceed the deflection limit state critical value increases. Data representing several intermediate values are also plotted in Figure 5-35 (blue dots and line). As the girder diameter decreases the safety index also decreases linearly.

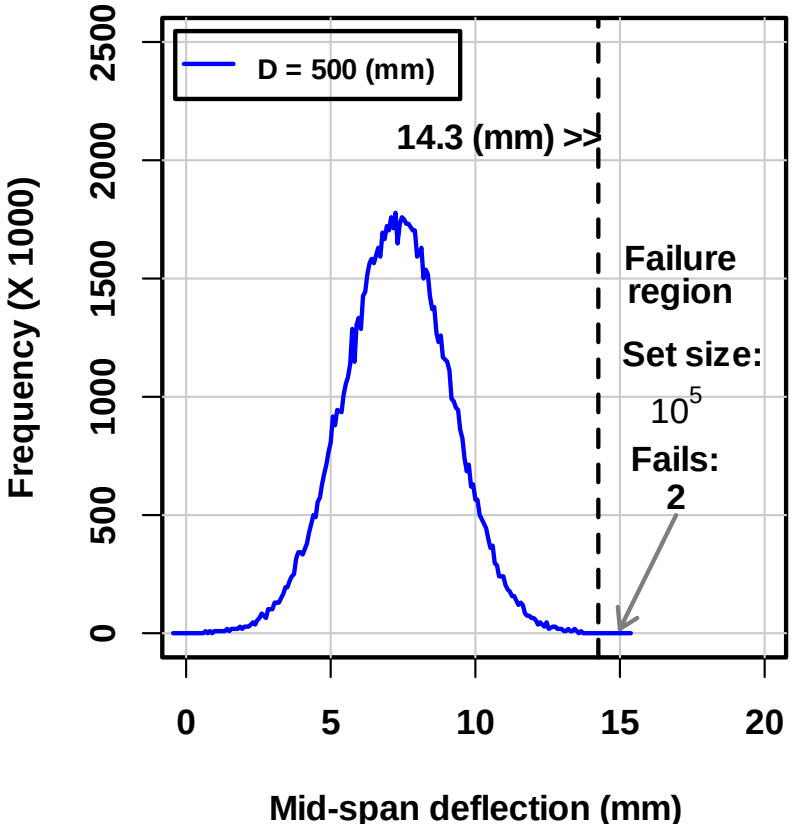

Figure 5-34: Mid-span deflection distribution compared to limit state; girder diameter 500 (mm)

Table 5-15: Deflection limit state failure rates

Limit State	*D* (mm)	Number of Failures	Year	Rate	Safety Index, β
1:600	500	2	0	0.00002	-4.1
1:600	490	61	25	0.00061	-3.23
1:600	488	96	30	0.00096	-3.1
1:600	480	404	50	0.00404	-2.65
1:380	464	1	90	0.00001	-4.27
1:380	440	99	150	0.00099	-3.09
1:380	436	395	160	0.00395	-2.66

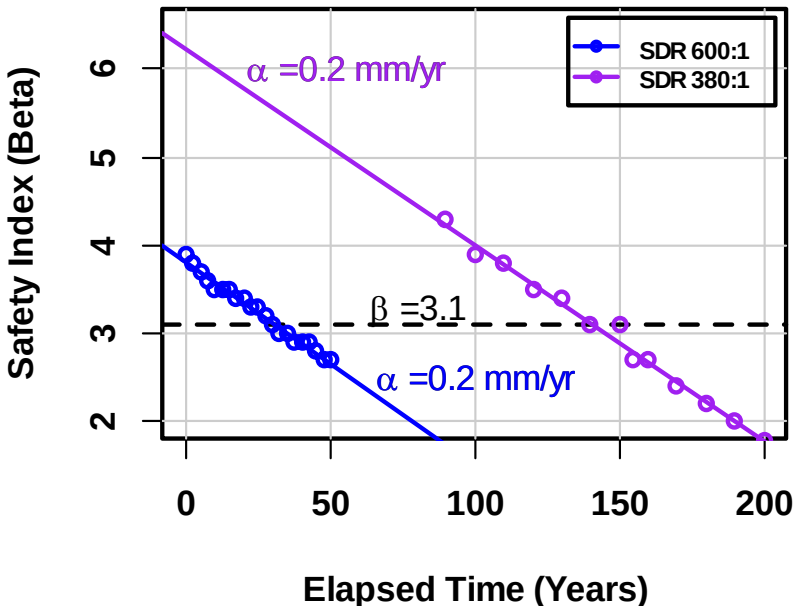

Figure 5-35: Safety Index β-v-elapsed time for a main girder as the girder loses surface material at 0.2 mm year^{-1}

At a girder diameter of 488 mm the safety index, β, reaches the −3.1 limit state. The deflection distribution for this case is shown in Figure 5-36 and its failure rate data tabulated in Table 5-15. The number of failures for this case was 96. At a diameter of 480 mm the number of failures increased to 404 and the distribution for this case is shown in Figure 5-37.

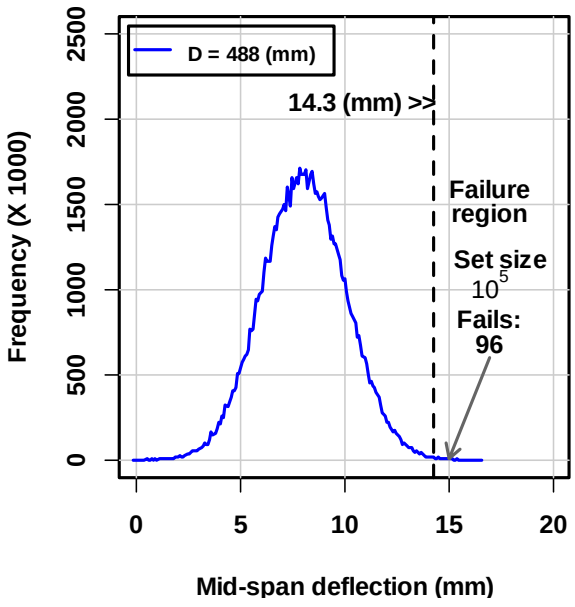

Figure 5-36: Mid-span deflection distribution compared to limit state; girder diameter 488 (mm)

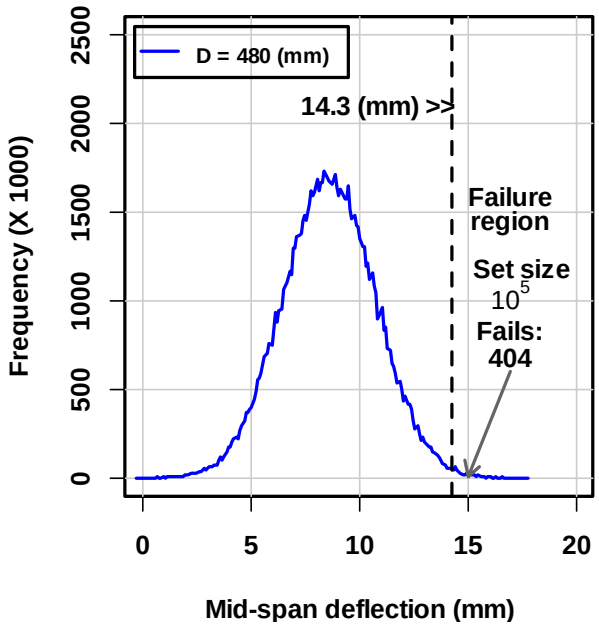

Figure 5-37: Mid-span deflection distribution compared to limit state; girder diameter 480 (mm)

The safety index has now declined to a value of −2.65 and the girder would need to be strengthened or replaced. The part of the distribution in the failure region has increased such that it can be readily observed and is shown, with expanded axes, in Figure 5-38. The time to reach this situation is 50 years.

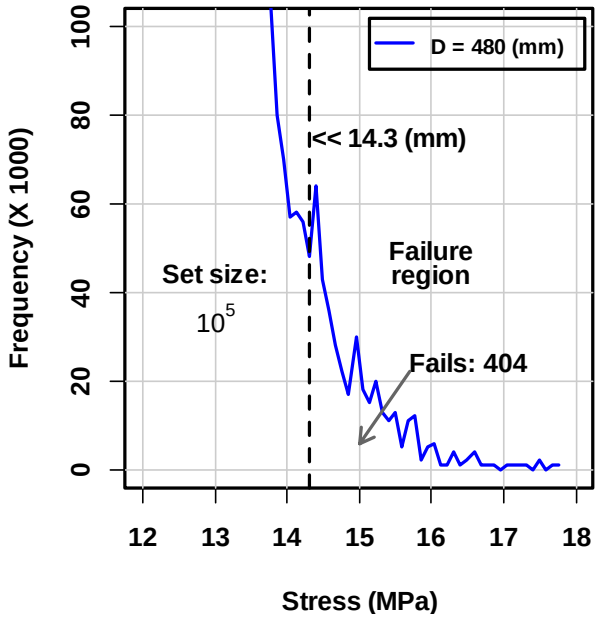

Figure 5-38: Mid-span deflection distribution compared to limit state; girder diameter 480 (mm) – with expanded axes

After 25 years the safety index reached −3.23 from an initial value of −4.1 and by proportion will reach −3.1 after about 29 years. As identified in Table 5-15, the calculated value for the safety index to reach −3.1 is 30 years. This safety index-v-time curve can thus be utilised to predict the limit state failure many years before it occurs. A second set of calculated data are also shown in Table 5-15. This second set is calculated for a span to deflection limit state ratio of 380:1.

5.7 SHM Application 4: Calculation of Condition Alarm from Traffic Flow

The probability of the structural failure of a bridge, identified as where girder MoR is exceeded, is quantified by firstly determining both its material constant distributions and the loading distributions. Then these distributions are numerically compared. As already indicated (Section 5.1) this requires the capabilities of a medium capacity computer and can consume many hours; it can be a power intensive process. However, such extensive numerical comparisons are not required to provide the first indication of structural concern. Such comparisons can be readily carried out on current desktop computers when required and after there is an indication of structural concern. It is not necessary to keep extensively repeating complex calculations for a structure that has not changed. This approach is typified by the current maintenance approach that visually identifies structural concern and follows-up with a more detailed engineering assessment to address that concern. Therefore, there is need for a method to identify specific structural concerns. Such a method must be easily applied to remote timber-bridges. A remote bridge monitoring system will rely on the local generation of power and only low power consumption instrumentation can be installed. It is important, therefore, that any measurement algorithm is also designed to minimise power consumption.

As one example method, demonstrated in this section, the daily running sum of vehicle activity is recorded and the ratio of heavy to light vehicles computed. Trends or significant changes in this computed ratio can be used as a condition alarm to trigger more detailed assessments, such as determining the probability of structural failure. Computing such a ratio is not an intensive procedure and can be readily carried out with remote bridge low power instrumentation. Only the concern that a structural change has occurred needs to be reported immediately to a service centre and the associated detailed data. Again, the signalling of a single alarm requires little power input.

5.7.1 Experiment aim

This section used a theoretical model to examine the hypothesis that the mid-span deflections caused by the number of light vehicles, compared to the deflections caused by the total traffic could be used as an indicator for the stiffness of a timber beam bridge.

5.7.2 Experiment method

A database was created from ABS data (refer Section 2.7.5) of the number of light vehicles, on NSW roads, with a GVM of less than three tonnes. These data were scaled in number to produce a set of 300 randomised vehicle loads to represent the daily bridge traffic data, as obtained in Experiment 3, and applied as loading to a theoretical model bridge. Three levels of stiffness were specified for the bridge and a hypothetical BDM used to measure the resultant deflections. Mid-span measurement thresholds were created at 2, 4 and 8 mm; Threshold 1, 2 and 3 respectively. The deflections caused by the randomised traffic were compared with the deflection thresholds to determine the number of vehicles, each day, exceeding each threshold. The algorithm employed is shown in Figure 5-39.

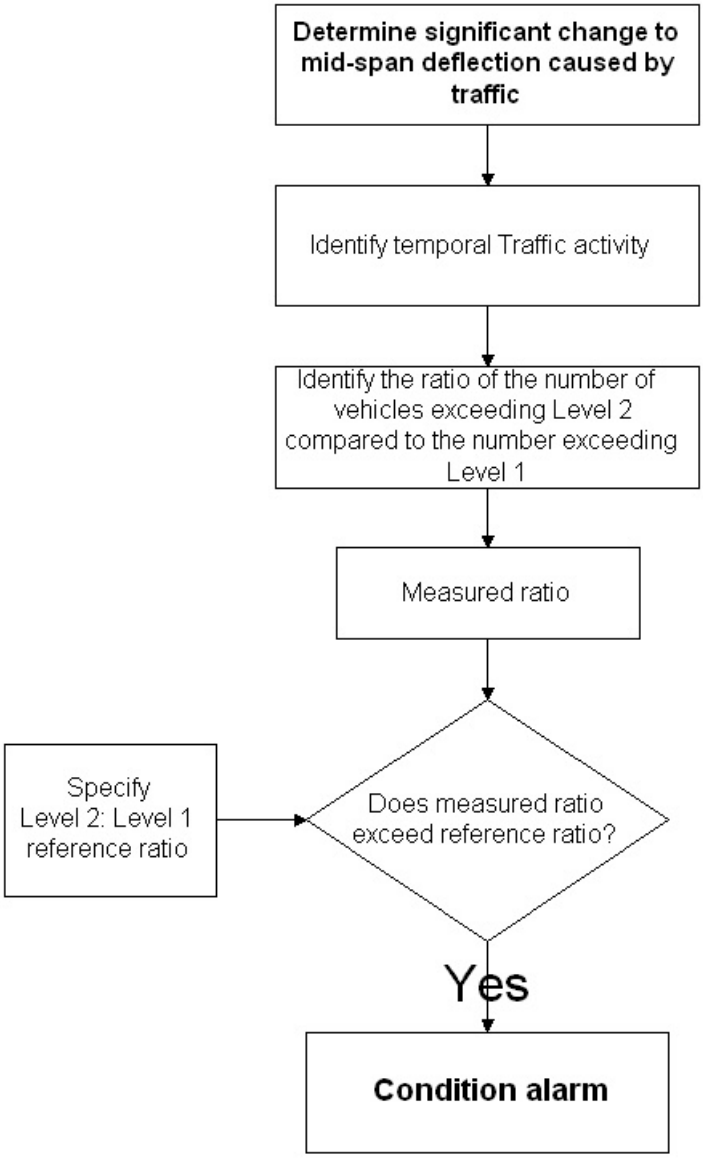

Figure 5-39: Flow chart: Determination of condition alarm from traffic flow

5.7.3 Results: Calculation of simple Condition Alarm

In New South Wales the number of registered vehicles is recorded by the ABS while the number of vehicles and their related kerb weights can be inferred using manufacturers' data, as for the example shown in Section . Refer to the example tabulation shown in Section 2.4.4. By restricting this ABS data set to those manufacturers that have more than 50 000 vehicles registered and models with more than 5000 vehicles registered, a typical model set of light vehicles of known weight is created, as represented by the histogram in Figure 5-40.

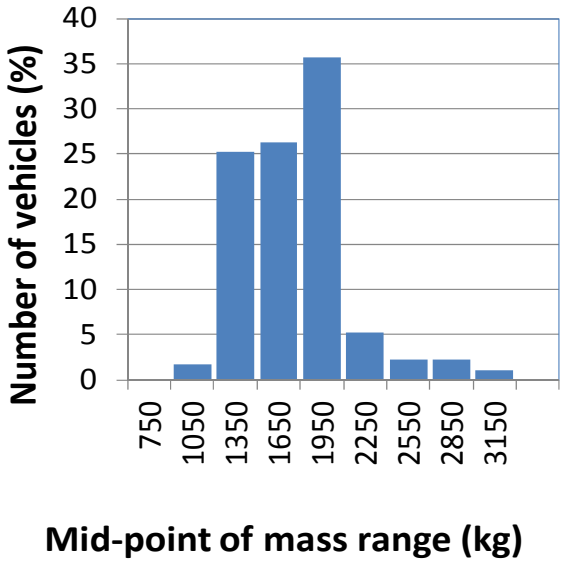

Figure 5-40: Percentage of vehicles registered in NSW in 2008-v-Vehicle weight

By scaling the number of vehicles shown in Figure 5-40 to 300 and assigning a range of loading factors to them, such as number of passengers and freight, a model range of randomised vehicle loads was created as shown in Figure 5-41. This randomised set represents the range of light vehicles that could pass over a test bridge daily. Also shown in Figure 5-41 are the first two threshold detection levels; Threshold 1 (1200 kg) which is exceeded by most vehicles and Threshold 2 (2400 kg) which is only exceeded by heavier vehicles. The loadings required to exceed the three defined thresholds are as shown in Table 5-16.

Table 5-17 shows the number of vehicles that will exceed the model thresholds and the ratio of the number of vehicles that exceeds Threshold 2 to the number that exceeds Threshold 1. The number of vehicles that will exceed Threshold 1 is zero for a bridge with a high stiffness but then rises as the bridge stiffness declines. A typical in-service bridge will thus have a low percentage of traffic exceeding Threshold 2 (4%) but a degraded bridge might have as much as 50% of traffic exceeding Threshold 2.

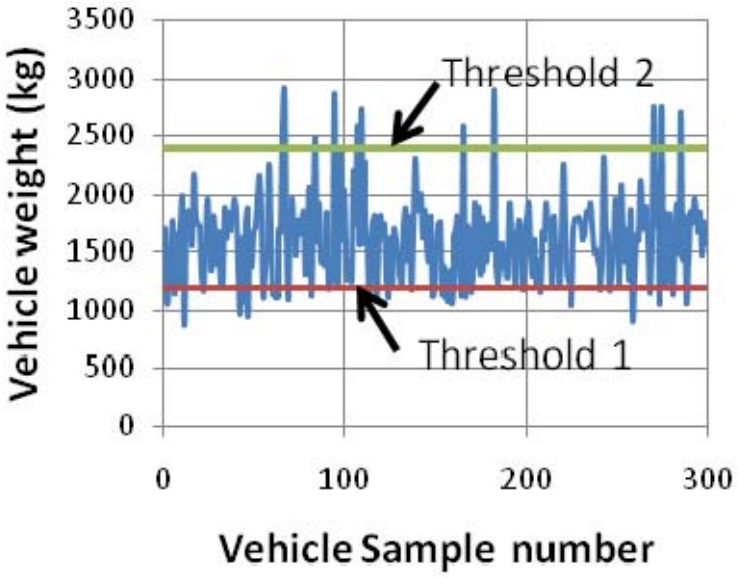

Figure 5-41: Randomised set of Vehicle weights crossing the model bridge per day for a bridge stiffness of 600 kg mm^{-1}

Table 5-16: Effective static loading required to equal pre-defined measurement thresholds for bridge stiffness values of: 750 kg mm^{-1}; 600 kg mm^{-1} and 400 kg mm^{-1}

Threshold	Mid-span deflection (mm)	Effective static loading to equal threshold with a bridge stiffness of:		
		750 kg mm^{-1}	600 kg mm^{-1}	400 kg mm^{-1}
Reference	0	0	0	0
Level 1	2	1500 kg	1200 kg	800 kg
Level 2	4	3000 kg	2400 kg	1600 kg
Level 3	8	6000 kg	4800 kg	3200 kg

Table 5-17: Number of vehicles per day exceeding thresholds 1 and 2 for particular bridge stiffness values in a model system

Threshold	Stiffness		
	750 kg mm^{-1}	600 kg mm^{-1}	400 kg mm^{-1}
	Number of vehicles exceeding threshold		
Level 1	189	261	300
Level 2	0	11	159
Level 3	0	0	0
Level 2: Level 1	0%	4%	53%

5.8 Summary

In Chapter 3, data representing over 300 girders removed from service were analysed. This analysis enabled both MoR-v-MoE vector prediction bands to be determined and MoE to be identified as a parameter to predict girder strength. In Chapter 4, in-service deflection experiments were used to demonstrate firstly, that girder load-v-deflection was linear for loadings below about 35% of the maximum legal axle loading; secondly, that bridge stiffness could be determined with a variation of less than 5%; and thirdly that the bridge traffic loading distribution could be determined.

In this chapter numerical bridge models are created and used in combination with measured deflection data to determine both girder MoE and the percentage of the total loading applied to each girder. Then girder MoE data were used in conjunction with the MoR-v-MoE prediction band data to demonstrate how to determine single valued load limits. Next these data were used in two SHM applications. The first was the determination of probability of span to deflection limit state failure. The second was the determination of the probability of ultimate girder stress limit state failure. Safety indices were determined, in these applications, for each of the two main girders for each of the three test spans.

Two additional methods were developed. The first was a condition alarm to enable early warning of significant structural change. The second was the use of a temporal safety index to demonstrate how limit state failure can be predicted. The particular case examined was that of girder surface erosion causing increased deflection and an increased probability of failure of the span to deflection limit state.

SHM applications 1 and 2, as developed, represented bridge structural health at one moment in time. These applications could be expanded to provide temporal safety indices as was demonstrated in Application 3. The algorithms used in these applications rely on the use of continuous deflection monitoring and can be used to determine the probability of timber-bridge girder failure

6 DISCUSSION

6.1 Introduction

Of the thousands of timber-bridges on NSW regional roads, most were built in an era when structural components were expected to survive without failure for many decades. Because many of these bridges are now degraded many require maintenance, in some cases urgently. The current maintenance approach is to assess structural integrity at somewhat regular intervals or if accidental damage is reported. Visual inspections, for instance, might be scheduled to occur every two years, but more detailed engineering inspections may be as infrequent as every 10 years. Whilst this is appropriate for a structure that is expected to survive for its lifetime, it is not for a structure that is known to be liable to fail at any time because of a random degradation process or fault. In the case of degraded timber-bridges such a process could take the form of a heavy vehicle overload (refer Chapter 1). To make a structure that is resistant to random faults, it is necessary to introduce monitoring systems to continuously decide when operation is no longer satisfactory or only satisfactory at a given level. The structure then has a known structural integrity.

To determine whether a timber-bridge is structurally sound requires an SHM methodological approach. Parameters indicative of satisfactory operation must be identified together with a set of conditions that indicate when the structure has stopped performing correctly. To identify whether a timber-bridge is structurally sound is a straightforward but complex process. As an example, a possible SHM methodology that can be used to determine that a bridge is operating in a satisfactory manner is shown in Figure 6-1. This process involves ten steps, each step is a straightforward measurement or calculation and the complexity only occurs because of the number of steps that are involved.

It is important to follow that what is being calculated is a safety index and not a FoS. A safety index is calculated from experimental data whereas FoS is an arbitrarily chosen factor. If the safety index is greater than the minimum required limit state then the bridge is operating correctly. If the safety index is less than the limit state then maintenance is required. In this process, bridge integrity is ensured by temporally monitoring the safety index. The definition of a failure is a safety index less than the limit state. An example safety index limit state is – 4.75. This value represents a failure rate of 1 in 10^6 and is the limit state used when human life is threatened by structural failure (Section 2.5). If the safety index magnitude is greater than the limit state magnitude then the structure is considered sound.

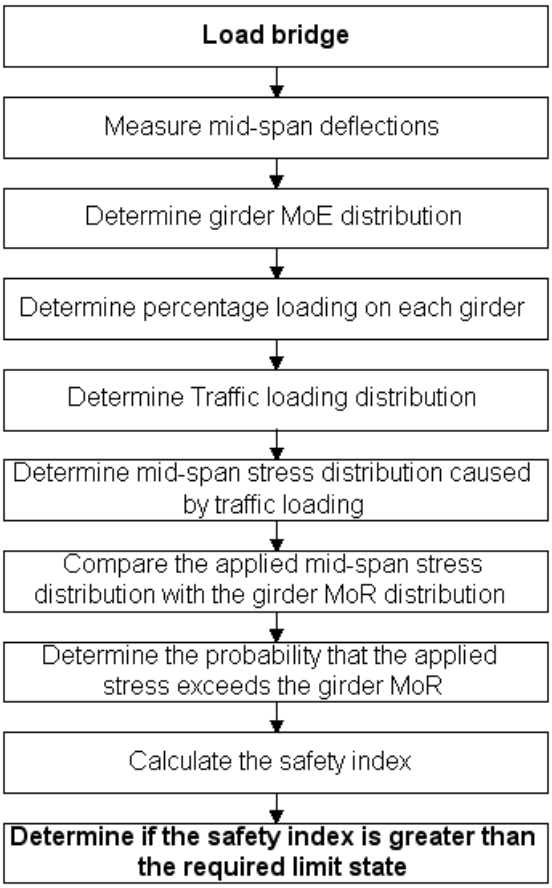

Figure 6-1: SHM flow chart, example determination of a safety index

The aim of this research was to test the hypothesis that continuous deflection monitoring can be used to assess the probability of timber-bridge girder failure. Specific SHM methodologies were developed to show how this aim could be validated. This validation was achieved by demonstrating that continuous deflection data can be transformed into a timber-bridge safety index and that this index can be used to identify when a bridge is no longer operating in a satisfactory manner. New measuring equipment was required to record deflection data that could be used to create a baseline of bridge performance and also be used to identify temporal change. This equipment, involving new laser based deflection measuring devices together with high speed camera techniques, was created such that data could be recorded without interrupting traffic flow.

In this chapter the research data are discussed, starting with the results of Chapter 3, where the analysis of data of previous researchers, representing over 300 timber girders removed from bridges, was reported. These girder data were combined from several independent sources and more rigorously statistically analysed than has previously been attempted. An introductory

section reviewing the individual datasets is provided in Appendix B. The pooled data are discussed. Following this analysis both MoE and condition state were identified as suitable parameters to predict girder MoR. Then, the experimental deflection data measured on in-service structures are described (Chapter 4). These deflection data were used to determine both girder stiffness and traffic loading for test case bridges. The numerical models of the test structures that were used to determine girder MoE, percentage loading and MoR as reported in Chapter 5, are described next. This is followed by details of the SHM methodologies that were developed to transform the deflection data into failure probabilities and safety indices. Finally a summary is provided in which the achievement of the set objectives and the aim are discussed.

6.2 Theoretical Analysis: Prediction of Girder Strength from Historical Datasets; Pooled datasets

Each dataset examined thus far, DS-1 to DS-6, is examined independently. A discussion of each dataset is provided in Appendix B. As introduced in Section 3.8, the next step is to determine what can be inferred by pooling the data. However, before this can be accomplished the effects produced by a confounding variable need to be examined, that of confounding variable of girder moisture content (MC). It is common industry knowledge that moisture content affects both the MoE and MoR of commercial timber, as identified in Equations 2-18 and 2-19. If a girder is unseasoned (green) when installed, then its MoR and MoE will vary during service as its MC adjusts to ambient conditions. However, as already indicated by data in Figure 2-37, once it has stabilised it does not vary significantly thereafter. DS-3 and DS-5 are examined to determine if it can be inferred whether MC is significant in affecting the change in bending performance between excised samples and girders.

The determinations presented in Chapter 3 are discussed in the order as identified in Section 3.8. These determinations were used to identify both girder MoE and girder MoR behaviour. In particular, they were set out to examine:

1. the effect of MC on in-service girder MoR-v-MoE vector
2. the range of in-service girder MoR prediction bands
3. prediction of in-service girder MoR from standardised data
4. the range of in-service girder MoE
5. the MoR-v-MoE vector path of in-service Ironbark girder.

6.2.1 Determination 1: The effect of MC on girder MoR-v-MoE vector

To what degree large round timber girders are affected by moisture content is not well documented. Examination of the ambient humidity records for a large section of NSW (Figures 2-38 to 2-40) provides an indication that the long term mean variability is very low. The running mean, as shown in Figure 2-40, is effectively a constant. It can be inferred from one example of measured data, Figure 2-37, that the MC of a large in-service girder is constant to within a tolerance of about $\pm$3% RH. Thus, as humidity varies throughout the day, moisture does not have time to significantly penetrate into a girder from the atmosphere. Providing a girder is kept clear of pooled moisture, it should remain at a relatively constant MC. One important outcome of this determination is that because girder MC does not vary significantly, it does not significantly affect temporal mid-span deflection measurements.

Determination 1 was designed to examine the likelihood that the girder MC could be influencing the girder material constants in a manner sufficient to cause the measured difference in MoR-v-MoE vectors between girder and excised clears (refer Figure 3-35). The moisture content of these girders is not clearly reported. For example, if the girders had a moisture content of 25% and they were dried to 12%, girder MoR and MoE would vary according to Table 2-17. The results of such a transformation are shown in Figure 3-36. It is quite clear from this calculation that merely a change in MC is not the reason that the excised clear MoR-v-MoE vectors are different from the girder MoR-v-MoE vectors. The level of change that would be required to transform the girder MoR-v-MoE vectors to be similar to the excised clear MoR-v-MoE vectors is shown in Figure 3-37. This change is a simple doubling of MoR with no change to MoE.

The reason for the difference between the two clusters, clears and girders (refer Figure 3-35, brown and green dots), is not explained by this simplistic calculation. The transformed data (Figure 3-37) is still not realistic since some of the values are greater than the characteristic mean values for Ironbark. The relationship between the two clusters must involve additional parameters, which have not yet been defined. As a further example, data for girder #14 were also examined (Figure 3-38). In this case a transformation of the girder MoR-v-MoE vector according to a change of MC of 13% produces an MoR-v-MoE vector that is clearly not the correct transformation (blue dot). To produce a transformed MoR-v-MoE vector near the mean of the excised sample MoR-v-MoE vector for girder #14, the transformation is MoR x 1.3 and MoE x 0.7 (orange dot). The determination and explanation of the correct transformation will require further research beyond the scope of this thesis.

6.2.2 Determination 2: Range of in-service girder MoR prediction bands

The total data examined, DS-1 to DS-6, are pooled (Figure 3-39) and then clustered into sub-sets that are indicative of individual girder performance. The significant outcomes of this process are:

1. The cluster of clear samples excised from DS-3 girders, identified as DS-5, were very similar to the cluster of clears excised from a wide range of species, identified as DS-6. Since the 95% confidence bounds of these two clusters are similar, these two clusters can be nominally considered to be from the same population of clear samples (Figure 3-40 and Figure 3-41).
2. The 95% confidence bounds of the four girder datasets, DS-1 to DS-4, appeared to be similar. It is inferred, therefore, that the four sets are from the same population of girders (Figure 3-42 to Figure 3-45).
3. The first pooled dataset of girders, identified as DS-1 to DS-4, was significantly different to the second pooled dataset of clear excised samples, identified as DS-5 and DS-6. The slopes and 95% confidence bounds of these two pooled datasets were not the same. DS-5 and DS-6 have a regression slope of about 7 MPa GPa^{-1} and DS-1 to DS4 have a regression slope of about 3 MPa GPa^{-1}. The 95% confidence bounds only overlap below the S2 limit states. It is inferred, therefore, that they can be considered to be from different populations.

There is, therefore, an apparent anomaly in these data since:

1. The clears were similar and could be treated as one set;
2. The girder sets were similar and could be treated as one set;
3. The clears and girders were different sets; but
4. The clears should represent young girders, they should be the same.

But items 3 and 4 are mutually exclusive, they are anomolous. Two possible hypotheses for this apparent anomaly are proposed. The first hypothesis is that large section timber behaves differently to small section timber. The second hypothesis is that a significant change occurs early in the life of a girder to change its MoR-v-MoE vector from the characterised clear value to the in-service girder value. Both hypotheses appear to contain inconsistencies and will be discussed further following this summary.

The major outcomes from pooling DS-1 to DS-6 are (refer Figure 3-46):

1. Any excised clear from any species will have an MoR-v-MoE vector contained within the green zone.
2. Any bridge girder of any species will have an MoR-v-MoE vector contained within the brown zone.
3. These outcomes are to a confidence level of 95% ($p < 0.001$).

These outcomes affect how data for an individual girder are interpreted. For example, data for girder #14 are plotted overlaid on the in-service prediction band background data (refer Figure 3-47). The girder MoR-v-MoE vector is at the centre of the girder prediction band. The excised clears MoR-v-MoE vectors are within the excised clears prediction band. Although the MoR-v-MoE vector for the excised clears varies significantly, it does so within the excised clears prediction band.

Whatever the mechanism is behind the first hypothesis, it must also explain why MoR-v-MoE vectors of small sections remain within the excised clear prediction band. Further research is required to identify such a mechanism. There were no data available to test the second hypothesis because DS-1 to DS-4 does not contain any values for the MoR of girders less than two years old. Girders less than two years old were used in new work and were not available to be stressed to bending failure. Also, any results from proof-testing have seemingly not survived. However, using the girder prediction band (Figure 3-46) regression model, girder MoR can be predicted from measured girder MoE. An indication of the capacity of a girder less than two years old can, therefore, be inferred by examining the value of MoE of those girders and an interesting pattern is obtained, thus:

1. The mean MoE of all girders of age less than two years is within 1% of the characterised mean value for Ironbark.
2. The mean MoE has fallen about 38% after 15 years.
3. The MoE variation of girders less than two years of age is about 27% CV.
4. The MoE variation has almost doubled to about 53% CV after 15 years.
5. The maximum value of MoE was about 40 GPa for both girders less than two years old and for girders over 15 years old.

The inference is that girders less than two years old had values of MoE that were similar to Ironbark clears and were effectively un-degraded. However, after 15 years there was a significant number of girders that had degraded such that the mean value of MoE had fallen by

about 38% and the variation in the set had almost doubled. Since the maximum values had not significantly changed, the increase in CV had occurred by degradation, thereby reducing the minimum values. An individual girder could, therefore, follow two different paths. It could be within an MoE range of about 5% CV or less when first installed and then degrade to a be within a range of about 50% CV within 15 years. Alternatively it could stay un-degraded and within the original 5% CV range throughout its service life. The girders with un-degraded MoE that were tested to destruction still had MoR-v-MoE vectors within the girder prediction band and not within the excised clear prediction band. Further research, beyond this thesis, is required to explain this anomaly.

The outcomes from the theoretical analysis are that:

1. A girder with a MoE below 14 GPa will have an MoR less than 86 MPa, to a 95% confidence level.
2. A girder with a MoE above 36 GPa will have an MoR above 86 MPa to a 95% confidence level.
3. MoR can be predicted using MoE, condition status and age in the region between 14 GPa and 36 GPa MoE;
4. The ‘as new’ excised clear sample MoR-v-MoE value for a girder can be obtained by excising a clear sample in a region of low stress. This process can determine the initial MoE for a girder with an unknown history, which can then be compared with the current girder MoE.
5. Girder moisture content is not a prime influence of MoR-v-MoE variation.

The MoR of an in-service girder can, therefore, be assessed by measuring the girder MoE and determining MoR using a statistical model equation relating MoR to MoE. It is this approach that is employed as an SHM procedure guiding the remainder of this thesis. DS-1 to DS-4 contained significant variations and represented girders removed from service. Only about 15% of these girders had an MoR above the S2 limit state of 86 MPa. A CS-1 girder that was well within its operating lifetime is, therefore, not well represented in these data. After further research, it is anticipated that the variation of the MoR prediction band for an individual girder can be significantly reduced from that obtained with the current data.

6.2.3 Determination 3: Using standard MoE data to predict in-service girder MoR

This determination examined firstly the possibility that existing data could be found that provides a better prediction of MoR from known MoE than data examined in Determination 2. Three sources were considered:

Case 3-A. species data compared to prediction bands

Case 3-B. AS/NZS 2878 characterised data compared to prediction bands

Case 3-C. AS 1720.1:2000 strength group data compared to prediction bands.

Then the measured range of MoE was examined:

Case 3-D. measured MoE compared to prediction bands.

Case 3-A: As a baseline, the CSIRO data from Tables 2-2 and 2-3 are overlaid on the background in-service prediction band data (refer Figure 3-46) as shown in Figure 3-48. These data are the characterised MoR-v-MoE for Australian hardwoods and are located within the excised clear prediction bands. The location of the MoR-v-MoE vectors are situated where they are expected to be found since they are part of the data that were used to create the prediction bands for the excised clears. What is of interest is the range of these hardwood species. As expected, they are all above the S2 limit state (refer Figure 3-48).

Case 3-B: Next, AS/NZS 2878 species mean data (refer Table 2-6) are overlaid on the background data as shown in Figure 3-49. These data are also located within the excised clear prediction bands (green dotted lines). They do not, therefore, represent the MoR-v-MoE vectors of in-service girders. These data are specified to be mean values but they are not appropriate for predicting MoR of in-service girders, they can only be used to predict the MoR of excised clears.

Case 3-C: In this case AS 1720.1:2000 data are overlaid on the background data as shown in Figure 3-50. While these data (blue circles) are within the girder prediction bands (dotted brown lines), there are no prediction bands provided in the Standard. There is a related statement that the 5th percentile can be computed by calculating half the quoted value. The 5th percentile data (blue crosses), calculated by this method, are also shown in Figure 3-50. These two sets of standard data are similar to the DS-1 to DS-4 calculated regression line and lower prediction bands respectively. However, the standard data only covers strengths below the S2 limit state and cannot be used reliably above this value because the slopes are different.

Case 3-D: DS-2-2 represents girders very early in their service life. They cover a surprisingly wide range of MoE from 13 GPa to 38 GPa. Although the species of these girders was not

reported, there is no reason to believe that they were not all suitable species for their role. DS-3 was gathered as part of the same research project as DS-2 and represented girders that were all of hardwood species as shown in Figure 3-48. Girder #30, with a MoE of 13 GPa is, therefore, anomalous with a surprisingly low value. Girder #119 is also anomalous with a very high MoE of 38 GPa. This range is shown in Figure 3-51 where it is compared with the mean value of Ironbark, which is also about the mean of the girder #30 and girder #119 MoE. Note that the shaded orange area in Figure 3-51 only represents the MoE range and not MoR.

Case 3-E: In Figure 3-52 the full expected range of Ironbark is shown. Three limits are outlined with the outer dashed line representing the six sigma range of individual samples. There are two unexpected features of this data. The first, as already identified in Case 3-D, girders #30 and #119 are anomalous since they are respectively both below and above the six sigma range limits. The second is that there are MoR-v-MoE vectors representing Ironbark that appear to be outside the 95% confidence band for clears. The reason for this is that there is no identified available data to verify this scenario. To determine the true limits requires the measurement of a large number of samples. For example, is there evidence of any Ironbark sample that has an MoE of about 30 GPa and an MoR of about 130 MPa? Which the true limits are, the confidence bands or the six sigma limit rectangle as shown in Figure 3-52 will require further targeted research which was beyond the scope of this thesis.

6.2.4 Determination 4: The range of in-service girder MoE

DS-3 and DS-5 were examined theoretically in Section 3.4 and detailed in Appendix B. One outcome was that girder MoE could be both higher than the characterised mean values for Ironbark and higher than the excised samples from the same girder (refer Figure 3-22). This anomaly is now examined in relation to the DS-1 to DS-6 background.

The range of DS-3 MoE is about 2.4 times the range of the DS-5 MoE while the average of both clusters is about 18 GPa. While it is to be expected that DS-3 girder MoE might be lower than their equivalent DS-5 MoE it is not expected that DS-3 girder MoE are higher than DS-5 MoE. This change in MoE is examined in more detail in Figures 3-53 and 3-54. DS-3 and DS-5 represent data obtained from the same girders. DS-3 was obtained from mid-span girder bending failure (Figure 3-53, brown dots). DS-5 was obtained from the bending failure of excised samples from those same girders. Up to eight samples were obtained from each girder. The mean MoR-v-MoE vectors, representing the eight samples from each girder, are as shown in Figure 3-53 (green dots). These data are overlaid onto the DS-1 to DS-6 background. For each

girder the MoR-v-MoE trajectories from DS-3 to DS-5 are plotted. The outcomes to be observed are:

1. In-service girder MoR always declines. This is inferred because all of the arrows in Figure 3-53 are pointing downwards.
2. In service MoE sometimes decreases and sometimes increases. This is inferred because some arrows point to the left and some to the right.

Both decreasing MoR and MoE are not a surprise, increasing MoE is a surprise. To emphasise that this effect is not because of an odd erroneous data point, the complete cluster with increasing MoE is plotted in Figure 3-54. This cluster is otherwise correctly located within the background prediction bands.

To explain this anomaly, two processes appear to be occurring. The first process causes a girder to have a value in the MoR-v-MoE vector space within the girder prediction band (Figure 3-53, brown dotted lines). The value adopted may be above or below the excised value for the species of timber of the girder. The second process causes an in-service girder MoR-v-MoE vector to move from a value with higher MoR and higher MoE to a value with lower MoR and lower MoE while remaining within the girder prediction band. These two processes are only inferred as an explanation of the available data, they have not been observed.

Within the available data there are examples of girders that have been removed from service with values of MoE as low as 12 GPa and others with MoE as high as 40 GPa. These girders generally begin their structural life with a characterised value of 24 GPa (Ironbark). Whilst in-service the surface of the girder deteriorates and splits occur. The girder SMA, and the effective diameter are expected to decrease. If the decreased diameter is computed for a girder MoE moving from 20 GPa to 15 GPa, then the effective radial loss is −17 mm (Table 3-21), that is, 17 mm has been lost from the surface all around the girder. Although a significant loss, this is not at all surprising. If the effective diameter is computed for girder MoE moving from 20 GPa to 25 GPa then the effective surface loss is +12 mm. Such a change is currently inexplicable. It is not a simple change to the MoE, since an MoR change also occurs synchronously.

While this apparent increase in MoE is an anomaly, which can only be explained by further research, it does not affect the aim of this particular research. The fact that these processes appear to occur synchronously is an advantage. The in-service girder MoR-v-MoE vector is only found in the girder prediction band. Therefore, MoR can, within the statistical limits of the prediction band, be predicted by appropriate and significant prediction parameters.

Quantification of these parameters allows MoR to be predicted to a known confidence level. This process of MoR quantification was considered further in the following SHM Applications.

To understand why an increase of MoE appears to be an anomaly requires some explanation. When a steel structure is first fabricated the detailed material characteristics are accurately known. Any variation in the measured value of its MoE will be less than 0.5% and much of this variation is due to measurement error (refer Experiment 4). Any change in MoE by more than a few per cent is likely to be indicative of a change in a material or environmental constant. As an example, the temperature of the steel might substantially change and it softens or hardens accordingly. As another example, the crystallographic structure may alter over time. In the literature referred to in Section 2.2.12 (Gordon, 1991) the possibility is discussed of increasing the MoR of glass by reducing the level of surface imperfections. In this literature cited in this thesis, there is no discussion of a related change in MoE. A material is characterised by its MoE. Ironbark has a six sigma range of values that are different from that of other hardwoods, such as Tallowwood (*E. microcorys*). While the variation in timber MoE might be substantially affected by defects, there are limitations on how much it is affected.

Excised clear samples have been traditionally used to characterise timber. They are used to provide an indication of the upper boundary of timber properties for the species from which they are cut (refer Section 2.2.2); an upper boundary of both MoR and MoE. A carpenter will select timber with a minimum of visual defects and known MoE when selecting timber for load bearing use. Similarly bridge girders are normally selected from premium stock of specific species; they are expected to be of Condition State 1. When new, the variation in strength of large timber components is about 10% – 15% (refer Section 2.4.6). After extensive structural use, this variation can increase to cover a range of 10% – 33%: a doubling in variation.

As already discussed there are two common reasons for such a variation. The first is degradation caused by mechanical defects, the second by biological attack. Degradation by mechanical defects, such as surface erosion, splits and piping will change the effective SMA, which if not measured accurately will be attributed to a change in MoE. Biological attack, such as fungal rot, will change the chemical and mechanical makeup of the timber and will lead to a change in the effective MoE. Both reasons are commonly accepted to cause a decrease in MoE. No evidence was found, in the literature reviewed for this thesis, of mechanical or biological degradation causing an increase in bridge timber MoE. Why the girder data presented in Figure 3-22 has higher MoE than its excised clears has not been explained and will require further research.

6.2.5 Determination 5: The MoR-v-MoE vector path of an in-service Ironbark girder

In this Determination the variation of MoE is examined in more detail. In Determination 4 it was identified that some values of effective girder MoE can be found that are above their related clear MoE and some below their related clear MoE. How the in-service path of a girder MoR-v-MoE vector varies can be inferred by examination of girders in increasing states of degradation. In Figure 3-29 DS-4 Ironbark girders were presented. These data were repeated in Figure 3-55 and overlaid with the background prediction bands (refer Figure 3-46). Also overlaid were the MoR-v-MoE vectors for girders from DS-2. A description of the individual points is explained in Section 3.13.

Point 1 is the start; it represents the characterisation of the timber used to make a girder, and is a reference point. Since data for the MoR-v-MoE vector of a newly installed girder were not available, the first in-service vector is, therefore, Point 2. This point represents CS-1 girders. These are the type of girders that are expected in a bridge. They are components that are in the middle of their operating life (refer Figure 2-3). Point 3 represents a girder that has reached the end of its operating life and is starting to wear out (refer Figure 2-3). A girder in this phase of its operating life needs to be constantly monitored to ensure that it is operating within its design specification. Point 4 and Point 5 represent girders that have deteriorated and are below the S2 strength limit state. They are in advanced wear out and should be replaced.

These data Points 2 to 5, represent some, but not all, girders. There are other girders, represented by Points 2A, 2B and 2C, which have MoE above the reference value of Point 1. These girders are also in the middle of their operating life. They have MoR and MoE above the S2 limit states. Based on this research, the inferences from the data presented in Figure 3-55 are:

1. Girders that have MoE that is above their characterised value and is increasing are probably structurally sound. They would need to be checked that their predicted MoR is within their design specification but they may actually increase in strength.
2. Girders that have MoE that is decreasing should be continually checked to verify that their predicted MoR remains within their design specification.

Although every MoR-v-MoE vector examined only represents one girder at one point in its life, it is a general observation that girders do degrade and their strength declines with service life. It is, therefore, reasonable to hypothesise that the Points 2 to Point 5, together with Points 2A, 2B and 2C do represent the in-service MoR-v-MoE vector path of a girder. Different girders will

enter, and exit, this path at different places, but they will all follow the solid brown trend line shown in Figure 3-55 and remain within the prediction bands.

In Figure 3-56 a diagrammatic summary is shown for these inferences. A girder with MoE below the 14 GPa S2 limit state, should be regarded as unsatisfactory for use in a bridge. It will have an MoR that is also below the S2 limit state. This range is identified by a red band. A girder above 36 GPa will, at a 95% confidence level, have an MoR value above the S2 limit state and can be used unreservedly. The girders with MoE between 14 GPa and 36 GPa will need to be assessed for their suitability in a bridge. Although some may not have MoR above the S2 limit state to a 95% level of confidence they may not need to do so. As an example, a girder with a mean MoE of about 20 GPa will have a mean MoR of about 72 MPa. The minimum value that is to be expected is 32 MPa to a 95% confidence level. If the percentage of the total applied load (legal maximum load) is such that the applied load does not cause the MoR (32 MPa) to be exceeded, then it has a high probability of not failing. This is discussed further in SHM Application 2 (Section 5.3).

6.3 Experimental measurement of Deflection

In the previous section (Section 6.2), data are examined and outcomes identified as a result of testing bridge girders that have been removed from service (refer Chapter 3). In some cases, these girders were transported over long distances to be measured in a laboratory. In other cases, they were measured using a purpose built testing machine. The testing machine was transported to the vicinity of a particular bridge, the girders were removed, tested and discarded on site. None of the girders described in Chapter 3 were tested in an in-service situation. The cost of this type of testing process can be considerable, while a draw-back is that there is no immediate feedback about how any particular bridge is performing. The only feedback is ‘after the event’, so to speak. Characteristics are only gained after a girder has been removed from service, by which time it has been replaced with a new girder with different characteristics. General design information is gradually gathered, but knowledge about the in-service performance of a particular bridge is not significantly advanced.

Experiment 1 to Experiment 3 as introduced in Chapter 4 and discussed in this section, examined the measurement of mid-span deflection of in-service girders. Then in Chapter 5, it is shown how SHM techniques can be applied to determine the in-service performance of these girders using the measured deflections. Implementation of these techniques can significantly reduce the cost of girder testing. The cost of in-field measuring equipment can be significantly less than laboratory

equipment. There is no need to transport the girders. In the case of councils, the measurements can be made by in-house technical staff as outside specialist staff are not required. The test loads that need to be applied are less than 35% of the legal axle limit. Standard bridge maintenance vehicles can be used to provide loading. No special heavy loading vehicles were required. The measurement of traffic activity is required regardless of whether girders are measured on site or removed to a laboratory. This can be achieved in a low cost manner by the use of equipment that continuously records mid-span deflection throughout the life of the structure or individual members.

6.3.1 Experiment 1: Deflection caused by Static Loading

Powers Creek Bridge was loaded with vehicles of known loads and load versus deflection curve plotted (Figure 4-18). The calculated regression line through the measured data had a coefficient of determination of 0.999. This high degree of linearity was only achieved by accurately and consistently locating the wheels of the test vehicles on the bridge. Smaller vehicles were located with both axles loading the bridge and with each axle about one metre either side of the mid-span. The deflections resulting from such loading required correction since their wheel loadings were not at the mid-span. Larger vehicles with inter-axle distances greater than 4.5 m could be positioned with one axle on the mid-span and the other axle off the bridge; the deflections for these axles did not need correction. Because the loads were distributed laterally across more than one girder in each span, the correction factor was determined using a finite element model (Figure 5-5). Although the measured deflections were only read to a desired level of accuracy of about 0.5 mm, the load-v-deflection relationship was highly linear with low variation. The calculated tolerance in the slope of the load-v-deflection curve was about 5% to a confidence level of 95%. In SHM Determination 1 (Section 6.4.1) these deflection measurements are used to determine the girder MoE. The accuracy achieved in that determination is of a similar order. The girder MoE is determined about 1 GPa in 20 GPa; about 5%. Three inferences can be made from these results:

1. Increased measurement accuracy, below 0.5 mm, is not currently justified.
2. The use of low cost equipment is justified.
3. The use of standard light vehicles as loads is justified.

The slope of the load-v-deflection curve provides an indication of the bridge stiffness, as shown in Table 4-3. This stiffness figure quantifies the bridge at one point in time and can be regarded as a baseline figure. It should not be directly compared with another bridge without accounting

for the loads applied to each case. What is intended is that a temporal record is kept for each bridge so that temporal change can be identified. This concept of quantified temporal comparison contrasts with current regular assessment procedures, which are only concerned with visually identifiable parameters.

Example stiffness data for the three evaluated spans are shown in Table 4-4. Munsie Bridge Span G-6 has acceptable stiffness at about 0.6 tonne mm^{-1}. By comparison, a CS-1 span of 10 m with a main girder of 450 mm diameter, MoE 24 GPa and 35% loading, would have a stiffness of about 0.7 tonne mm^{-1}. The stiffness of the other two spans is lower than expected. Munsie Bridge Span G-4 is about 70%, and Powers Creek Bridge about 60% of the stiffness achievable for 450 mm diameter main girders of MoE 24 GPa. However, what is more important than the specific value is how the value might temporally vary. Unfortunately, there appears to be no available data in the current literature with which to compare such variations. Bridge carers have not been in the habit of broadly publishing such data and the scantly available accounts of bridge maintenance do not refer to records of deflection measurements. Although it was possible to record data of sufficient accuracy when these structures were first constructed in Australia, c. 1860 and larger truss bridges were quantified, records of small timber-bridges are hard to find.

It is important to initially determine and characterise the stiffness of a bridge by plotting a complete load deflection curve, as indicated in Australian Standards (AS 1720.1, refer Section 2.2.9). This determination ensures that the bridge under test is operating appropriately and behaving linearly. Once characterised, the bridge can be regularly checked using a single known vehicle. Bridge crews commonly utilise a vehicle with axle loads of about 50 kN, which are ideal for the purpose, but are not used as such. By using the same vehicle each time, the same loading distribution can be readily achieved by positioning the vehicle at the same place repeatedly. As can be identified in Figure 4-18, the load deflection curve for vehicles in the range of about 40 kN to 60 kN GVM is essentially linear. If such a vehicle is regularly weighed before transiting the bridge, then small variations in vehicle mass can be accounted for in the measured deflections. Many bridges can be readily modified to enable quick attachment of a staff and vernier measurement system, such as shown in Figure 4-10. This measurement process can, therefore, be readily utilised in comparison with normal visual inspection to quantify bridge temporal stiffness. Regular readings could be used to create a temporal deflection record. Once the mean and limits of normal variation are known, any anomalous deflections can be readily identified.

In the laboratory situation it was cited (Wilkinson, 2008) that a single bridge girder could deflect more than 40 mm at mid-span and the deflection curve to that point would be highly linear (refer Figure 2-28, Section 2.6.1). However, that data analysis was not published. In Figure 4-19 data from Figure 2-28 was recreated to show the degree of linearity that was achieved. A coefficient of determination of 0.999 was calculated for the regression line through the data below the 50% load level; it is a high coefficient, as is to be expected for a linear process with no confounding influences. The degree of linearity that might be expected to be measured for a timber sample is examined further in Experiment 4 (refer Section 6.3.4).

It was determined from these results (Experiment 1), that for loads below about 80 kN the load-v-deflection curve of an in-service bridge can be linear. What is not known is at what load might lose its linearity. This concern is addressed by using a hypothetical girder in a hypothetical bridge as described in Figure 4-19. In Chapter 5, the level of percentage loading and the MoE of the test bridge girders were determined. These data were recalculated with one of the test girders replaced by the hypothetical girder as shown in Table 4-5. This hypothetical girder supported about 50% of the load, whereas the actual girder supported only about 39% of the load. The reason for this was that the hypothetical girder MoE was 27 GPa, compared to the test girder's 20 GPa. When loaded up to about 70 kN, the span including the hypothetical girder, performed in a comparable manner to the test span (refer Figure 4-20).

This level of loading is only about 35% of the maximum loading which is to be expected for a legal single axle load. Thus, by load testing with vehicles of about 80 kN or less, a bridge can be expected to operate linearly. This situation may not be true if girders are highly degraded. However, bridges are structures that are expected to be highly reliable. The girders should always be CS-1 or CS-2. By following the procedures just described, it should be possible to determine the onset of girder degradation, before a higher level of degradation occurs.

6.3.2 Experiment 2: Traffic loading

The prime difficulty in determining the probability of failure of a bridge girder is to identify the in-service loading. The historical method used to overcome this difficulty was to proof load a bridge. Such a method involved subjecting the bridge to load and, by necessity, this had to be done with the bridge closed to traffic. However, as has been inferred from the results from Experiment 1, bridge girders deflect in a linear manner at loads up to about 80 kN. Hence, if a span is initially characterised by measuring the girder stiffness, subsequent measurement of girder deflection can be translated to an effective applied mass for each vehicle. If the deflection

of every vehicle is recorded, then these records can be converted into an in-service loading distribution.

The traffic that crosses any particular bridge span is within predictable bounds. A similar set of vehicles uses it regularly. Even heavy vehicles are related to activities in the area. Large stock trucks regularly cross Munsie Bridge because a business in that area transports stock from one side of the bridge to a livestock selling centre on the other side. Heavy concrete trucks, fuel tankers and construction equipment might enter the area for their various exploits, but otherwise unrelated heavy traffic is unlikely to cross the bridge. However, although heavy vehicles are most likely to cause damage to timber-bridges, it is not mandatory to use heavy vehicles to test a bridge.

Light vehicles comprise by far the major type of vehicles crossing the two bridges that were examined. Measuring the loading effect of light vehicles provides more than ten times the data compared to the effect caused by heavy vehicles. As shown in Table 4-7, some 90% of the vehicles exceed a mid-span deflection of about 2mm (Threshold 1), but not a mid-span deflection of about 4.5 mm (Threshold 2). Less than 1% of the vehicles, crossing each of the spans investigated created deflections above 20 mm (threshold 5). At a stiffness of 6 kN mm^{-1} a deflection of 20 mm is equivalent to 120 kN. This is only about 60% of the maximum legal axle loading set at about 200 kN for a single axle (refer Section 2.2.5). If for any reason a bridge becomes degraded, then its effective bridge girder MoE will decrease, as identified in Chapter 3. This change in MoE can be readily detected by loading the bridge with light vehicles, which apply less than 80 kN load.

Traffic volumes were sequentially recorded for each of the three measured spans, each for a separate period of about three weeks. The histograms for each (refer Figure 4-24) are somewhat similar, with the percentage of vehicles crossing each span and at each threshold, being of the same order of magnitude. The fact that the percentages for G-4 and G-6 are not identical is indicative that the actual traffic distribution may vary over time spans of several weeks. Specifically, traffic can alter because of the change in local activities. The recording period of one span was interrupted with a public holiday. During this period schools were closed for two weeks, which led to a change in the traffic density (i.e. the school bus did not run during this period, parents were not transporting children to after school activities). A detailed discussion of actual traffic flows will require both a more detailed examination of the traffic characteristics and a sufficiently long recording period to exclude any change of use irregularities, such as holidays. Such an evaluation was not attempted as part of this research. What was attempted, and

successfully achieved, was a demonstration of the fact that vehicle distributions can be readily recorded by using a mid-span peak deflection recording system such as a BDM.

The advantage of using automatic recording equipment, such as a BDM, is that a bridge can be monitored on a continuous in-service basis, thus precluding the need to keep manually repeating static load-v-deflection measurements. For example, if there is a BDM threshold set at 4.5 mm (Threshold 2, as specified for the BDM used in this Experiment), then that equates, via the model equation (refer Table 4-3,) to an applied load of 31 kN. If a vehicle mass is adjusted to apply a load of 29 kN, then the mid-span deflection should not exceed Threshold 2. If the vehicle mass is then adjusted to apply 33 kN, it should just exceed Threshold 2. A small truck of four tonne GVM can be readily used to achieve this result. If such a truck regularly traverses the bridge at these two different masses and only the higher mass caused the deflection to exceed Threshold 2, then it would provide verification that the bridge stiffness was unchanging. If the lower mass caused the deflection to exceed Threshold 2, then there should be concern that the girder or bridge stiffness has diminished.

Once a baseline condition has been established for a particular bridge span, then about 90% of the vehicles crossing the bridge will not exceed Threshold 2. The actual percentage will, of course, depend on the bridge span's structural quality and the type of traffic distribution. If, at any time after the baseline has been established, the percentage exceeding Threshold 2 changes significantly, then there is cause for concern. A significant change would not include a small variation up or down caused by seasonal variation of the timber. It would include a continuing temporal increase in the percentage of vehicles exceeding Threshold 2. Example baseline data for the test spans is given in Table 4-7. In each of the three spans, only about 11% of vehicles exceeded Threshold 2. These percentages may not vary for many years and any continuous record may just indicate that no change has occurred. In order to demonstrate that degradation can be measured a bridge in the act of degrading has to be found. One method to overcome this delay is to artificially degrade the girder, but this is only permissible on an experimental structure and not on a public bridge. Another method is to find a bridge that has advanced degradation and because of the piping and termite degradation present in G-4 it may not be many years before a significant change occurs in that span. A further method is to strengthen a span such as G-4 such that it is returned to CS-1 quality but to do so in a way that the strengthening can also be reduced in a controlled way. The strengthening can then be varied over time and the temporal changes recorded.

The traffic data (Table 4-6) were fitted to lognormal distributions as a first step in creating a load distribution. These results are shown in Table 4-8 and Figure 4-25. These distributions were created by first transforming the vehicle deflection to mass using the standard Euler-Bernoulli beam theory while assuming that each vehicle represented a point load at mid-span. There is of course some error introduced in this translation since, as discussed in relation to Experiment 2, many of the smaller vehicles would have had both axles on the bridge at the same time and there would not have been a single point load. However, it is a relative measurement which is being carried out here and not an absolute one, so, providing the distribution of vehicle types does not change significantly, the deflection distribution will be indicative of the vehicle mass distribution. Average vehicle axle spacing does not change significantly from year to year and a new baseline figure could be determined if this parameter did become a concern. The distributions shown in Figure 4-25 are all different because they are for different spans and different traffic. Over a longer period it is to be expected that the distributions for span G-4 and span G-6 might become more similar.

What is of greater concern are the data shown in Figure 4-26. Here, the lognormal fitted distribution is plotted over the histogram that represents data for Powers Creek Bridge. While it can be shown numerically that there is a reasonable fit for the lower mass vehicles, there is not a good fit for the higher mass vehicles. The distribution of heavy vehicles is not well represented by the lognormal distribution. This is a concern because it is the higher mass vehicles that will cause the bridge span to be over-stressed. Because of the lower incidence of higher mass vehicles, a much longer period of recording is required. This recording period may need to be 100 times that of low mass vehicles. Thus, if a reasonable recording period for the low mass vehicles is one week, then the recording period for high mass vehicles could be as much as two years (104 weeks). This period should not be an operational concern since the lifetime of a girder should be at least 10 years and a baseline traffic distribution can be established within the first few years of operation. In Chapter 3, some girders were identified as being degraded when only 15 years old and some still not degraded and still in-service after 60 years. Therefore, a two year characterisation period will normally be significantly less than the overall service life.

The concern then is related to what distribution should be used to fairly represent heavy vehicle activity. The BDM used to record this activity had thresholds set at increments of 10 mm for loads above 60 kN. Therefore, there was insufficient resolution at the higher loadings to clearly define the higher mass traffic activity. The best fit to the available heavy vehicle data appeared to be a uniform distribution. This distribution would be truncated at a specific maximum value and

its density set to suit the actual vehicle density. This maximum value might first be chosen to be 10% above the actual legal axle load, but higher loads were experienced across Munsie Bridge.

A normal distribution was an alternative choice. However, to match the required distribution required a complex multi-modal distribution. The MatLab® distribution tool was also tried but a good fit was not found. The choice of this or another approach will require further research. The maximum threshold was pre-set at 55 mm, which for a stiffness of 6 $kN.mm^{-1}$ is equivalent to 325 kN (33 tonne). In the design phase of the BDM, this was chosen as a suitable upper limit, which was unlikely to be exceeded. Yet it was exceeded while recording data for G-6. G-6 appears to be in sound structural condition and this excessive deflection must be accepted as real. Before and after this excessive value was recorded the deflection returned to zero. Therefore, there was no indication of any inconsistency in the measurement process either before or after the excessive load.

An axle load of 33 tonnes is significantly above the legal limit of 20 tonne (refer Section 2.2.5) yet it occurred on five occasions during the measurement period of G-6 and once on G-4 (non-concurrent periods). In terms of creating a realistic equivalent distribution, the concern is where the upper limit should be set and the only sensible choice is at a percentage above the legal limit. This percentage might be as high as 50%. The overall traffic load distribution could thus be a combined distribution of a lognormal one representing 99% of the traffic and a uniform one representing the 1% of traffic with equivalent single axle loadings above 100kN. It was, however, not possible to clearly identify the magnitude of such a uniform distribution because of insufficient data collected during each three week period. As both the Powers Creek Bridge and Munsie Bridge (spans G-6 and G-4) are rural bridges on the outskirts of urban areas, a much longer recording period is required to measure sufficient heavy traffic to create a heavy traffic distribution.

6.3.3 Experiment 3: Dynamic Loading

Case A: Influence Line

This experiment was devised to ensure that the recording system had sufficient response time to record moving vehicles. The level of detail that was captured was not apparent from the deflection-v-time response curve initially plotted. This only became apparent after examining the influence line (Section 2.2.7). As a vehicle progresses across a bridge, the deflection caused at the mid-span will depend on whether one or more axle is on the bridge at a time. The passage of a vehicle travelling at 5 $km.h^{-1}$ and with an axle spacing 30% of the bridge span is shown in

Figure 4-31. The first important feature is that the combined actions of the two axles, as calculated using standard theory mirror the measured data. The inflection in the measured data curve, as the second axle arrives on the bridge and departs from the bridge, can be readily identified. The measurement process involved recording the movement of a graduated chart, relative to a fixed laser beam, with a high speed camera. This process effectively modelled the BDM recording technique. The interpretation process using the camera was very labour intensive since every individual picture frame had to be viewed to determine the position of the laser image on the graduated chart. In the case of the BDM, high speed electronics and software provide an immediate result. The major functional difference between the two systems is that the camera provides a proportional signal whereas the BDM has a number of pre-set thresholds. When recording with a camera the position of the image can be read to within 0.25 mm for all displacements. The BDM provided one signal when the image was above and another signal when below a pre-set threshold. The switching indecision between thresholds is about 0.2 mm. The advantage of using a limited number of pre-set thresholds is that it leads to low cost instrument design, but the pre-set thresholds must be appropriately chosen to suit the required data. If interest is in heavy traffic then higher more closely spaced thresholds are required such as: 0, 15, 20, 23, 26, 30, 35, 50 mm. If interest is in light traffic then lower more closely spaced threshold are required (refer Table 2-15). The BDM should be pre-set according to the recording need.

The deflection curve (Figure 4-31) was determined using parameters representing the stiffness of the structure. These parameters included the girder diameters, the girder MoE and the actual placement of the girders. As indicated in Table 4-10, the effective girder MoE was specified to suit the bridge span parameters. It was specified as 17 GPa, which was a realistic value as reported in Section 4.3.3. However, it is the form of the curve that is of primary interest in this comparison and not the absolute magnitude. The two features shown in Figure 4-31 are the inflections and the peak value. The detail of the two inflections can be identified in the measured data and the peak value can be identified as the sum of the two axle values. The measurement system, at 240 fps (about 4 ms per frame), is clearly of adequate frequency to record the detailed deflections. The effective BDM response time, as used, was slightly faster at about 3 ms per data point. A vehicle crossing the bridge at 100 $km.h^{-1}$ will spend about 36 ms in the central 1 m of the bridge while causing the maximum mid-span deflection. The BDM can thus record ten data points during the time the vehicle is at mid-span. The particular BDM used was designed as a

low cost measurement system. A higher performance can be readily achieved but would require increased processing speed leading to an increased cost.

It can also be inferred from data presented in Figure 4-31 that the peak deflection is less than the sum of the two peaks caused by each axle; as is theoretically expected. This is true whether the vehicle moves continuously across the bridge or whether it is parked centrally at mid-span. It is for this reason that a correction factor, accounting for the presence of the two axles, was used in Experiment 3. It can be inferred from these measurements that a theoretical concept such as line of action can be clearly identified on an aged in-service timber-bridge with low cost measurement equipment. The corollary of this inference is that local councils do not need highly priced measurement equipment to adequately measure the performance of their timber-bridges if they use the equipment and strategies developed in this research.

Case B: Transient response

In the previous case, the vehicle was moving at a low speed (5 km h^{-1}) and the vehicle mass was low (43 kN). Data in Figure 4-32 were representative of the type of dynamic data that can be readily captured by a vehicle moving at typical speeds of 60 km h^{-1}. The purpose of this experiment was to indicate that deflection data, reflecting the movement of high speed vehicles, can be readily collected. Because of the volume of data gathered, it was not possible to adequately analyse all of it within the research period. So, what are you proposing? What should be done? You could mention that this will be discussed in Conclusion.

The transient presented in Figure 4-32 comprises major vibrations at about 1.3 Hz and 8 Hz. The 1.3 Hz transients represented the impacts caused by the vehicle and the 8 Hz transient represented a natural vibration of the bridge. The 8 Hz vibration can be inferred to be a natural bridge vibration because it continued for several seconds after the vehicle had departed, as recorded by the BDM. The vibration in the structure was not critically damped, otherwise the vibration would have ceased within one or two oscillations instead of continuing for more than ten oscillations without a noticeable change in amplitude. This vibration is of concern in relation to bridge design since hardware components would be unnecessarily stressed. Further research will be required to determine if such vibration concerns are typical of timber beam bridges and what level of damage it could incur.

The peak mid-span girder deflection that was measured was 15 mm, refer Figure 4-47, which for a stiffness of 6 kN mm^{-1}, refer Table 4-18, was equivalent to a mid-span point load of 90 kN. The bridge behaved in an elastic fashion in response to this vehicle loading, returning to its

initial unloaded state after the vehicle had departed. This was similar behaviour to that seen using the BDM recording traffic in Experiment 2. Many tens of heavy vehicles produced deflections of more than 20 mm and six were recorded above 55 mm. After each traverse, the girder returned to its initial rest state, followed by many other lighter mass vehicles that produced peak deflections of only 2 mm. From all these results both dynamic, in Experiments 2 and 3, and static, in Experiment 1, it is inferred that the girders were still dynamically deflecting in an elastic manner. However, because of a lack of historical records, it is not known whether the current MoE has temporally changed from its original commissioned value.

As with Case A, the full significance of these data is not apparent when plotted as a deflection-v-time curve, but better understood when transformed into an influence line (Figure 4-34). Because of the speed and the mass of the vehicle, the instantaneous deflection oscillates about the nominal static influence line. The dynamic effect is to cause increased stress which, in the region of the peak deflections, is about 30% higher than for an equivalent static case. The inference from this measurement is that the test equipment can be readily used to identify peak dynamic deflection. Further research will be required to examine this aspect in detail.

Case C: Influence of speed

In designing a bridge, an impact factor allowance is made for the impact loading that is produced by heavier vehicles at higher speeds. To examine whether this effect could be readily identified in deflection data, a vehicle of mass of two tonnes was driven across Munsie Bridge, Span G-6, at speeds up to 40 km h^{-1}. Higher speeds were not considered viable because of the uneven timber deck and low sight distances on approaching the bridge. The results, normalised to the deflection readings with the vehicle parked at mid-span, are as shown in Figure 4-35. At speeds below 10 km h^{-1} there was no change in the deflections compared to the static case, but at 20 $km.h^{-1}$ and above, there was a significant increase in mid-span deflection; + 40% at 40 km h^{-1}. Because of this speed effect it cannot be known, from the traffic deflection data recorded by the BDM, what the actual vehicle mass is unless a vehicle is known to have crossed at 10 $km.h^{-1}$ or less. However, to determine if a girder is overstressed, it is of interest to know the actual deflection that occurs regardless of whether it is caused by a faster and lighter vehicle or a slower and heavier vehicle.

The increase in deflection caused by speed is a possible reason for an anomaly in the Powers Creek Bridge data (refer Table 4-7). The number of vehicles exceeding the second threshold for Powers Creek Bridge was 11.6% whereas Munsie Bridge spans were 10.8% and 10.0%. The

Powers Creek Bridge data appear anomalous because it was a shorter single span, which should, with similar diameter girders produce a stiffer structure. There was one particular difference between the two bridges that would have affected this result and that was the quality of the decking. The Powers Creek Bridge deck was smooth and the road either side was relatively straight and level. Lower mass vehicles, below about 6 tonne, were able to cross the bridge at 100 km h^{-1} and many did so as experienced during site visits. The deck on Munsie Bridge was uneven and caused significant vibration in a vehicle crossing it. Munsie Bridge is not clearly visible to traffic on the approaches and traffic will naturally slow down before arriving at the bridge. Because of the unevenness of Munsie Bridge and the immediate vibration that occurs as soon as a vehicle begins to cross the bridge, crossing speeds tend to reduce to about 20 km h^{-1}. The impact loading of the two bridges was, therefore, quite different.

If 30% of the lower mass vehicles crossing Powers Creek Bridge, below a mass of 30 kN, were travelling at 100 km h^{-1}, they would have had an increased loading that produced a mid-span deflection above 4.5 mm. If, conversely, 30% of these higher speed vehicles are removed from the number of vehicles that created a deflection above 4.5 mm and attributed to those that only created a deflection of 2 mm, then the ratio is 8.4%. That is only 8.4% of vehicles would cause a deflection exceeding 2 mm and not 11.6%. To verify this inference, that the ratio is increased by about 3% because of vehicle speed, will require an experiment to determine a traffic loading distribution for vehicles of known speed. Either all vehicles need to be speed limited for a period or the speed of each vehicle, and of known mass, needs to be correlated with the deflection produced. Such experiments should be the subject of future research.

6.3.4 Experiment 4: Determination of level of variation in a timber load-v-deflection curve

This thesis examines the possibility that continuous deflection monitoring can be used as a method of assessing the probability of timber-bridge failure. As part of the process of determining the probability of failure, variation of girder material parameters are assessed; in particular the variation of in-service girder MoE is assessed. However, the level of variation that can be expected for an individual girder could not be gleaned from the reviewed literature. In Section 2.4.6 it was identified that a distribution of in-service power poles could have a 15% CV, increasing to 33% during service. In Section 2.3 it was identified that excised specimens from a population of one tree species can have an 8% CV. What is not identified in the literature is the level of variation that can be achieved in measuring the in-service MoE of a specific girder. This

experiment was designed to quantify the lower bound of variation that might be experienced, thus filling the gap in the published literature.

A stainless steel specimen was used as model material. Its material characteristics would not change significantly while being measured in a laboratory situation and it is known to be a very resilient material when measured. The dimensions of the sample were chosen such that it would produce similar deflections to timber samples loaded in a similar manner.. The steel characteristics were determined with a load-v-deflection curve and a regression model. The regression model achieved an exceptionally high coefficient of determination of 0.99996. This experiment was then repeated on a sample of *P. radiata* and again a very high level of linearity was achieved with a coefficient of determination of 0.99998.

Samples of timber (*P. radiata*) were then measured repeatedly while ensuring that the MC of the timber was kept constant. The CV in MoE for a single sample was determined to be 0.5%, or less (refer Table 4-12). A single sample was also kept at constant MC and measured repeatedly over a period of two weeks. Again, the MoE variation was less than 0.5% CV (Figure 4-41). The timber samples were carefully maintained at a constant MC to achieve this low variation. Each sample had a significant surface area through which moisture could diffuse and it was possible, by weighing, to determine the quick changes in mass. Since the measurement of in-service girder MoE occurs in a less controlled environment, it is most likely that the variation of in-service MoE will be higher than 0.5%.Thus, a measurement technique set to determine in-service girder MoE need not achieve a higher systematic accuracy than about 1%. The variation in bridge stiffness determined in Experiment 1was about 5%. To achieve a significantly lower variation may not be cost effective for an in-service measurement. However, it will be possible to statistically review the level of accuracy that should be attained with the future collection of temporal data.

6.3.5 Experiment 5: Cypress Pine destructive test

The CSIRO species characterisation data (refer Table 2-3) were obtained from the bending to failure of clear specimens. The level of defects present in these specimens was not published nor was the reason for the level of variation that was reported. These omissions are not surprising because the tests were to a standard for the purposes of determining the characterisation of a species and not to determine how accurately a single sample can be measured. Because timber is a natural material, it is accepted that there is a significant level of variation between samples. However, what has not been identified is the temporal variation that can be expected in a single

sample and it is temporal variation that is of interest in characterising changes in a single girder. It was not possible for this thesis to repetitively bend full girders to determine what level of variation might occur. As a first model, small clear samples were tested in Experiment 4. Girders include defects and it is important to understand how such defects can affect in-service measurements. As a simple model, a randomly chosen scantling of White Cypress Pine (*C. glaucophylla*), which had a surface defect on the compression side, was tested to failure.

The MoR-v-MoE vector for this sample was not a complete outlier. Its MoR was below and its MoE was above the species mean, but both values were within the expected range for the species. The combined MoR-v-MoE vector was also within the prediction band for excised clears. This positioning is despite the presence of a defect having a significant effect on its MoR. That the defect was significant can be inferred because the sample failed in a brittle fashion. There was no region of non-linearity. Further research will be required to determine if the major cause for the measured variation in the MoR-v-MoE prediction bands is due to intrinsic material variation or because of the presence of defects. If it is caused by the presence of defects, then processing technology is available to screen out girders that contain such defects. An alternative approach is of course to engineer girders to have no significant defects, resulting in much more consistent properties. This is the approach currently being taken in Europe and North America as espoused by Moore et al. (2011).

Three inferences can be made from this measurement. The first is that since girders are selected for quality, they should not fail outside the identified prediction bands (brown dotted lines, Figure 4-46). Girders are chosen, as are excised clears, to have minimal defects. If a girder is selected with a defect, then that defect will not be placed in a highly stressed region. The type of brittle failure that occurred in the Cypress sample should not occur in an in-service girder. Although a girder may not have a defect in the mid-span high stress region when it is installed, it may incur damage during its service life. This could then lead to a failure of the type demonstrated in Experiment 5. The second inference is that reinforcement of this region should inhibit any tendency for brittle failure. Such reinforcement has been applied to concrete structures, but the use of techniques to strengthen aged timber-bridge girders was not evident in the reviewed literature. The third inference is that if an aged timber girder contained a defect that could cause the girder to fail in a brittle manner, then it would be unwise to proof test it. This inference is important since such a defect may not be visible. It is, therefore, important to only test aged timber-bridges to a light loading level to minimise the possibility of brittle failure.

6.3.6 Summary

The experiments reported in Chapter 4 were set to examine the deflections produced by both static loading and in-service traffic loading. This approach is consistent with the following Australian Standards, where it is recommended that:

1. Load testing should be used to quantify bridge load capacity in a scientific manner (AS 5100.7: Section 6.1).
2. A load test should be used to determine the onset of non-linear behaviour (AS 5100.7: Section 6.3.3).
3. A minimum of six points is required to define the load-v-deflection curve if it is predominately linear (AS 1720.1: Section D3.4).
4. A minimum of ten points is required if the curve is significantly non-linear (AS 1720.1: Section D3.4).

However, the approach recommended in AS 5100.7 also has the following unspecified limitations:

1. A single proof load test can only enable the determination of the current strength of a bridge; it cannot by itself be used to predict future performance.
2. The determination of temporal bridge degradation requires a succession of proof tests to be conducted at regular intervals.
3. Proof testing is a time and labour intensive process and requires the bridge to be closed for the period of the test.
4. Regular proof testing is not currently affordable by many bridge owners. This can be inferred because very few aged bridges are currently being tested (Roorda, 2006). In recent years, many have simply been replaced when their performance was believed to be sub-standard.

There is a need to determine temporal change in MoE. This need was inferred from the theoretical evaluation of data in Chapter 3, where it was identified that effective MoE varies during the service life of a girder. It was also inferred that the temporal path of the MoR-v-MoE vector can be used to predict girder performance. This need is not specifically identified in AS 5100.7 or AS 1720.1 and neither is the significance of quantified temporal change. In Australian Standards (AS 5100.7) it is recommended that, to cater for changes in bridge

performance, comprehensive investigations and inspections should be carried out. However, small, but continuous changes in MoE will not be detected by a single proof loading test and many tests would be required to detect these changes.

It was also identified in Chapter 3 that there is a relationship between MoE and MoR. However, no evidence was found in the literature that defined any relationship between MoE or MoR and the onset of non-linearity for Australian hardwood bridge girders. Further research is, therefore, required to establish whether any relationship does exist. In Chapter 3 it was determined that there were girders with high values of MoE. These girders may have always had high MoE or their MoE may have increased during their service life. A question that can be posed in relation to this change in MoE is: Does the onset of non-linearity increase and decrease as MoE increases and decreases, respectively or conversely?

As a method of determining temporal MoE, the temporal deflections caused by vehicles can be recorded. This was demonstrated in the experiments described in Chapter 4, where it was identified that:

1. Recording temporal deflection need not be time and labour intensive.
2. Accuracy can be achieved by repeating a measurement many times with the same vehicle.
3. The measurement need not be static but can be dynamically recorded.
4. Temporal deflection measurements can be used to predict future performance. How this can be achieved is explained in Section 6.4.

It was not evident in the reviewed literature what level of variation would occur in the measurement of a single sample girder. It was also not clear what effect a significant defect might have on girder testing. To fully understand both of these effects would require significant research. Because of high cost and Occupational Health and Safety (OH&S) matters, the initial plans to test complete girders and excise samples of adequate quality as part of this research were aborted. Having carried out in-service measurements, it is now apparent that full girder deflection tests can be carried out using a method modified from that used in Experiment 1. However, in the absence of such research, Experiments 3 and 4 were set to provide an indication of in-service girder measurement. From the results of those experiments it is inferred firstly, that measured variations of a few per cent should be the target for an in-service measurement situation. Secondly, it is inferred that care should be taken in proof load testing. Since the measured MoR-v-MoE vector of a sample with a significant defect was not an outlier, a similar

condition could apply to an in-service girder. An unrecognised girder defect could lead to brittle failure at less than the expected maximum load.

Timber is not a material of the past; it is a material of the future. In Europe and North America it is now recognised that timber is cost-competitive with other materials. However, it should not be regarded as a new material that has unknown properties. There is an important reservoir of information held in current timber-bridge girders that needs interpretation. To improve understanding in this area, it should be possible to compare a girder removed from service with currently known data (Section 4.1.9). Unfortunately, there have been many cases of local councils contracting the removal of timber-bridges to companies who remove the timber for second-hand sale and the important strength data are lost forever. These are data that have been slowly stored in these girders for many decades. To understand the strength of large aged timber beams for use in highly reliable structures, this practice must be modified and girders tested before being sold on. When and where timber-bridges are removed from service, some girders should be tested in bending, then a sample should be excised from an unstressed region and also tested. Girder bending tests can be carried out in the vicinity of the bridge before the girders are transported and should to be part of any de-commissioning process. It need not be an expensive process. Using the techniques developed in these experiments, it is now possible to propose methods that enable load-v-deflection data to be recorded on-site using simple jacks, lasers and vernier scales. Large purpose-built testing rigs are no longer necessary. It is only after this end-of-life testing that these data will be retained and can be used to more optimally design structures using large timber beams and an SHM methodology.

6.4 Application of SHM to timber beam bridge girders

In Section 6.3, the discussion focussed on in-service measurements, which were described in Chapter 4. These measurements were:

1. static deflection and load, used to determine stiffness (Experiment 1)
2. the deflection caused by each vehicle, used to determine both the traffic distribution and the ratio of heavy to light vehicles (Experiment 2)
3. the peak deflection caused by a vehicle regardless of its speed and used to determine the effect of impact (Experiment 3).

In Chapter 5, the outcomes of those in-service measurements were combined with the theoretical outcomes developed in Chapter 3. By combining those outcomes, it is possible to calculate the

probability of failure, a safety index and to identify bridge structural health, as will be discussed next.

6.4.1 SHM Determination 1: Girder MoE and percentage loading

It is necessary to determine the following objectives in order to identify both the safe carrying capacity and the probability of failure of a bridge girder:

1. the girder MoE
2. the fraction of the load applied to the bridge that is applied to the girder
3. the strength of the girder, that is its MoR, and for the purpose of determining:
    a) a single valued safe carrying capacity the required MoR is the lower prediction band value, at a confidence level of 95% two standard errors below the mean.
    b) the probability of failure, this is the predicted mean value.

SHM Determination 1 was set to achieve only objectives 1 and 2. These were achieved by creating numerical models of the in-service test spans and comparing the measured deflections with the calculated ones. This approach worked well. One surprise was the lack of stiffness in the deck planking and the subsequent lack of load transfer to girders not directly loaded. The Educational SAP2000® software package was adequate for the task, but further, more detailed analysis is required. To achieve a more detailed analysis, a full account of the complete bridge deck is required, which would require more nodes and equations than were available. Even with the restricted model that was employed, it was possible to readily adjust the MoE of girders to within 1 GPa to achieve deflection comparisons within 0.5 mm. That MoE data were then used in a spreadsheet model to determine the percentage of load applied to each girder. Again the level of adjustment had sufficient resolution; it was necessary to adjust the girder load to within ±0.1 kN to achieve deflection comparisons to within ±0.1 mm. It would require a number of tests and comparisons at a higher level of accuracy than was possible during this research to determine the possible accuracy of this process. This is a possible area of future targeted research to realise an effective numerical software model for a timber-bridge that takes into account the outcomes from Chapter 3.

On first examination of an unknown bridge it is necessary to determine reasonable operating limits. The span, girder diameter range and girder MoE range are specified and nominal span to deflection ratio and stiffness ranges calculated. For example, the effective stiffness range for the Powers Creek Bridge span can be determined to be between 0.6 and 1.9 tonne mm^{-1}. Thus, a

four tonne load applied at mid-span should not deflect more than about 6.6 mm (total bridge load/minimum stiffness). This calculation was based on a nominal girder load of 35% of the total load. The bridge can be tested with a small mass vehicle and the deflection verified to be within the expected range. If the deflection is excessive, the bridge may be structurally unsound and require immediate maintenance. All three test spans performed within expected limits and did not deflect excessively under light traffic loading.

The range of measured MoE for the test spans was between 12 GPa and 34 GPa. The higher value of 34 GPa was 80% of the DS-2 upper limit of 42 GPa for a girder with both recorded MoE and MoR. The lower value of 12 GPa was 85% of the S2 limit state. The mean of the measured test span data was 22 GPa. That was higher than the mean of the DS-1 to DS-4 data which were 15 GPa. If only those girders that have MoE and MoR above the S2 limits are selected from the DS-1 to DS-4 data, then there are only 37 girders that qualify and the mean of this cluster was 24 GPa. That was a more appropriate comparison, the measured 22 GPa was 92% of the DS-1 to DS-4 data mean. By a comparison of working girders it is concluded that in both cases were expected to be above the S2 limit states. Therefore, both the range and the mean of the test span girders were similar to the DS-1 to DS-4 cluster data that represents in-service girders.

The loading of the girders of the test bridges was distinctly uneven. It certainly was not distributed evenly across each girder. The minimum loading on a kerb girder was 7% and the maximum on a main girder was 46%. Typically, a main girder and its associated kerb would support about 50% of the load. However, if one main was stiffer than another, one main and kerb pair could support more than the other pair. In one test case, one pair supported 5% more than the other pair. It was inferred from the test bridge measurements and the subsequent modelling that in a structurally sound bridge, with standard planking, the kerb and main girder load distributions would be 15% and 35% respectively.

6.4.2 SHM Determination 2: Bridge load limit

To identify the safe carrying capacity of a bridge girder, that is its load limit, it is necessary to first determine the following objectives:

1. The fraction of the load applied to the bridge that is applied to the girder.
2. The strength of the girder.

Objective 1 was determined as part of SHM Determination 1 discussed above. The strength was next determined using the model Equation 3.10. However, that regression model was designed to predict the mean MoR from mean MoE. What is required for a load limit determination is the lower 95% confidence limit of this equation, as identified in Equation 5.2. It is not straightforward to quantify the resultant data. One comparison that can be made is that all girders were expected to have MoR above the S2 limit state. That was not the case because the value determined was a low estimate, which had a very high chance of validity; all girders had MoR of less than 70% of the S2 limit. A second comparison can be made that is identified in AS 1720.1 (Standards Australia, 2010). This is that the fifth percentile is 50% of the mean value. If this criterion is employed, then the mean of the test span girder MoR is 80 GPa compared to the DS-1 to DS-4 cluster of 37 girders, which has a mean of 101 GPa. The inference here is that the strength of the test span girders may be underestimated, but these current estimates cannot be varied without additional information.

The first step in determining girder MoR is to determine the effective girder diameter. This determination can have significant variation depending on the level of sapwood (refer Section 2.4.3), or the degree of surface erosion (refer Figure 5-33). Once the diameter is determined, the girder MoE is calculated using Euler-Bernoulli beam theory, the measured loads and the deflections. The next step is to use a regression model to predict MoR, as shown in Figure 5-8. To compute the load that will create a mid-span stress equal to the predicted MoR, again using Euler-Bernoulli beam theory, is the final step. The resultant calculated loads are shown graphically in Figure 5-9.

In this process, there are two significant contributions to the standard error. The first is the error in identifying the effective diameter. The second is the variation in the prediction equation. However, this second contribution is statistically quantified, while the first is not. An indication of how a change in diameter can affect this error is examined in more detail by considering girder G4-MU. According to the current determination, while it will carry a legal load, a small overload may cause damage (Figure 5-9). By more careful visual examination of the girder it was realised that the initial determination of the effective girder diameter was overestimated because of extensive sub-surface degradation. After an improved diameter determination and a new calculation, the load limits were improved to those shown in Figure 5-11. Therefore, it is important to accurately determine the effective cross-section of solid wood of the girder.

These calculated load limits are such that the test bridges can be considered to be structurally sound, providing that they are not excessively overloaded. Such a determination is only true for

the time when the measurement is made. Any change in the girder material parameters, for whatever reason, will require a recalculation of the load limit. Also, at a later time, it will not not known whether any change has occurred without a second load test. It is important, therefore, to temporally monitor the bridge for any structural change. A bridge can only be considered structurally sound if the mid-span deflections are such that the safe load limit is not exceeded. In the particular case of G4-MU, a load had crossed the span several times that was significantly above the legally specified maximum load limit (refer Section 2.2.5). As a result of those crossings, there were no significant changes observed in the girder parameters. It is inferred from this unplanned experiment of excessive overload that the girder strength is significantly above the 95% confidence minimum value.

6.4.3 SHM Application 1: Probability of Failure of the Span to Deflection limit state

It is necessary to determine the following objectives to identify the probability of failure of the span to deflection limit state of a girder:

1. the stiffness of the girder (MoE)
2. the fraction of the load applied to the bridge that is applied to the girder
3. the applied traffic load
4. the mid-span limit state
5. the probability of the mid-span deflection exceeding the limit state.

Objectives 1 and 2 were determined in SHM Determination 1 and the applied traffic load in Experiment 2. Both the girder stiffness and the traffic load are determined as a distribution. If the girder stiffness is measured several times, the data will include measurement errors. The girder parameters may vary between measurements if the measurement times are separated by significant periods, then the data will include both measurement error and material parameter variations. As a girder degrades, the stiffness distribution variation will increase. As discussed in Section 2.4.6, the variation of a large number of timber power poles can increase from about 15% to 30%. The variation in stiffness of a single girder may, therefore, increase from 5% to 20%. It will increase from a small, well quantified value when a girder is first placed in service to a larger, less well quantified value towards the end of its serviceable life.

While it is trivial to include a variation in the stiffness data, it was not included for two reasons. Firstly, it had been measured and could be regarded as known. Secondly, its inclusion would have hidden the concern about the accuracy of the traffic distribution. The traffic distribution, as

measured and as discussed in Section 6.3.2, did not adequately represent the heavy traffic, therefore. The probability calculation cannot be considered realistic until a suitable distribution is determined. The first probability of failure calculations, using the traffic distributions as calculated, did not indicate failure. By creating an artificial distribution that was a better fit to the heavier traffic, a failure rate of 155 in 10^6 was determined which is equivalent to a safety index of −3.6.

It should be mentioned that it is not the absolute value of the failure rate that is of primary importance. In this case, the index is acceptable; its magnitude is above the limit state of −3.1 (refer Section 2.6.3). What is important is the rate of change in the safety index. If the safety index is constant, then the bridge is not deteriorating. If the safety index is declining, then the bridge is deteriorating and the time it will take for the limit state to be exceeded can be estimated. The time for the safety index to vary significantly should be many years and it was not realistic to measure a change within the research period of this project. One example of this will be discussed in more detail in SHM Application 3 (Section 6.4.5).

6.4.4 SHM Application 2: Probability of girder structural failure

It is necessary to determine the following objectives to identify the probability of girder structural failure:

1. the MoE of the girder
2. the fraction of the load applied to the bridge that is applied to the girder
3. the MoR distribution predicted using MoE
4. the applied traffic load
5. the probability of the failure.

In SHM Determination 1 (Section 6.4.1) the fraction of the load distribution and girder MoE were calculated. Girder MoR was then calculated using a prediction equation. As an example, the prediction equation used (Section 5.3) was Equation 5.2 (refer also Equation 3.10); an example of an improved prediction equation is Equation 3.9. Equation 3.9 is not used for two reasons. Firstly, it is based on a much smaller dataset than was used to create Equation 5.2 and it is not known how well it models the full range of in-service girders. Secondly, it is necessary to know the condition state of the girder being evaluated and for the test bridge girders this was not known since an experienced assessor was not available. In the absence of such better quantified

data, Equation 5.2 is used as a demonstration model. Because of the variation in both the MoE and MoR data, the MoR is specified as a distribution.

As indicated in section 6.4.2, the first expectation was that all girders would have an MoR above the S2 limit state. That was not the case. Only the main girders for span G-6 were above 86 MPa. The strength comparison that was applied in Section 6.4.2 can also be applied here. The mean of the test span girder MoR was 80 GPa compared to the DS-1 to DS-4 cluster of 37 girders that had a mean of 101 GPa. It may be that the strength of the test span girders may have been underestimated by 30%. The alternative inference to be made about those data is that the test span girders were of lower strength but, without testing them to destruction, this cannot be known.

The higher G-6 MoR values are also reflected in the safety indices for these two girders. The magnitude of G6-MU and G6-MD are above the magnitude of the limit state of −4.75. Of the three test spans, only G-6 (−5.1) is acceptable without reservation. The other two spans were both in need of maintenance ($-4.2 < \beta < -3.7$). This is not to suggest that the strength of the other two spans is deficient. As indicated in Section 6.4.2, at the time of testing, all three spans were capable of supporting legal loading. What is suggested is that the probability of failure is greater than expected. If the magnitude of the safety index is declining, then a time will come when the structure will fail under legal loading. This cannot be known without recording the temporal change in safety index. Again, as indicated in Section 6.4.3, if the safety index is not changing, the probability of failure will not change, providing, of course, that the bridge is not severely overloaded.

One important feature of these calculations is that they are straightforward. They can be encapsulated into a software program which could include the variations and distributions of all the relevant variables. The inclusion of a distribution in diameter in the determination of MoE is possible if a SP2000® calculation engine is incorporated. That was a level of complexity that was not possible to evaluate as part of this research. Engineers would then be able to assess a timber-bridge on a regular basis using temporal data. Maintenance regimes could be reliably planned as changes in safety indices occur.

6.4.5 SHM Application 3: Calculation of temporal safety index variation caused by surface erosion

As indicated in Section 2.4.3, the material parameters of outer layers of in-service girders can temporally change. One example is the temporal change of sapwood MoE and MoR due to

moisture. Another is the temporal loss of external material. The level of checking in a girder can vary significantly between girders and over time. An example of a low level of checking is shown in Figure 5-31. That girder was removed from a timber beam bridge at Puddledock, NSW, when the bridge was decommissioned and replaced with a concrete and steel structure c. 2009. Checks of a few millimetres depth occur that are spaced about 50 mm apart.

An example of a high incidence of checking is shown in Figure 5-33. In this example there are many checks of about 15 mm depth spaced about 15 mm apart. Both examples are from different sections of the same girder. Whether girder strength is affected by checking will depend on where it occurs. It may have little impact if the degree of checking shown in Figure 5-31 occurs near the underside of the mid-span where the girder is highly stressed in tension. Similarly, it may have little impact if the checking shown in Figure 5-33 only occurs near the neutral axis and away from both the mid-span and from the support region. However, if a high incidence of checking occurs in the highly stressed mid-span region, it will have an impact because the SMA will be decreased. How much the strength is affected will depend how on much the SMA is decreased.

In SHM Application 3 a surface erosion rate was specified and a safety index calculated. The erosion of the girder surface caused several other parameters to change synchronously. Loss of surface material, no matter where it occurs, causes a reduction in the effective girder diameter. Reduced girder diameter causes the effective SMA to decrease. The declining SMA increases the mid-span deflection to load ratio. As the mid-span deflection to load ratio increases, the span to deflection safety index decreases. There are three features of interest in this calculation. The first feature is the very low erosion rate α_d specified as 0.2 mm yr^{-1}. The second is that the effective girder lifetime calculated is similar to the lifetime of an in-service girder. The girder lifetime in this determination was specified as: the time it takes for the span to deflection limit state to be exceeded and the safety index magnitude to fall below 3.1 (refer Section 2.6.3). The third feature is that the erosion rate will probably start as soon as a girder is installed, although it may not progress linearly, as specified in this example. Because of the slow erosion rate, it will not be visible at first, but will be quantifiable by continuous deflection measurements. As the loss of surface material will progress faster in some locations than in others, the rate of change of the safety index trajectory can provide an indication of how soon girder maintenance might be required. It is important to quantify it soon after the girder has been commissioned into service since this effect is active throughout a girder's in-service life.

6.4.6 SHM Application 4: Calculation of Condition Alarm from traffic flow

A bridge load limit was estimated by performing measurements and calculations at one moment in time, as reported in SHM Determination 2. SHM Application 1 and 2 required temporal measurements and complex calculations to identify a bridge's safety index. To apply the concepts of SHM requires that an appropriate parameter is measured and intelligent action taken on the detection of a significant change in that parameter. Although the methods described in SHM Application 1 and 2 can be used to apply SHM principles, they provide outcomes that are more than required to identify a significant change. Such a significant change can be identified by examining the measured data more directly.

As indicated in relation to Experiment 2, light vehicular traffic crossing a small regional timber-bridge is of known range. The daily number of vehicles exceeding each threshold (Table 5-15) will be the same if the bridge stiffness is constant and the same vehicles cross the bridge daily. In practice, this does not happen. Some vehicles, which normally cross the bridge every day, might miss a day. Some vehicles will vary in gross mass. However, these variations can be statistically accounted for by recording running averages. The number of vehicles causing each threshold to be exceeded will vary statistically, but in an identifiable manner. A different statistical variation will occur if the bridge stiffness alters. For example, the data presented in Table 5-16 represent the number of vehicles causing the two thresholds to be exceeded for three values of bridge stiffness. At the initial bridge stiffness (750 kg mm^{-1}) all the vehicles cause Threshold 1 to be exceeded and none cause Threshold 2 to be exceeded. While at the final bridge stiffness (400 $kg.mm^{-1}$) about half the number of vehicles cause Threshold 2 to be exceeded. A ratio is obtained that will vary according to bridge stiffness if the number of vehicles that exceeds Threshold 2 is divided by the number of vehicles that exceed Threshold 1.

The Threshold 2 to Threshold 1 ratio (Table 5-16) will temporally vary according to the variation in vehicle mass. Whereas a CS-1 bridge will have a low ratio, a CS-4 bridge will have a high one. To monitor the structural health of a particular bridge, a limit state ratio would first have to be determined, based on bridge stiffness, traffic mass distribution and the threshold settings. Then the Threshold 2 to Threshold 1 ratio would be measured daily and compared to the limit state ratio. A remote alarm could be triggered if the limit state ratio is exceeded. The advantage of this type of monitoring procedure is that it depends on direct measurements, running averages and simple calculations. It can be economically performed directly at a bridge site in a low cost control and alarm telemetry system.

6.5 Discussion summary

The aim of this research was to test the hypothesis that continuous deflection monitoring can be used as a method of assessing the probability of timber-bridge failure. This required nine main objectives to be achieved:

1. the determination of the strength and elastic behaviour of a single girder
2. the determination of a measurable parameter indicative of bridge girder strength (MoE)
3. the identification of the load-v-deflection curve for an in-service girder
4. the deflection distribution caused by traffic loading
5. the effect of dynamic activity on the measurements
6. the determination of girder in-service MoE
7. the identification of the percentage of applied load supported by an in-service girder
8. the determination of girder MoR
9. the use of these data to identify a bridge limit state safety index.

Objectives 1 and 2 are discussed in Section 6.2 by interpreting data from the destructive testing of over 300 in-service girders and excised clear samples from over 100 species of timber. Detailed prediction bands for both the girders and their excised clears are calculated outcomes from this examination. Surprisingly, the prediction bands for these girders are characteristically different from those for the clears. Further outcomes are MoR model prediction equations. Coefficients of determination as high as 0.86 were achieved when both MoE and condition state were used as prediction parameters. After averaging and then regressing MoR-v-MoE data an improved coefficient of determination of 0.98 was achieved. Therefore, the prediction of individual girder MoR should be improved and the coefficient of determination significantly increased by more accurate assessments of degraded girder SMA. However, it was possible to make worthwhile predictions of MoR as shown in Chapter 5, even with coefficients of determination of about 0.6. The most important inference from these data and from the model equations generated is that to enable girder strength to be predicted in-service temporal MoE should be measured.

There are two confounding measurement concerns that can potentially influence the determination of in-service MoE. The first concern relates to the level of accuracy to which MoE can be measured and the second is the importance of timber MC. The first concern was addressed in Experiment 4 where it was experimentally determined that MoE can be measured to 0.5% tolerance. The second concern relates to whether MC contributes to the anomaly between

girder MoR-v-MoE and excised clear MoR-v-MoE. This was addressed in Determination 1, where it was demonstrated that the changes in MC were not the cause of this anomaly. This information, in combination with the data discussed in Section 2.7.3, enables the conclusion to be drawn that MC is not of prime importance in the measurement of in-service girder MoE.

Objectives 3, 4 and 5 were addressed in Experiments 1, 2 and 3, where in-service bridge parameters were measured practically with the use of low cost equipment. The first step was to determine how accurately in-service girder MoE could be measured. Others have shown in the laboratory that linear girder load-v-deflection plots can be achieved with coefficients of determination of 0.999, but they have not identified the level of variation that can occur. In Experiment 1 the same high level of linearity was achieved for an in-service girder. In addition, the statistical tolerance in the slope is shown to be about 5% to a confidence level of 95% for a single determination. This sets a minimum level to the expected variation in the measurement of MoE. In Experiment 2 it was shown that a traffic distribution can be readily attained and in Experiment 3 that dynamic vehicle activity can be readily measured.

Objective 6 was addressed in the Theoretical Analysis (Chapter 3) in Determination 2 that any girder MoR-v-MoE vector was to be found within predictable bands. In Determination 3 the hypothesis was examined that existing data in International Standards can be used to predict individual girder strength. That hypothesis failed because of insufficient standardised data. Current standards do not provide an adequate relationship for Australian hardwoods that enables individual girder MoR to be predicted from the MoE of that same girder with a known level of confidence.

In Determination 4 it was shown that in-service girder effective MoE does not remain constant. It can be both more than twice and less than half the characterised mean value of Ironbark. It is not straightforward to identify actual changes in MoE because they must be separated from those in effective SMA. The determination of any change of in-service SMA requires accurate quantification of both the girder section and of mechanical defects such as checks, splits and surface erosion. Currently, such prediction is not possible because of the lack of suitably accurate measurement equipment. However, the presence of such mechanical defects can be determined since they directly affect mid-span deflection, which can be measured accurately. The hypothesis that only SMA varies and that MoE does not vary is shown to be false. If all the changes in mid-span deflection are caused by mechanical defects, then the girder would have to increase in diameter which does not happen. Both MoE and SMA must, therefore, vary.

Reduction in MoE can be attributed to biological decay chemically altering the timber material parameters, but there is no current explanation for increases in MoE.

In Determination 5 the vector path of in-service girder MoR-v-MoE was established. This path was shown to be consistent with the model girder prediction bands, as identified in Determination 2. The major outcome from Determinations 2 to 5 is that girder MoE can be used as a predictor of girder MoR. Therefore, it is a measurable parameter, which is suitable for SHM purposes. Although there is a significant variation in the MoR-v-MoE relationship, it should be possible to reduce the level of variability in the model prediction equations with more appropriate in-service data. The data examined was derived from girders mainly at the end of their service life. To reduce the variation in these prediction equations will require data that represent the complete life cycle of a single girder.

Objective 7 was addressed in Section 6.4 (refer also Chapter 5) where three methods of calculating a bridge safety index and one method of producing a bridge condition alarm were identified. The first three methods involved the use of a numerical model. That model was created using both Timoshenko beam theory and finite element theory to represent a particular bridge span. The model and the actual span were loaded and the resulting mid-span deflections compared. These comparisons enabled the girder MoE to be calculated (Objective 7). Using these calculated values of MoE, the probability of span to deflection limit state failure was determined for each main girder. Girder MoR was predicted using the prediction models identified in the theoretical analysis and used to identify a bridge load limit (SHM Determination 2, Objective 8). The predicted values of MoR were also used to determine the possibility of structural failure using numerical Monte Carlo type techniques (SHM Application 2). These failure probabilities were then used to compute girder safety indices (Objective 9).

The nine objectives of this research were achieved and the overall research aim supported. Continuous deflection monitoring can be used as a method of assessing the probability of timber-bridge failure. Both parameters, MoE and MoR, can be determined by measuring the deflection of a timber-bridge under load. But, these parameters will vary temporally. The incidence of both heavy traffic and biological decay will also vary. The possibility of over-stress by a heavy load will increase as a timber-bridge girder temporally degrades. Any resulting small changes in MoR can be quantified by continuous deflection measurement even though they may not be visually apparent. These changes can especially be identified by using light vehicles as test loads to detect changes in effective MoE. The mid-span deflections of a timber-bridge, obtained by

continuous monitoring, can be used to calculate both a temporal safety index and the probability of bridge failure.

7 CONCLUDING REMARKS

7.1 Summary and Conclusions

Prior to this work, timber-beam bridges have been maintained by methods involving visual inspection and proof loading. This type of maintenance approach was created when timber-bridges were expected to last for decades without significant structural repair. More recently, however, this has not been the case and a large number of timber-bridges are in need of repair. In NSW, a few degraded timber-bridges have been replaced with mixed timber and concrete structures. In some instances, replacement has also occurred because the bridge service function needed upgrading; the bridge needed to be straightened and widened. However, in many other instances, a timber-bridge has been replaced by a multiple section concrete culvert and the service requirement has not changed. In these instances, an improvement is gained because the old structure is replaced with a new one that should last for decades without needing repair.

Concurrent with many timber-bridges reaching the end of their life, vehicle GVMs are also increasing. This increase in bridge loading has partly occurred because of the need to carry more freight per vehicle and partly because of the increase in the number of heavy vehicles carrying more freight. Now many of the heavier trucks are new and cross small bridges at high speed. A short single span bridge that is shorter than the distance between the axles of a large truck is only affected by the legal group axle load which is less than 20 tonne and not the total GVM. However, such a short bridge is deleteriously affected by the impact load generated by a high speed truck. A multiple span timber-bridge must of course support the total GVM as well as survive the impact loading. These types of concerns, increased loading and structural degradation, have created a need for new ways of maintaining aged timber-bridges.

Timber-bridge girders, when newly commissioned, have been well able to survive under legal loading. Excessive loading can cause excessive deflection and members of the public are aware that excessive deflection should be treated with caution. However, degraded girders can contain defects that lead to premature failure when excessively loaded and accidents have occurred when bridges have failed unexpectedly. Chapter 1 related examples where heavy vehicles were driven several times over a degraded bridge before it eventually failed. What has not been apparent to the transporters, in such instances, is whether they have contributed to the bridge deterioration. Such contribution can only be identified by continuous measurement and regular calculation of a safety index.

To be able to identify whether a structure has changed integrity, a stepwise approach must be followed. Initially, a baseline of performance must be established that is representative of a structure that has a low probability of failure. Then, at some later moment in time, the performance of the structure has to be re-assessed and compared with that baseline. If significant changes occur then the probability of failure must also be re-evaluated. Since a random excessive load or other degradation event can occur at any time, it is important that a structure is assessed on a continuous basis. This is not to suggest that any particular random load or event will necessarily cause failure, but what it may do is incrementally increase the level of girder degradation. When a temporal change in structural performance can be quantified, then any trend in degradation can be identified. Once a performance trend has been established the time to failure can be predicted within statistical limits.

The aim of this research was to determine that continuous deflection monitoring could be used to assess the probability of timber-bridge girder failure. To achieve this aim, new SHM strategies were developed to demonstrate how deflection measurements could be used to identify both the probability of girder failure and a girder safety index. It was also shown that future limit-state girder failure could be predicted by establishing a girder temporal safety index. As well as new SHM strategies, new measuring equipment was developed such that the girder mid-span deflections could be measured continuously, without interfering with traffic flow. This new equipment involved the use of new laser-based deflection measuring equipment together with high speed camera recording techniques. A commercial high resolution, high speed camera was used to capture static and dynamic mid-span deflection under low and high speed traffic loading. A proprietary low resolution and low data volume, high speed camera was developed to monitor girder mid-span deflection relative to a fixed horizontal laser beam for long term continuous measurement.

Introduction

In addition to new SHM strategies and new measurement equipment nine objectives were set to establish the aim (refer to Chapter 1). All nine measurement objectives were successfully achieved which verified that, by the measurement of continuous mid-span deflection and the application of the developed SHM strategies a bridge safety index could be computed for each of three in-service case study bridge spans. These objectives were addressed in Chapters 3 to 5. In Chapter 3, the theoretical objectives 1 and 2 were addressed by analysing DS-1 to DS-6. The results showed both a consistent relationship between MoR and MoE and that girder MoE varies throughout the life of an in-service girder as it deteriorates. Objectives 3, 4 and 5 related to in-

service measurement and were addressed in Chapter 4. In that chapter it was demonstrated how the mid-span deflection of an in-service timber-bridge could be continuously measured without interrupting traffic flow. Then in Chapter 5 objectives 6 to 9 were achieved where mid-span deflection measurements were used in the developed SHM strategies to calculate bridge safety indices.

Literature Review

The literature review revealed shortcomings in the current methods used to determine the strength of timber-bridge girders. These methods involved the use of arbitrary factors of safety that can lead to structures that may be stronger than they need be. Methods identifying how to determine the probability of failure of an aged timber-bridge were not found. It was identified that new methods of measuring deflection and new strategies for calculating probability of failure need to be developed to determine the safety of aged timber-bridges.

Datasets analysis

In Chapter 3, DS-1 to DS-6 were theoretically examined. The data examined represented two distinct groups. The first, DS-1 to DS-5 represented 338 girders removed from service while the second, DS-6 represented new and un-degraded samples from over 100 different species of tree. DS-1 to DS-4 were gained after the removal of complete bridge girders from service and the original researchers testing them in three and four point load testing frames. After examination of these data it was concluded that the complete dataset was consistent and that it comprised two independent clusters of data.

The first cluster comprised all the full sized girders and the second all the excised clears from both girders and tree species. Both clusters had a different MoR-v-MoE relationship. The DS-1 to DS-4 girder MoR-v-MoE relationship had a slope of t 0.003 (3 MPa GPa^{-1}) and the DS-5 and DS-6 excised clear relationship had a slope of 0.007 (7 MPa GPa^{-1}). Within the DS-1 to DS-4 cluster it was concluded that the data were consistent and that the only group of girders that was sparsely represented were un-degraded girders early in their service lives. However, there was a statistically significant number of girders to conclude that any girder found would have an MoR-v-MoE vector within the 95% prediction bands identified for DS-1 to DS-4 ($p < 0.0001$). The standard deviation from the mean regression line was 20 MPa. When a girder is assessed and found outside the DS-1 to DS-4 prediction bands, it should be carefully examined to determine the source of this discrepancy.

As well as there being a defined girder MoR-v-MoE relationship it was concluded that as a girder degrades, its MoR-v-MoE vector changes. Early in a girder's life it would have an MoR-v-MoE vector above the S2 limit states, but if degraded to CS-3 or CS-4 it would have an MoR-v-MoE vector with both low MoE and MoR. Further long-term research will be required to substantiate this fact/. However, , it was concluded from the available data that a girder MoR-v-MoE vector would remain within the MoR-v-MoE prediction band and move down as it deteriorated from a position of both high MoE and MoR to a position of both low MoE and MoR. In addition it was concluded firstly, that girder strength could be determined from measurements of MoE and secondly, that to determine girder MoR girder MoE should be measured.

Within the available data, relationships were discovered that were not explained in the reviewed literature. The first was the relationship between the MoR_g-v-MoE_g vector of a girder and the MoR_c-v-MoE_c vector of an excised clear sample. For an Australian hardwood such as Ironbark they were characteristically different. The possibility that the difference was just caused by differing MC was investigated and this was found not to be the case. The second relationship was that between MoR_g and MoE_g. Higher values of MoR_g were associated with higher values of MoE_g and lower values of MoR_g with lower values of MoE_g. There were also data examples found of girder MoE_g that were above the characterised mean species range for Ironbark. It was concluded from these data that explanations are required to identify how both MoR_g and MoE_g can change synchronously and how effective MoE_g can increase. These explanations will require further research.

Measurements

Experiments for measuring the variables of timber-bridge girder performance were addressed in Chapter 4. Firstly, static load-v-deflection data were gathered that showed the girder operated in a linearly elastic manner when the applied mid-span loads were restricted to about 35% of the maximum legal axle load limit; about seven tonnes. It was also shown that dynamic traffic loading data could be continuously recorded for all vehicles above about one tonne. Further, the effects of impact loads were verified by measuring the mid-span deflections caused by moving vehicles. Displacement-v-time transient response data were recorded and used to determine influence lines for an in-service test span. It was concluded that recording deflection data to an accuracy of 0.5 mm was sufficient to enable adequate accuracy for the determination of MoE using the SAP2000® finite element models examined in Chapter 5.

SHM Applications

SHM strategies were developed to determine the probability of failure from measured in-service deflection data. Finite element models were used to determine both girder effective MoE and the load distribution across the bridge deck planking. It was concluded that a CS-1 deck would not distribute the applied load evenly but would transfer 35% to the main girders and 15% to the kerb girders of a four girder timber-bridge. If the girders and deck were deteriorated, the load transferred to the kerb girders could be as low as 8%. Therefore, it is concluded that if a bridge is only inspected visually and not quantified with deflection measurement, the main girder loading for a degraded bridge could be about 20% higher than anticipated.

Girder MoE was estimated for the test bridge span girders and found to vary over the range of 12 GPa to 34 GPa. This range was similar to that found in the DS-2-2 data of 13 GPa to 38 GPa. This DS-2-2 data represented CS-1 girders of age less than two years. It was concluded that both these data sets were consistent with the S2 limit state (14 GPa) specified in this thesis as a minimum indicator of girder MoE.

Girder MoR was estimated for the test span girders using regression analysis and found to have a range of 70 MPa to 97 MPa. Only the G6-MU and G6-MD girders were above the S2 limit state of 86 MPa, the rest were below. This variation can be compared to the DS-4-1 range of 12 MPa to 130 MPa which also included girders with MoR above and below the S2 limit. It was concluded that it was reasonable to expect an in-service girder to be above the S2 limit state and that most of the test span girders needed strengthening. This conclusion was further supported by calculating the probability of failure for the test span girders. Only those girders with MoR above 90 MPa had acceptable safety indices and only the one girder (G6-MU) with MoR of 97 MPa had a safety index magnitude above 4.75 at a magnitude of 5.1. This was equivalent to a failure rate of 0.0000002 and a probability of failure of 2 in 10^7.

As part of this research new measurement equipment was developed. This equipment was used to determine the mid-span deflections of in-service test timber-bridges and those deflections then used to determine girder MoE and MoR distributions. Applied traffic load distributions were calculated directly from these deflection data. Applied stress distributions were calculated using these load distributions, then compared with the girder MoR distributions to calculate a probability of failure. Since these are in-service bridges, comparison with exact failure data will not be possible until the test girders are removed from service. The only current comparison that can be made is that those girders that were assessed visually as being of low probable strength

were also verified as being the lowest in strength. One test girder, G4-MU, had a safety index of 3.6 and significant surface rot. Another test girder was G4-MD which had a safety index of 3.7 and evidence of termite activity with a significant central pipe at one end of the girder.

In Section 5.6 it was demonstrated, using a hypothetical bridge with continuous recording, that mid-span deflection could be used to identify a declining trend in safety index. Thus, if the mid-span deflections of the test spans are continuously monitored, it will be possible to identify any change in safety index. If one of those degraded spans is strengthened, the safety index will increase. Thus, the research aim has been demonstrated by recording in-service mid-span deflection and demonstrating by calculation how those deflections can be transformed into probability of failure data and safety indices for the respective in service test span girders.

Summary

This research has shown that it is practicable to monitor timber-bridges in a continuous mode to predict degradation to a point where the bridge becomes unsafe. Unpredicted or unexpected girder failure should not occur. Girders can be maintained within known safety indices and rates of degradation can be quantified. The simple and inexpensive measurement equipment required is readily available and remote bridges can be easily instrumented with telemetry. Monitoring equipment can be mounted on one of more girders for long-term appraisal. There should be instrumentation installed, at least initially on all suspect bridges, such that SHM principles can be applied on a daily basis such that all bridge owners know the structural integrity of their bridges.

In Chapter 4 it was shown that a BDM could be used to record the mid-span deflection caused by traffic. By calibrating these deflections with known loads a traffic loading distribution was obtained. The deflection data for known loads was also compared with a finite element model to determine the in-service girder MoE. In Chapter 3 a relationship was determined that related MoR to MoE. Using this relationship enabled the determination of an in-service girder MoR distribution. The applied stress produced by the traffic loading distribution was then calculated and compared with the MoR distribution and the probability that the applied stress would exceed the ultimate material stress calculated. When such monitoring is conducted on a continuous basis, in an SHM system, it is possible to determine the probability of failure, the safety index and thereby the structural health of a bridge. By using known vehicles on a regular basis, maybe the school bus twice every weekday, the system can be kept in a known calibrated state. Any

significant change in the deflection distribution can be used to create an alarm for bridge maintenance staff.

The vehicle monitoring period should be sufficiently fast to capture the effect of every vehicle. The calculation and distribution comparison rate should be at least daily and probably hourly. The actual rate chosen will depend on the type of traffic pattern and the cost of the computing equipment. Although a low failure rate may require faster processing times to enable an hourly reporting rate, higher failure rates can be computed with standard computers. Using such a SHM system enables bridge maintenance staff to be aware that every bridge under their supervision has an adequately high safety index and also when, within half an hour, any situation of significant overload occurs.

7.2 Recommendations for further work

The measurement data recorded and the numerical calculations based on that data were of sufficient accuracy to meet the intended objectives within the scope of this research. However, in the theoretical analyses of DS-1 to DS-6 several areas were identified that need further research. It was also only possible to monitor case study bridges sufficient to set baseline performance histories. These and other test structures need to be continuously evaluated to determine the statistical limits of both the measurement and the SHM strategies developed in this research. Some of those areas that require continuing research are discussed next.

Experimental Study

1. There is a need to determine if there is a relationship between the on-set of non-linearity and MoE. This could be modelled using small clears and multiple species. If a relationship is established, then girders should be examined to determine if that same relationship is present. If such a relationship does exist, it would avoid the need for breaking girders to determine MoR. Even if there is significant variation in the relationship, the research would still be beneficial. Any girder, which because of hidden defects and a potential to fracture in a brittle manner, should not be used in a bridge. The corollary is that all bridge girders should have a non-linear region and should be tested prior to installation.
2. Structural temporal change may take a decade or more to occur to an individual girder. In addition it is not acceptable to artificially degrade an in-service girder to enable measurement theory to be verified. However, there are many degraded timber-bridges still in-service. To examine the SHM strategies developed as part of this research a degraded in-service girder

could first be strengthened, a performance baseline recorded and then gradually artificially weakened again while recording the temporal changes. This could be achieved while maintaining, at all times, a girder with an appropriately high safety index.

3. The effect of sapwood on MoR-v-MoE is not well understood. Research is needed to determine whether it is structurally better to remove or to treat it. There are two possible approaches. The first is to categorise a girder with a CAT scan to determine a typical cross-sectional density and then relate its cross-section to MoR-v-MoE measurements. The second is a theoretical analysis of a girder with a varying cross-section density, elasticity and strength.
4. Because of the variation in surface quality and degraded timber under, but near, the surface it can be difficult to accurately determine the effective SMA of an in-service girder. New methods are required to determine girder SMA.
5. It is not apparent how and why effective MoE varies. The parameters that are related to this effect need to be qualified since it may be a real change of MoE or it may be a change in a related parameter. Girders need to be examined at a cellular level to determine if damage at a micro level is significant and whether it is related to stress. This effect can be examined by comparing unstressed timber with stressed timber to determine if there is a change in MoE and relate any change to measured MoR. Cellular changes could be determined using microwave, ultrasonic or stress wave analysis techniques.
6. In the DS-1 to DS-4 data there were examples of girders with MoE twice the characterised magnitude for the species. No reason for this was found in the literature reviewed. These data need to be reproduced and could be first modelled using commercial softwood and then repeated for hardwood. It was also found that the characterised values of excised specimens did not represent full girders. Again the reasons were not explained in the reviewed literature. This experimental work might require the support of a girder or pole manufacturer to ensure appropriate samples are obtained.
7. The data examined here was for hardwood girders. The regression of MoR-v-MoE for excised samples was consistent between hardwood and softwood. Because the excised clear and the girder regressions are similar at low values of MoE and MoR, the difference between softwood clears and softwood girders might not be as significant as for hardwood. This relationship should be examined because it may lead to a better understanding of the

differences in hardwood and the outcome might have implications in relation to predicting the strength of commercial softwood beams.

8. It was demonstrated that a dynamic influence line could be developed for high speed vehicles. There is need for further research to accurately quantify the impact effect on small timber-bridges.

Experimental equipment development

9. It is expensive to transport girders to a laboratory and also expensive to use a large machine bending jig to measure girders in the vicinity of an in-service bridge. There is need for the development of a field portable device which uses two (or three) on-site bridge girders. Loading is achieved by bending one against the other with a small hydraulic jack. Laser measurement equipment is used to measure the relative deflection between the supports and a load cell to measure force applied by the jack. This type of equipment could be carried on a small vehicle.

10. Any test bridge to be evaluated requires the attachment of measurement support brackets to enable both static and dynamic deflection to be recorded. Since there are thousands of these bridges it is appropriate to create some standard measurement aids. There is a need for a bracket that is flush with decking but provides a small hole of about 30 mm that a staff can be fitted through from the top of the deck. The bracket should attach tightly around the girder and move rigidly up and down with the girder. There are two applications for such a bracket. The first application is for a bridge span above water. On the bottom end of the staff a graduated scale is fitted. A laser mounted on a tripod or other stable support is pointed at the scale. A camera is used to record the relative movement of the laser on the scale as the girder is deflected under load. The laser and camera are mounted either on bridge supports or dry ground. The dry ground could be on the bank of the water course. The second application is for a bridge span above dry ground. In this case a vernier is fitted to the bottom of the staff and a graduated scale mounted on a fixed stable tripod. A camera is used to record the vernier deflections. The bracket should be fitted to all girders on a bridge and a light vehicle used to apply a load. Any bridge with the brackets fitted can then be tested as described in this thesis.

Theoretical study:

1. There is a need to apply comprehensive finite element analysis to a range of bridges to determine the accuracy of the load percentage that is applied. Bridges that should be evaluated include both single span timber beam bridges and multiple span bridges.
2. In this research, it was demonstrated that SHM reliability based analysis techniques could be used to determine bridge safety indices. There is a need for further research on these concepts and for them to be used assessing a large variety of regional multi-span bridges constructed from both timber and other materials.
3. In Europe and North America it has been defined that timber is a cost competitive material that can be used to build structures such as bridges and multistorey buildings. There is a need to identify the economies of building large timber structures in Australia.

References

ABS. (2008). Motor Vehicle Census, Australia, 9309.0 (File mvc2008nsw.srd) Retrieved 23 February, 2010, from www.abs.gov.au

Allan, P. (1895). Timber Bridge Construction in New South Wales. Journal and Proceedings of the Royal Society of New South Wales, 29.

Ashby, M. F. (1983). The Mechanical Properties of Cellular Solids. *Metallurgical Transactions A, 14A*(September), 1755 - 1769.

Austenfeld, R. B. J. (2001). W Edwards Deming: The story of a truly remarkable person. *Research Society of Commerce and Economics, XXXXII*(1), 49-102.

B.J.P. (1969). Timber Bridge Maintenance, No. 6 District. *Queensland Roads*, 51 - 56.

Bakht, B., & Pinjarkar, S. G. (1989). *Review of Dynamic Testing of Highway Bridges*. (TRB 880532 SRR-89-01). Ontario: Ministry of Transportation.

Bazovsky, I. (1961). *Reliability Theory and Practice*. Englewood Cliffs, New Jersey: Prentice-Hall.

Bergander, A., & Salmén, L. (2002). Cell wall properties and their effects on the mechanical properties of fibers. *Journal of Materials Science, 37*(1), 151-156. doi: 10.1023/a:1013115925679

Biggs, J. M., Suer, H. S., Louw, J. M., Engineering, M. I. o. T. D. o. C., & Works, M. D. o. P. (1956). *A Theoretical and Experimental Investigation of the Vibration of Simple-span Highway Bridges*: Joint Highway Research Project.

Bodig, J. (1985, 12 September 1985). *Timber Engineering, The Strength and Durability of Timber Structures.* Paper presented at the Timber Engineering Seminar, Sydney,

Boland, D., Brooker, M., Chippendale, G., Hall, N., Hyland, B., Johnston, R., . . . Turner, J. (1984). *Forest Trees of Australia*. Collingwood, Australia: CSIRO Publishing.

Bolza, E., & Kloot, N. H. (1963). The Mechanical Properties of 174 Australian Timbers: CSIRO.

Bootle, K. R. (2004). *Wood in Australia, types properties and uses* (Second ed.): McGraw-Hill Australia Pty Ltd.

Boughton, G. N., & Crews, K. (1998). *Timber Design Handbook*. Sydney: Standards Australia.

Boughton, G. N., & Juniper, P. M. (2010). *Revision of Australian MGP Stress Grades 2009.* Paper presented at the World Congress of Timber Engineering, Italy,

Bowyer, J. L., Shmulsky, R., & Haygreen, J. G. (2007). *Forest Products & Wood Science* (Vol. Fifth). Carlton, Victoria, Australia: Blackwell Publishing Asia.

Britannica. (1975). Douglas Fir *The New Encyclopaedia Britannica* (Vol. III, pp. 641). Sydney: Helen Hemingway Benton.

Bull, J. W. (1993). The unseen timber roofs of the choir, north transept, 1-2 The College and the dorter of Durham Cathedral *Engineering a Cathedral, Durham*. London: Thomas Telford.

Canty, J. N. (1995). USA Patent No.: U. P. Office.

Carter, D., Crews, K., & Keith, J. (1991). *Stress laminated timber bridges: Old material - New technology*. Paper presented at the Bridges - Part of the Transport system, Brisbane, Australia.

Carter, D., Crews, K., & Taylor, R. J. (1992, 13-15 November). *Timber Bridges - Its time for a rethink.* Paper presented at the Timber Bridges Conference, The University of Melbourne, pp 165-171,

Chan, T. H., & Thambiratnam, D. P. (2011). *Structural Health Monitoring in Australia*. New York: Nova Publishers.

Chan, T. H., Wong, K., Li, Z., & Ni, Y. (2011). Structural Health Monitoring for Long-Span Bridges - Hong Kongexperience and Continuing onto Australia. In T. Chan & D. Thambiratnam (Eds.), *Structural Health Monitoring in Australia* (pp. 1-32). New York: Nova Science Publishers, Inc. ISBN 9781617288609

Chen, M.-H., Wang, H.-L., Chen, C.-S., & Wang, C.-Y. (2008, 27-30 October). *A study for evaluating the loading capacity to a damaged prestressed bridge.* Paper presented at the 3rd World conference on Engineering Asset Management and Intelligent Maintenance Systems (WCEAM-IMS 2008), Beijing, China, pp 308-317,

Chiswell, B., & Grigg, E. C. M. (1971). *SI UNITS, University of Queensland*. Sydney: John Wiley & Sons Australasia Pty Ltd.

Coltheart, L., & Fraser, D. (1987). Landmarks in Public Works: Engineers and their works in New South Wales 1884 - 1914 Hale & Iremonger.

Interstate road transport regulations - schedule 4, Division 2A C.F.R. (1986), Retrieved from: http://www.austlii.edu.au/au/legis/cth/consol_reg/irtr1986417/

Crawley, M. J. (2007). *The R Book*. Chichester, UK: John Wiley & Sons Ltd.

Crews, K. (1998). *Strength Assessment of Utility Poles in Australia*. Paper presented at the Electricity Association of New South Wales (EANSW) Non-destructive Evaluation (NDE) Poles Seminar, Schofields Pole Testing site and Mercure Hotel.

Crews, K. (2005). *Making Sense of Risk Management for Timber Bridges.* Paper presented at the The Australian Small Bridges Conference, Powerhouse Museum, Sydney,

Crews, K., & Ritter, M. A. (1996). *Development of limit states Design Procedures for Timber Bridges, Gen. Tech. Rep. FPL-GTR-94.* Paper presented at the National Conference on Wood Transportation Structures,

CSI. (2010). Static and Dynamic Finite Element Analysis of Structures, SAP2000® (Version Educational 14.2.4). Berkley, California: Computures and Structures, Inc.

CSIRO. (1974). Testing Timber for Moisture Content (D. o. B. Research, Trans.). Melbourne: Commonwealth Scientific and Industrial Research Organisation, Australia.

CSIRO. (2011). Light Detection and Ranging (lidar), from http://www.csiro.au/en/Outcomes/Food-and-Agriculture/LightDetectionLidar.aspx

Curling, S., Clausen, C. A., & Winandy, J. E. (2001). *The effect of hemicellulose degradation on the mechanical properties of wood during brown rot decay.* Paper presented at the The International Research Group on Wood Preservation, Nara, Japan,

Dalgaard, P. (2008). *Introductory Statistics with R* (Second ed.). New York, USA: Springer.

Dare, H. H. (1903). *Recent Road-Bridge Practice in New South Wales*. Paper presented at the Institution of Civil Engineers, London.

Decosterd, L. (1998). Description of Physical Tests and Post Mortem Procedures.

Desch, H. E. (1968). *Timber: Its structure and properties* (Fourth ed.). London: Macmillan and Company Limited.

Doyle, C. (2012). Fibre Bragg Grating Sensors: An introduction to Bragg gratings and interrogation techniques, from http://www.smartfibres.com/Attachments/Smart%20Fibres%20Technology%20Introduction.pdf

Elishakoff, I. (2004). *Safety Factors and Reliability: Friends or Foes?* : Kluwer Academic Publishers.

Faherty, K. F., & Williamson, T. G. (1995). *Wood Engineering and Construction Handbook* (Second Edition ed.): McGraw-Hill.

Farruggia, F., & Perré, P. (2000). Microscopic tensile tests in the transverse plane of earlywood and latewood parts of spruce. [10.1007/s002260000034]. *Wood Science and Technology, 34*(2), 65-82.

Ferguson, W. (2012, 18 August). Nature's wonder stuff. *New Scientist*, 24.

Fuller, A. H., Eitzen, A. R., & Kelly, E. F. (1931). Impact on Highway Bridges. *Transaction, ASCE, 95* (Paper 1786), 1089-1117.

Garratt, G. A. (1931). *The mechanical properties of wood*. New York, USA: John Wiley & Sons, Inc.

Glencross-Grant, R. (2009). Large Road Bridges in Northern NSW: 19th Century Evolution from Timber to Iron and Back Again [online]. . *Australian Journal of Multi-disciplinary Engineering, 7*(2), 117-127.

Glencross-Grant, R. (2011). The evolution of large-truss road bridges in NSW, Australia. *Heritage Engineer, Institution of Civil Engineers (ICE), UK, 165*(EH2).

Gordon, J. E. (1991). The New Science of Strong Materials or Why you don't fall through the floor (Second ed.): Penguin Books.

Brodie v Singleton Shire Council, 29 C.F.R. § 206 (2001).

Hepworth, D. G., Vincent, J. F. V., Stringer, G., & Jeronimidis, G. (2002). Variations in the morphology of wood structure can explain why hardwood species of similar density have very different resistances to impact and compressive loading. *Philosophical Transactions of the Royal Society of London. Series A: Mathematical, Physical and Engineering Sciences, 360*(1791), 255-272. doi: 10.1098/rsta.2001.0927

Heywood, R., Karagania, R., & Baade, B. (2003). *Working Together to Manage The Bridge Risk.* Paper presented at the IPWEAQ State Conference, Mackay, Queensland,

Hibbeler, R. C. (2012). *Structural Analysis* (Eight ed.): Prentice Hall.

Horrigan, A., Crews, K., & Boughton, G. N. (2000). In-Grade Testing of Utility Poles in Australia. *New Zealand Timber Design Journal, 9*(2), 17-24.

Howard, J. (2009). Road Asset Benchmarking Project 2008, Timber Bridge Management Report (pp. 32). Springwood, N.S.W., Australia: IPWEA (NSW) Roads &Transport Directorate.

Jauregui, D. V., White, K. R., Woodward, C. B., & Leitch, K. R. (2003). Noncontact photogrammetric measurement of vertical bridge deflection. *Journal of Bridge Engineering, 8*(4), 212-222.

Jiang, R., & Jauregui, D. V. (2007). A Novel Network Control Method for Photogrammetric Bridge Measurement. *Experimental Techniques, 31*(3), 48-53. doi: 10.1111/j.1747-1567.2007.00150.x

Kadar, P., Zavitski, J., Manamperi, P. B., & Mann, P. (2011). *Optimised Maintenance Program for the Sydney Harbour Bridge*. Paper presented at the International Public Works Conference, National Convention Centre, Canberra.

Krzanowski, W. J. (1998). *An Introduction to Statistical Modelling*. Bristol, UK: Arnold, Hodder Headline Group.

Kuisch, H., Gard, W., Botter, E., & van de Kuilen, J.-W. (2012). *Brittleheart as a critical feature for visual strength grading of tropical heartwood - approach of detection.* Paper presented at the World Conference on Timber Engineering, Auckland, New Zealand.

Kumamoto, H., & Henley, E. J. (1996). Probabilistic Risk Assessment and Management for Engineers and Scientists (Second ed.): IEEE Press.

Kuo, M.-L., & Arganbright, d. G. (1978). SEM observation of collapse in wood. *IAWA Bulletin, 2*(3), 40-46.

Lake, N. J. (2001). *Evaluating the Health of Bridge Structures.* (Doctor of Philosophy PhD Thesis), Queensland University of Technology, Brisbane.

Law, P. W. (1989). Timber Bridge Maintenance Study: Progress Report No. 1, Project N150: RTA.

Law, P. W., Matheson, N., & Yttrup, P. J. (1992a). Report No. N150-GRT: Girder rig testing. Unpublished: Roads and Traffic Authority of NSW.

Law, P. W., Matheson, N., & Yttrup, P. J. (1992b). Report No. N150/06: Roads and Traffic Authority of NSW.

Law, P. W., & Morris, H. (1992). *Degradation of Round Timber Bridge Girders with Time.* Paper presented at the Timber Bridges Conference, The University of Melbourne, pp 202-212,

Law, P. W., Yttrup, P. J., McTackett, P. I., & McNaught, A. (1991). *The Testing of Old and New Timber Bridge Girder Elements*. Paper presented at the Bridges - Part of the Transport System, Brisbane, QLD.

Maas, H.-G., & Hampel, U. (2006). Photogrammetric Techniques in Civil Engineeering Material Testing and Structure Monitoring. *Photogrammetric Engineering & Remote Sensing, 72*(1), 1-7.

Mahini, S., Glencross-Grant, R., & Moore, J. C. (2011, August 21-24). *Structural Health Monitoring of Older Bridges: Current studies in Australia and Worldwide.* Paper presented at the International Public Works Conference, Canberra, Published on line by IPWEA.

MathWorks. (2011). MATLAB® Student version (Version 7.12.0.635 (R2011a)). Natick, Massachusetts 01760 USA The MathWorks.

McTackett, P. I. (1991). *Timber Bridge Maintenance Study*. Paper presented at the BRIDGES - Part of the Transport System, Brisbane, QLD.

Melchers, R. E. (1999). *Structural Reliability Analysis and Prediction*. Chichester: John Wiley & Sons.

Moore, J. C. (2009). *Monitoring Timber Beam Bridges for Structural Health.* (MSc Research Thesis), School of Environmental and Rural Science, University of New England (UNE), Armidale, NSW, Australia.

Moore, J. C., Glencross-Grant, R., Mahini, S., & Patterson, R. (2012). Regional Timber Bridge Girder Reliability: Structural Health Monitoring and Reliability Strategies. *Advances in Structural Engineering, 15*(5). doi: 10.1260/1369-4332.15.5.793

Moore, J. C., Glencross-Grant, R., & Patterson, R. (2009, 14 June). *How to stop the rot? Continuous monitoring of short span timber beam bridges.* Paper presented at the Institution of Engineers Australia NSW Regional Convention, Grafton, NSW, Australia,

Moore, J. C., Mahini, S., Glencross-Grant, R., & Patterson, R. (2011, August 21-24). *How do Australian Bridges Stack up? A comparative study with international timber bridge developments.* Paper presented at the International Public Works Conference, Canberra, Published on line by IPWEA.

Mufti, A. (2001). *Guidelines for Structural Health Monitoring*. Manitoba, Winnipeg: ISIS Canada.

Newell, H. H. (1938). Road Engineering and its Development in Australia 1788-1938. *Journal of the Institution of Engineers, Australia, 10*(3), 97-104.

Nolan, G. (2006). Experience with Concrete Overlayed Bridges in Tasmania Retrieved 19 May, 2011, from: http://oak.arch.utas.edu.au/research/bridge/sem2.asp

Roads Act No 33 (1993).

Oldfield, K. A., & McTackett, P. I. (1991). *Skinners Swamp - a new bridge*. Paper presented at the Bridges - Part of the Transport System, Brisbane, QLD.

Piot, S. (2010). *Novative Solutions for Heritage Structures Monitoring*. Paper presented at the Conservation of Heritage Structures, Proceedings of CSHM-3, Ottawa.

Putt, I., Chandler, I., & Margetts, L. (1992, 13-15 November). *A strength assessment method for timber bridges.* Paper presented at the Timber Bridges Conference, The University of Melbourne, pp 78-91,

QDMR. (2004). *Bridge Inspection Manual*. Brisbane, Australia: Queensland Government, Department of Main Roads.

QDMR. (2005). *Timber Bridge Maintenance Manual*. Brisbane, Australia: Queensland Government, Department of Main Roads.

Rasgsdale, J. (2004). Vibromet(tm) 500V: Single Point Laser Doppler Vibrometer *(Advertisement Brochure).*

Record, S. J. (1914). The Mechanical Properties of Wood, from http://www.freeinfosociety.com/media.php?id=2216

Roads and Maritime Services. (2012). Timber Bridge Partnership Retrieved 1 September 2012, from http://www.rta.nsw.gov.au/roadprojects/projects/maintenance/timber_bridges.html

Roorda, J. (2006). Road Asset Benchmarking Project, Timber Bridge Management (pp. 26). Springwood, N.S.W., Australia: IPWEA (NSW) Roads &Transport Directorate.

RTA. (2006). Bridges types in NSW, Historical Overviews. In N. R. a. T. Authority (Ed.), (pp. 126): RTA.

RTA. (2007). Bridge Inspection Procedure Manual (Second ed.): Roads and Traffic Authority of New South Wales.

RTA. (2008). Timber Bridge Manual. In E. T. B. Bridge Engineering (Ed.): Roads and Traffic Authority of NSW.

Samali, B., Li, J., & Crews, K. (2007). Load Rating of impaired Bridges Using a Dynamic Method. *Electronic Journal of Structural engineering, Special Issue*, 66 - 75.

Savino, T. (1988). 4843372. US Patent Office.

Simon, P., Maigre, H., Bigorgne, L., Eyheramendy, D., & Jullien, J.-F. (2010). *Multi-Scale Study of the Variability in Softwood Transverse Elasticity*. Paper presented at the WCTE 2010, Riva del Garda, Italy.

Standards Australia. (2000). AS 2878:2000 Timber - classification into Strength Groups. Sydney: Standards Australia.

Standards Australia (2004a). Australian Standard Bridge Design: AS 5100.1 Part 1: Scope and General Principles. (AS 5100.1-2004). Sydney, NSW: Standards Australia

Standards Australia (2004b). Australian Standard Bridge Design: AS 5100.1 Part 7: Rating of existing bridges. (AS 5100.7-2004). Sydney, NSW: Standards Australia

Standards Australia (2004c). Australian Standard Bridge Design: AS 5100.1 Part 2: Design Loads. (AS 5100.2-2004). Sydney, NSW: Standards Australia

Standards Australia (2010). Australian Standard Timber Structures: AS 1720.1 Part 1: Design Methods. (AS 1720.1-2010). Sydney, NSW: Standards Australia

Talebinejad, I., Fischer, C., Ansari, F., & Bojidar, S. Y. (2010). *Structural Health Monitoring of the Masonry Vaults of the Brooklyn Bridge.* Paper presented at the CSHM-3 International Workshop on Preservation of Heritage Structures Using ACM and SHM, Ottawa, ON CA

Tannert, T., Berger, R., Vogel, M., & Muller, A. (2011). *Remote Moisture Monitoring of Timber Bridges: A Case Study*. Paper presented at the 5th International Conference on Structural Health Monitoring of Intelligent Infrastructure, SHMII-5, Cancun, Mexico.

Taylor, J. S. (1985). *"Load Testing"* Paper presented at the Timber Bridges, Seminar at Monash University, The Centre for Continuous Education.

Tomiolo, A. (1989). USA Patent No. 4889997. U. P. Office.

Troy, M. (2011). Media Release - MIDGOC meeting Retrieved 25 April, 2011, from http://bellingen.local-e.nsw.gov.au/news/pages/7969.html

Tsakanika-Theohari, E., & Mouzakis, H. (2010). *A Post-Byzantine mansion in Athens. The restoration project of the timber structural elements*. Paper presented at the WCTE 2010, Riva del Garda, Italy.

Tsakiri, M., Ioannidis, C., Papanikos, P., & Kattis, M. (2004, 1 July). *Load Testing Measurements for Structural Assessment Using Geodetic and Photogrammetric Techniques.* Paper presented at the 1st FIG International Symposium on Engineering Surveys for Construction Works and Structural Engineering, Nottingham, United Kingdom, pp 1-14,

Tseng, T.-J. (2010). *Evaluation of wooden purlins using the drill resistance test.* Paper presented at the World Conference on Timber Engineering, Riva del Garda, Italy,

Tyson, G. R. (1992, 13-15 November). *A hydrostatic deflection measuring rig for timber bridges.* Paper presented at the Timber Bridges Conference, The University of Melbourne, pp 373-381,

US Department of Defense. (1991). Military Handbook: Reliability Prediction of Electronic Equipment, MIL-HDBK-217F.

VICROADS. (2011). *Road structures inspection manual*. Camberwell, VIC, AUS.

Wikipedia. (2012). LIDAR speed gun, from http://en.wikipedia.org/wiki/LIDAR_speed_gun

Wilkinson, K. (2008). *Capacity Evaluation and Retrofitting of Timber Bridge Girders.* (PhD Research Thesis), Queensland University of Technology, Brisbane.

Wolfram, J. (2004). *Structural Safety and Reliability* Heriot-Watt, University, Edinburgh.

Worden, K., Farrar, C., Manson, G., & Park, G. (2007). The fundamental axioms of structural health monitoring. *Proceedings of the Royal Society, 463*(2082), 1639-1664.

Yoneyama, S., Kitagawa, A., Iwata, S., Tani, K., & Kikuta, H. (2007). Bridge Deflection Measurement using Digital Image Correlation. *Experimental Techniques, 31*(1), 34-40. doi: 10.1111/j.1747-1567.2006.00132.x

Yttrup, P. J., Law, P. W., & Audova, H. (1991). *The mechanics of timber beam bridges*. Paper presented at the Bridges - Part of the Transport system, Brisbane, Australia.

Yttrup, P. J., Law, P. W., & Subramaniam, H. (1991). *Analysis and determination of safe working load limits for timber beam bridges*. Paper presented at the Bridges - Part of the Transport system, Brisbane, Australia.

Yttrup, P. J., & Nolan, G. (1996). *Performance of Timber Beam Bridges in Tasmania, Australia.* Paper presented at the International Wood Engineering Conference, New Orleans, Louisiana, USA, pp 75-80,

Appendix A

Example scripts

Thesis figures were produced using the following scripts. In some cases the data was directly available and the script was run using the R program. Details of the R program are provided in numerous texts such as Crawley (2007) and Dalgaard (2008), as identified in the reference list. In other cases data was first analysed using MatLab and then the figure was produced using R. Both R and Matlab could be used, in most cases interchangeably. Because of prior experience MatLab was used for engineering calculations and R for statistical data. Details of MatLab can be obtained from Mathworks (refer Glossary). In the R script all comments are preceded by the # symbol and in the Matlab script by the % symbol.

1. Figure 3-2, DS-1 source data and script
2. Figure 4-27, Truck transient source data and script
3. Figure 4-31, Static influence line, script
4. Figure 5-13 and 5-14, SHM Application 1, Evaluation of a deflection limit state
5. Figure 5-19, Evaluation of a combined Log-normal Stress & MoR distribution, Experiment PC-MU
6. Figure 5-36, Evaluation of a deflection limit state set by surface erosion

1. Figure 3-2, DS-1 source data and script

DS-1 data: DS1.TXT

"N"	"MoE2"	"MoR2"	"N"	"MoE2"	"MoR2"	"N"	"MoE2"	"MoR2"
1	23.74702	83.07692	33	6.563246	23.07692	65	8.711217	17.14286
2	15.33413	73.18681	34	6.181384	34.28571	66	8.830549	15.82418
3	15.99045	66.59341	35	6.443914	30.98901	67	9.427208	29.67033
4	16.40811	65.27473	36	6.682578	29.67033	68	9.844869	30.32967
5	16.82578	63.95604	37	7.875895	23.07692	69	10.08353	16.68132
6	17.74463	61.64835	38	8.114558	23.73626	70	10.44153	20.76923
7	19.45107	56.37363	39	8.448687	10.54945	71	10.50119	28.02198
8	10.02387	58.35165	40	7.458234	9.89011	72	10.50119	31.31868
9	14.37947	60	41	7.040573	10.54945	73	10.26253	33.62637
10	16.10979	60.65934	42	7.21957	13.51648	74	10.73986	34.94505
11	18.43675	52.74725	43	7.398568	14.50549	75	12.2315	13.51648
12	18.37709	32.96703	44	7.696897	13.84615	76	12.50597	18.65934
13	18.13842	19.45055	45	15.45346	46.48352	77	11.81384	19.45055
14	1.849642	7.582418	46	15.63246	36.92308	78	11.57518	20.24176
15	2.565632	10.54945	47	17.42243	41.86813	79	10.97852	25.05495
16	2.804296	8.571429	48	16.57518	46.81319	80	11.27685	24.3956
17	3.818616	9.89011	49	7.374702	44.17582	81	11.45585	30
18	4.272076	8.901099	50	9.844869	37.58242	82	11.51551	32.10989
19	4.868735	7.912088	51	7.362768	42.1978	83	11.69451	30.98901
20	4.713604	11.20879	52	7.5179	38.24176	84	12.3747	32.30769
21	4.116945	12.52747	53	8.591885	33.2967	85	13.38902	32.96703
22	3.329356	15.16484	54	8.472554	44.17582	86	11.19332	38.24176
23	4.653938	17.14286	55	7.637232	29.34066	87	11.69451	36.59341
24	3.699284	26.83516	56	7.875895	33.2967	88	10.38186	43.84615
25	3.102625	34.08791	57	7.995227	31.31868	89	10.40573	43.84615
26	5.883055	7.78022	58	7.875895	32.96703	90	12.74463	39.36264
27	5.727924	10.87912	59	9.785203	40.21978	91	13.24582	45.82418
28	6.026253	13.05495	60	9.486874	42.85714	92	11.57518	44.17582
29	5.906921	16.15385	61	8.890215	25.05495	93	11.19332	49.97802
30	5.429594	20.10989	62	9.725537	21.75824	94	11.63484	52.28571
31	6.026253	21.0989	63	8.830549	19.45055	95	14.34368	46.68132
32	6.682578	18.72527	64	8.591885	18.46154			

R script

```
# DS1.TXT contains data interpolated from Yttrup's Figure 4

library("car")
library("calibrate")

DMoE <- c(0,50)      # Default range
DMoR <- c(0,200)     # Default range


dev.new(width=4, height=3)
par(font.axis=2,font.lab=2,cex=1,mar=c(4,4,0.8,1),font=2,lwd=2)

plot(DMoE,DMoR,type="n",xlim=c(0,50),
 ylim=c(0,200),ylab="MoR (MPa)",xlab="MoE (GPa)")
grid(nx=NULL,ny=NULL,lty=1,lwd=1,col="gray80",equilogs = TRUE)

DS1 <- read.table("DS1.TXT",header=T)
attach(DS1)
```

```
DS1CC = DS1
# DS1CC[1,3]=NA
DS1CC <- DS1CC[complete.cases(DS1CC),]
DS1CC
MoE2 = DS1CC[,2]          # MoE2 = MoES in DS1.txt
MoR2 = DS1CC[,3]          # MoR2 = MoRS in DS1.txt

lm.DS1CC <- lm(MoR2~MoE2)
summary(lm.DS1CC)

pred.frame <- data.frame(MoE2=0:50)
pc <- predict(lm.DS1CC, int="c", newdata=pred.frame, level=0.95)
pp <- predict(lm.DS1CC, int="p", newdata=pred.frame, level=0.95)

# This will plot the data from DS1.txt as per Figure 3.2
plot(MoE2,MoR2,xlim=c(0,50),
 ylim=c(0,200), pch=1, col="purple",ylab="MoR (MPa)",xlab="MoE (GPa)")
pred.MoE2 <- pred.frame$MoE2
matlines(pred.MoE2,pc,lwd=c(3,1,1),lty=c(1,2,2), col="purple")
matlines(pred.MoE2, pp,
 lwd=c(3,1,1),lty=c(1,2,2), col=c("purple","red","red"))

grid(nx=NULL,ny=NULL,lty=1,lwd=1,col="gray80",equilogs = TRUE)

abline(h=86,lty=2)            # add horizontal line
abline(v=14.2,lty=2)          # add vertical line
text(5,96,"86 MPa")
text(8,190,"14 GPa >")

length(DS1CC[,1]) # = 95
# Tolerance on slope for df = 95 - 2 = 93
# L1*L2 = tolerance in slope = s x t*  (Keubler & Smith p276)
L1 <- qt(c(.025, .975), df=93)[2] #  = t* = 1.985802
L2 <- coef(summary(lm.DS1CC))[2,2] # Std Error wrt MoE
L1*L2 # MoRIB~ MoEIB, [ = t* x Std Error wrt MoE]  = 0.5505775

# This accentuates the data for girder #68

points(10,30,cex=1.5,pch=1) # Girder DS-1 #68

legend("bottomright",c("DS-1  ","95% Prediction Limit    ","Girder #68"),
 cex=0.7,lty=c(1,1,-1),pch=c(1,1,1),
 col=c("purple","red","black"),inset=0.02)
```

2. Figure 4-27, Truck transient source data and script

Data file: Truck4t4.txt

Time	Delta
0.00	-0.00
0.30	-0.20
0.91	-0.50
1.06	-1.00
1.50	-1.50
2.36	-2.00
2.78	-2.50
3.22	-3.00
4.00	-4.00
4.79	-4.50
5.10	-5.00
6.13	-5.00
7.54	-4.00
8.39	-3.00
9.17	-2.00
10.26	-1.00
11.14	-0.00

R script

```
# Figure 4-27, 4T4 Truck transient

library("car")
library("calibrate")

rm(list = ls()) # removes all in list
detach() # removes object in position 2
search()
ls()

# This will plot the Deflection transient (Delta)-v-time for the Truck4t4.txt data
XRange <- c(0,12)
YRange <- c(-6,0)
dev.new(width=4, height=3)
par(font.axis=2,font.lab=2,cex=1,mar=c(4,4,0.8,1),font=2,lwd=2)
plot(XRange,YRange,type="n",xlim=XRange,ylim=YRange,
 ylab="Deflection at midspan (mm)",
 xlab="Time from Front axle loading bridge (sec)")
grid(nx=NULL,ny=NULL,lty=1,lwd=1,col="gray80",equilogs = TRUE)

T4T4 <- read.table("Truck4t4.txt",header=T)
attach(T4T4)
lines(T4T4[,1],T4T4[,2],col="blue")                # T4T4[,1] = Time, T4T4[,2] = Delta
points(T4T4[,1],T4T4[,2],col="blue",pch=19)
```

3. Figure 4-31, Static influence line, script

R script

```
library("car")
library("calibrate")

rm(list = ls()) # removes all in list
detach() # removes object in position 2
search()
ls()

# Deflection transient-v-time graph ~ this creates the background graph axes
XRange <- c(-6,7)
YRange <- c(-6,0)

dev.new(width=9, height=3)
par(font.axis=2,font.lab=2,cex=1,mar=c(4,4,0.8,1),font=2,lwd=2)

plot(XRange,YRange,type="n",xlim=XRange,ylim=YRange,
 ylab="Deflection at midspan (mm)",
 xlab="Position of front axle from detector (m)")
grid(nx=NULL,ny=NULL,lty=1,lwd=1,col="gray80",equilogs = TRUE)

T4T4 <- read.table("Truck4t4.txt",header=T)
attach(T4T4)
Delta <- T4T4[,2]
# T4T4

# Calculate distance from time data
AxleSpacing = 2.6 # (m) wheelspan of 4.4 tonne light truck
S = 8.6 # (m) Span as at Power's Creek
HS = S/2 #  (m) Halfspan
Tmax = max(T4T4[,1])
speed = (AxleSpacing + S) / Tmax # (m/sec)
Dist <- Time * speed - S/2

points(Dist,Delta,pch=19,col="red",cex=1.2)

D = 0.463 # (m) Girder diameter
MoE = 17 # (GPa)
E = MoE * 1e9
I = pi * D^4/64 # (m^4) Second moment of area
PMA1 = 20.4 # (kN) measured front axle load
PMA2 = 22.8 # (kN) measured rear axle load
LS = 0.394 # load sharing fraction for PC-MU
PA1 = PMA1 * LS * 1000 # (N)
PA2 = PMA2 * LS * 1000 # (N)
F1 = -PA1/6/E/I
F2 = -PA2/6/E/I
```

```
Dist1 <- seq(0,S+AxleSpacing,0.1)
LD1 = length(Dist1)
Delta1 <- rep(0,LD1)
Dist2 <- Dist1
Delta2 <- rep(0,LD1)

# Calculate the effect of the first axle
for(i in 1:LD1)
{
 a = Dist1[i]
 Delta1[i] <- ifelse(a < S, F1*(HS*(S-a)/S*(2*a*S-a^2-HS^2)),0)
 Delta1[i] <- ifelse(a < HS, Delta1[i] + F1*(HS-a)^3, Delta1[i])
 }
lines(Dist1-HS,Delta1*1000,col="blue")

# Calculate the effect of the second axle
for(i in 1:LD1)
{
 a = Dist2[i] - AxleSpacing
 Delta2[i] <- ifelse(a < S, F2*(HS*(S-a)/S*(2*a*S-a^2-HS^2)),0)
 Delta2[i] <- ifelse(a < HS, Delta2[i] + F2*(HS-a)^3, Delta2[i])
 Delta2[i] <- ifelse(a < 0, 0, Delta2[i])
 }

# Now add the calculated influence line data to the background plot

lines(Dist2-HS,Delta2*1000,col="orange")

lines(Dist1-HS,(Delta1+Delta2)*1000,col="green")

abline(v=-4.3)
abline(v=4.3)

legend("bottomright",cex=0.7,inset=0.02,lty=c(1,1,1,-1),pch=c(NA,NA,NA,19),
 c("Front Axle  ","Rear axle  ","Combined axles   ","Measured  "),
 col=c("blue","orange","green","red"))
```

4. Figure 5-13 and 5-14, SHM Application 1, Evaluation of a deflection limit state

MatLab script

```
% Evaluation of a deflection limit state
% Traffic load distributions, Table 4-8
% These data account for bridge stiffness, BDM thresholds and
% traffic volumes and represent the total applied traffic load.
%         Mean        STD
% PC-MU   3.0         0.42
% G4-MD   2.3         0.40
% G6-MU   2.6         0.40

% Girder Data, Table 5-7
% PC-MU     PC-MD   G4-MU   G4-MD   G6-MU   G6-MD
% 0.463     0.490   0.450   0.430   0.455   0.456   Diameter, D
% 8.6       8.6     10.6    10.6    10.6    10.6    Span, L
% 0.394     0.463   0.344   0.320   0.381   0.38    Load factor, Lf
% 20        20      19      22      28      26      MoE

%The following calculates the data shown in Figure 5-15
% Girder G6-MD refer Section 5.4.3
mean_PLN = 4.0; % (kN) Mean load log-normal distribution
std_PLN  = 0.60; % (kN) Standard deviation log-normal distribution
D = 0.456; % (m)
L = 10.6; % (m) Span
Lf = .38; % load distribution factor
MoE = 26; % (GPa) Mean MoE
d_limit = 600; % deflection limit state 1:d_limit
% d_limit = 380; % deflection limit state 1:d_limit
setnum = 10^6;

MP = mean_PLN * Lf; % (kN) mean load
SP = std_PLN;  % (kN) std of load
d_crit = L/d_limit; % (m) Max deflection for 1:d_limit

P = zeros(setnum,1); % Applied bending stress
d = zeros(setnum,1); % deflection
CountFail = 0;

for g = 1:setnum
   % creating a set of uniformly distributed random numbers
   u1 = rand(1);
   u2 = rand(1);

   % Calculate randomised applied load (N)
   P(g) = exp(MP + SP * sqrt(-2*log(u1))* cos(2*pi*u2));
%    P(g) = exp(mean_PLN + std_PLN * sqrt(-2*log(u1))* cos(2*pi*u2));

   % Calculate deflection (m)
```

```
    d(g) = (4*L^3/3/pi)*P(g)*1000/(MoE * 1e9)/D^4; % (m)

    if ((d_crit - d(g)) < 0 )
     CountFail = CountFail + 1;
    end
end

index=find(d==max(d));

sprintf('Girder diameter = %0.3f (m)', D)
sprintf('MoE = %3.1f (GPa)', MoE)
sprintf('Limit state deflection for a 1:%d limit = %3.2f (mm)',...
    d_limit, d_crit *1000)
sprintf('Number of limit state failures = %d', CountFail )
sprintf('Maximum deflection = %3.1f (mm)', d(index)*1000)
sprintf('Number of calculations = %d', setnum)

[Y,X] = hist(d*1000,100);
plot(X,Y,'b','LineWidth',2);
set(gca, 'FontSize', 18);
% axis([ 0 15 0 15e5]);
hold on;
xlabel('Mid-span deflection (mm)','FontSize',18)
ylabel('Frequency','FontSize',18)
hold off

TX = X'; % Transpose to a column array
TY = Y'; % Transpose to a column array
TXY = horzcat(TX,TY); % Combine into a two column array
csvwrite('G6MD.txt',TXY);  # this is the data generated for girder G6MD
```

R script

```
# PCMU Limit state deflection
# This script is adapted to also suit PCMD, G4MU, G4MD, G6MU, G6MD
# first run above Matlab script to generate the required data set

XRange <- c(0,8)
YRange <- c(0,100000)

dev.new(width=4, height=3)
par(font.axis=2,font.lab=2,cex=1,mar=c(4,4,0.8,1),font=2,lwd=2)

plot(XRange,YRange,type="n",xlim=XRange,ylim=YRange,
 ylab="Frequency",
 xlab="Mid-span deflection (mm)")
grid(nx=NULL,ny=NULL,lty=1,lwd=1,col="gray80",equilogs = TRUE)

PCMU <- read.table("PCMUD.txt",header=T)  # this reads the required data
attach(PCMU)
```

```
lines(PCMU[,1],PCMU[,2],col="blue",pch=19)
# points(PCMU[,1],PCMU[,2],col="blue",pch=19)

legend("topright",c("PC-MU    "),
 cex=0.7,lty=c(1),inset=0.05,pch=c(1),col=c("blue"))
```

5. **Figure 5-19, Evaluation of a combined Log-normal Stress & MoR distribution, Test span PC-MU**

MatLab script

% The data to plot is first created using the following

```
% File Name: ExpPCMU_MoR.m
% Experiment PCMU

mean_MoR = 72.2; % (MPa)
std_MoR = 18.54; % (MPa)

mean_PLN = 3.0; % (kN) Mean load log-normal distribution
std_PLN  = 0.420; % (kN) Standard deviation log-normal distribution
L = 8.6; % (m) Span
D = 0.463; % (m) Girder diameter
LF = 0.394; % Load fraction
Fmax = 0;

setnum = 10^7;
F = zeros(setnum,1); % Applied bending stress
MoR = zeros(setnum,1);
XF = zeros(setnum,1);
YF = zeros(setnum,1);
XR = zeros(setnum,1);
YR = zeros(setnum,1);
CountFail = 0;

for g = 1:setnum
   % creating a set of uniformly distributed random numbers
   u1 = rand(1);
   u2 = rand(1);
   u3 = rand(1);
   u4 = rand(1);
   % Calculate randomised stress (MPa)
   F(g) = exp(mean_PLN + std_PLN * sqrt(-2*log(u1))...
      * cos(2*pi*u2))* 8 * L / pi / D^3 / 1000 * LF;
   if F(g) > Fmax
      Fmax = F(g);
   end
   % Calculate randomised MoR
   MoR(g) = mean_MoR + std_MoR * sqrt(-2*log(u3)) * cos(2*pi*u4);
   if ((MoR(g) - F(g)) < 0 )
      CountFail = CountFail + 1;
   end
end

CountFail % print out the number of fails ~ 87 IN 10^6
Fmax % print out the max stress ~ 13.92
```

```
[YF,XF] = hist(F,200);
[YR,XR] = hist(MoR,200);


OP = 0;
if OP == 1
   [NF,CF] = hist(F,200);
   plot(CF(1:200),NF(1:200),'k','LineWidth',2);
   set(gca, 'FontSize', 18);
%     axis([ 0 150 0 3500 ]); % 10^5
%     axis([ 0 150 0 45000 ]); % 10^6
axis([ 0 20 0 500 ]); % Amplified scale
%     text(250,2.4e5,'n = 10^7', 'FontSize',18);
%     text(250,2.7e5,'n^* = 6', 'FontSize',18);
%     text(5,2.5e5,'\leftarrow Demand Stress','FontSize',18);
%     text(200,2e5,'\leftarrow Capability Stress','FontSize',18);
   % bar(C,N,'hist','b');
   hold on
   [NR,CR] = hist(MoR,200);
   plot(CR(1:200),NR(1:200),'k','LineWidth',2);
   % bar(C,N,'hist','b');
   xlabel('Stress (MPa)','FontSize',18)
   ylabel('Frequency','FontSize',18)
   hold off
end

TXF = XF'; % Transpose to a column array
TYF = YF'; % Transpose to a column array
TXR = XR'; % Transpose to a column array
TYR = YR'; % Transpose to a column array
% TXYFR = horzcat(TXF,TYF,TXR,TYR); % Combine into a four column array
TXYF = horzcat(TXF,TYF); % Combine into a two column array
TXYR = horzcat(TXR,TYR); % Combine into a two column array
FR = horzcat(TXYF,TXYR);
csvwrite('PCMU.txt',FR);              %this is the resultant data
```

R Script

```
# Now use this script to plot results
# PCMU Load bending stress cp MoR
# This script is adapted to also suit PCMD, G4MU, G4MD, G6MU, G6MD

XRange <- c(0,200)
YRange <- c(0,600)

dev.new(width=4, height=4)
par(font.axis=2,font.lab=2,cex=1,mar=c(4,4,0.8,1),font=2,lwd=2)

plot(XRange,YRange,type="n",xlim=XRange,ylim=YRange,
 ylab="Frequency (X 1000)",
```

```
 xlab="Stress (MPa)")
grid(nx=NULL,ny=NULL,lty=1,lwd=1,col="gray80",equilogs = TRUE)

# Read required data created with Matlab
PCMUR <- read.table("PCMUR.TXT",header=T)
attach(PCMUR)

lines(PCMUR[,1],PCMUR[,2]/1000,col="blue",pch=19)
lines(PCMUR[,3],PCMUR[,4]/1000,col="purple",pch=19)

legend("topright",c("Applied stress   ","PC-MU MoR   "),
 cex=0.7,lty=c(1,1),inset=0.05,pch=c(NA,NA),col=c("blue","purple"))

# Deflection distribution ~ overlap region
XRange <- c(0,10)
YRange <- c(0,1)

dev.new(width=4, height=4)
par(font.axis=2,font.lab=2,cex=1,mar=c(4,4,0.8,1),font=2,lwd=2)

plot(XRange,YRange,type="n",xlim=XRange,ylim=YRange,
 ylab="Frequency (X 1000)",
 xlab="Stress (MPa)")
grid(nx=NULL,ny=NULL,lty=1,lwd=1,col="gray80",equilogs = TRUE)

lines(PCMUR[,1],PCMUR[,2]/1000,col="blue",pch=19)
lines(PCMUR[,3],PCMUR[,4]/1000,col="purple",pch=19)

legend(1.5,1,c("Applied stress   ","PC-MU MoR   "),
 cex=0.7,lty=c(1,1),inset=0.05,pch=c(NA,NA),col=c("blue","purple"))
text(3,0.5,"Failure region")
arrows(3,0.48,5,0.2,length =0.1,col="gray70")

text(2.2,0.05,"Failure rate:",col="red")
text(5,0.05,"742 in",col="red")
text(6.3,0.06,expression(10^7),col="red")
text(3.5,0.7,"Fmax = 16.4 MPa",col="blue")
```

6. Figure 5-36, Evaluation of a deflection limit state set by surface erosion

MatLab script

```
% File Name: S_erosion
% Evaluation of a deflection limit state set by surface erosion
% Source data is first defined [Refer file: Deflection Limit States.123]

mean_E = 23.65; % (GPa) Mean Ironbark

mean_P = 40; % (kN) Mean load
% std_P  = 20; % (kN) 50% of 40 kN
% std_P  = 12; % (kN) 30% of 40 kN
std_P  = 10; % (kN) 25% of 40 kN
% std_P  = 4; % (kN) 10% of 40 kN

% mean_P = 15; % (kN) Mean load
% std_P  = 5; % (kN) 33% of 15 kN

L = 8.6; % (m) Span

OD = 0.488; % (m)
d_limit = 600; % deflection limit state 1:d_limit
d_crit = L/d_limit; % (m) Max deflection for 1:d_limit

Decade = 5;
setnum = 10^Decade;
P = zeros(setnum,1); % Applied bending stress
Xd = zeros(setnum,1);
Yd = zeros(setnum,1);
CountFail = 0;

K = (4*L^3/3/pi)/ (mean_E * 1e9)  / OD^4;

for g = 1:setnum
   % creating a set of uniformly distributed random numbers
   u1 = rand(1);
   u2 = rand(1);

   % Calculate randomised applied load (N)
   P(g) = (mean_P + std_P * sqrt(-2*log(u1)) * cos(2*pi*u2)) *1000;

   % Calculate deflection (m)
%    d(g) = (4*L^3/3/pi) * P(g) / (mean_E * 1e9)  / OD^4; % (m)
    d(g) = K * P(g); % (m)

   if ((d_crit - d(g)) < 0 )
      CountFail = CountFail + 1;
   end
end
```

```
sprintf('Girder diameter = %0.3f (m)', OD)
sprintf('Limit state deflection for a 1:%d limit = %f (m)', d_limit, d_crit)
sprintf('Number of limit state failures = %d in 10^%d',...
    CountFail,Decade )
sprintf('Maximum deflection = %0.3f (mm)', max(d)*1000)

[Yd,Xd] = hist(d,200);

TXd = Xd'; % Transpose to a column array
TYd = Yd'; % Transpose to a column array
TXYd = horzcat(TXd,TYd); % Combine into a two column array
csvwrite('SE7.txt',TXYd*1000);      % Data Output
```

R script

```
# Now plot the data
# SE1-7 Surface erosion deflection cp limit state

SE7 <- read.table("SE7.TXT",header=T)
attach(SE7)

# Create background graph axes
# Deflection distribution
XRange <- c(0,20)
YRange <- c(0,2500)

dev.new(width=4, height=4)
par(font.axis=2,font.lab=2,cex=1,mar=c(4,4,0.8,1),font=2,lwd=2)

plot(XRange,YRange,type="n",xlim=XRange,ylim=YRange,
 ylab="Frequency (X 1000)",
 xlab="Mid-span deflection (mm)")
grid(nx=NULL,ny=NULL,lty=1,lwd=1,col="gray80",equilogs = TRUE)

# Add data created with Matlab
lines(SE7[,1],SE7[,2]/1000,col="blue",pch=19)
abline(v=14.3,lty=2)
text(10.8,2100,"14.3 (mm) >>")     # Annotate graph
text(17.1,1600,"Failure")
text(17.1,1450,"region")

legend("topleft",c("D = 500 (mm)  "),
 cex=0.8,lty=c(1),inset=0.02,pch=c(NA),col=c("blue"))

text(17.6,1200,"Set size:")
text(17,980,expression(10^5))
text(17,750,"Fails:")
text(17,600,"2")
arrows(17,500,15,20,length =0.1,col="gray50")
```

APPENDIX B

Theoretical Analysis: Prediction of Girder Strength from Historical Datasets

This section is a discussion of the results related to the individual data sets.

DS-1

DS-1 comprised data representing 95 Tasmanian bridge girders removed from service, as discussed in Section 3.2. The inferred data (Figure 3-2) compares well with the original data (Figure 2-12). Both the inferred and the original datasets have a coefficient of determination of 0.52 and a regression model identical to two significant figures (Equation 3.1, Table 3-1). The mean values of MoE (9.9 GPa) and MoR (31 MPa) are significantly lower than the S2 limiting values of 14 GPa and 86 MPa respectively. Of the 95 girders, only about 18% have an MoE above the S2 limit and none have a value above the S2 MoR limit strength. Within the limits of one standard deviation of both means, MoE and MoR, the distribution of DS-1 is similar to normal, but outside those limits it has slightly higher upper and lower tails (Figure 3-3). These data, therefore, contain extreme values that do not fit within the 95% confidence bounds of a true normal distribution. These extreme values represent both girders with high elasticity (refer Figure 3-3) and low strength girders (refer Figure 3-4). The DS-1 dataset does not represent girders suitable for bridge construction because they are below the S2 limit states.

The total population of Tasmanian bridge girders must include girders that are both of sufficient elasticity and strength to be used in structures constructed according to national standards. The data's authors (Yttrup & Nolan, 1996) suggest that Tasmanian girders have low strength (refer Section 2.4.1). However, this possibility is unlikely. If it were the case, then a large number of Tasmanian bridges would use five girders yet Yttrup & Nolan (1996) only report bridges with four girders. It is more likely that DS-1 represents a set of girders that were appropriately removed from service because they were degraded and of insufficient strength for their intended purpose by not meeting specific strength criteria.

DS-2

DS-2 (169 girders reported by NSW RTA, Section 3.3) is particularly characterised by the fact that the age of most of the girders is quoted, thus leading to an understanding of how age affects

both MoE and MoR. It is apparent from the box plot and quantile statistical summaries (Figures 3-5, 3-6, 3-8 and 3-9) that these data contain a number of outliers (represented by DS-2-4) which, when removed, creates DS-2-3. This subset conforms to a normal distribution (refer Figures 3-7 and 3-10). The eight outliers (DS-2-4) represent girders from a variety of sources, but they have high MoE in common. These girders were of significant estimated age: 15-45 years. Their prior in-service history is not known, but the inference from these data is that girders need not temporally degrade in MoE. Whether these girders (DS-2-4) were different in any other manner was not recorded in the available source data. These girders will be discussed further in relation to Figure 3-13.

The values of MoE and MoR are both calculated from measured data and will only be correct if the SMA is accurately determined. In creating this dataset, the NSW RTA (Law and Morris, 1992) identified that no attempt was made to accurately determine the true SMA (refer Section 2.4.3). The girder diameter recorded was that of the outside diameter, which provided a nominal upper limit on the diameter and a lower limit on the values of MoE and MoR. The diameters of the DS-2-4 girders, the outliers, did not appear to be significantly different when compared to DS-2-1 (refer Figures 3-11 and 3-12). What was significant in DS-2-1 was firstly, that there were more girders with widths greater than their depths, the mean depth to width ratio being 0.96; and secondly, only 16% had both depth and width that were greater than 450 mm. There was only one girder, #32, that had:

1. reported width and depth of 450 mm
2. measured values of MoE and MoR above the mean values for DS-2-1
3. measured values above the minimum expected values of 14 GPa (MoE) and 86 MPa (MoR).

Set DS-2 comprised girders that were removed from service c. 1990. Some 84% of them would not be suitable for use in a new structure, c. 2012 in NSW, because their diameters were less than 450 mm. What their strength levels at new is unknown. Thus, DS-2 did not contain girders that would be suitable for a modern timber-bridge. From a contemporary perspective, these girders should have been replaced.

Two features can be inferred from the relationship of DS-2 MoE-v-age. The first feature is that DS-2-4 girder MoE has not declined with age. A nominal degradation rate of about −30 MPa yr^{-1} is obtained from a regression of these data (Figure 3-13 and Table 3-4). The hypothesis that, the degradation rate for some girders is zero, cannot be discounted. DS-2-4 represents those girders with MoE greater than 30 GPa, there were no other selection criteria. They could have all been girders less than two years of age, but this was not the case. DS-2-4 girder age was from less than two years to 45 years. It is inferred, therefore, that there is no reason to expect girder MoE to decline with age. Even at the nominal rate a girder will only decline about 2 GPa in 50 years (−30 MPa × 50). It is not apparent from these data whether the MoE of these girders remained constant or whether it varied temporally. All that is known is that both girders only two years old and over 40 years old had MoE significantly above the six sigma mean range characterised for Ironbark (refer Table 2-5).

This is surprising since in the reviewed literature there were no other bridge timbers characterised (Bolza & Kloot, 1963) higher than Ironbark (refer Table 2-5). As discussed in Section 2.2.12, a material is specified by its MoE. Defects can reduce the MoR, but they do not necessarily modify the MoE of that material and they are unlikely to increase girder MoE. It is not clear, for example, why girder #92 has such a high value of MoE. Questions that therefore that arise are:

1. What has caused the high value of girder MoE?
2. Is the timber different in some way?
3. Does the MoE value temporally change?
4. Are the characterised values of excised sample MoE representative of large girders or not?
5. Does the mid-span stress allow, or cause, the timber to change?

Such questions cannot be answered from the available data that describe these datasets and will require further research. However, the presence of apparently anomalous high values of MoE does not preclude the prediction of MoR and, as was seen in Section 5.5, these high values are not anomalous, but entirely consistent with other girder data.

The second feature, in the DS-2 MoE-v-age relationship, is that DS-2-3 girder MoE has declined with age. The mean rate of temporal MoE decline can be inferred from the regression data shown

in Figure 3-14 and Table 3-6. This mean rate, approx. 137 MPa yr^{-1}, is a reasonable indicator of the average performance of the set (confidence level 95%, Pr < 0.0001). At this mean rate, an Ironbark girder with MoE of 24 GPa will take between 52 and 123 years to degrade to 14 GPa. Any girder decaying at a faster rate should be assessed to determine why it is decaying so quickly. As an example, after 10 years at this degradation rate a 24 GPa girder will have declined to 22.6 GPa. Therefore, on average a girder should not decline more than 6% within 10 years. The corollary of this is that if the mid-span deflection to load ratio of a girder increases by 10% or more in less than 10 years then that girder will be assessed to determine if it needs maintenance.

As with MoE, MoR also declines with age, as shown in Figure 3-15, and the scatter of these data is again high. Not all girders that had measured values of MoE also had recorded values of MoR. DS-2-7 was obtained by removing all data from DS-2-3 representing girders without recorded MoR. Data for 38 girders were removed such that only 110 girders were represented. One high outlier, girder #24, was also removed to retain a normal distribution. The mean decline of DS-2-7 MoR was about 0.4 MPa yr^{-1} (confidence level 95%, Pr < 0.001) and it is to be inferred that the strength of a DS-2-7 girder would be more likely to decline than not. The level of this mean decline is not of concern in relation to an Ironbark girder. If a girder has initial MoR of 183 MPa and declines in strength at the higher mean rate of 0.73 MPa yr^{-1}, then it will still have an MoR 28% above the S2 limit after 100 years. However, such a low rate of decline in strength is not true of all girders, since 76% of the girders aged 15 years were below the S2 limit. Of these girders, over 90% had values of MoE below the S2 limit and their MoE values were typically declining at a rate significantly more than 10% in ten years. If they had been temporally quantified, it should have been possible to determine that they were degrading at a rate faster than they should otherwise have.

In order to determine the MoR prediction band, a multiple analysis of variance was performed with both MoE and age as prediction parameters (refer Figure 3-16 and Table 3-7). The first regression model obtained was Equation 3.3 with a coefficient of determination of 0.48 (95% confidence, p < 0.001). This coefficient was improved by 6% to 0.54 by including age as an additional parameter in the regression (Equation 3.5, 95% confidence, p < 0.001). Age was not a good prediction parameter since it did not substantially improve the coefficient of determination.

DS-3 and DS-5

DS-3 and DS-5 were obtained from the measurement of 21 girders that were removed from service and reported by NSW RTA as set out in Section 3.4. In combination, these two sets contained data for both girders and excised clears. DS-3 contained the results from mid-span destructive bending and DS-5 contained results from the bending to failure of excised specimens. Because the excised specimens were taken from areas other than in the mid-span region, they represent lower stressed regions of the girder. No discussion of the effect of bending stress at a cellular level in relation to in-service timber-bridge girders was found in the reviewed literature (refer Section 2.6.5).

It seems intuitive that highly stressed regions will suffer cellular damage and low stressed regions will not. This hypothesis is supported by work examining compression failures and is described in literature reviewed in Section 2.6.5, by authors such as Kuisch, Gard, Botter, & van de Kuilen (2012). Observable cellular damage does occur in timber that might be otherwise graded as CS-1. In a new girder operating well within its elastic limit, negligible cellular change may occur. As the girder ages, degrades and is operated closer to its elastic limit, a point will be reached when cellular damage does occur. At this point, the MoR and MoE will be affected. The point of SHM is to detect that point and then take intelligent action (refer Section 2.5). A comparison of the MoR and MoE of highly stressed girders with the MoE and MoR of less stressed excised specimens should provide some indication of whether that point has been passed or not.

A first step towards examining the possibility that there are differences in cellular structure can be made by comparing low stressed specimens with highly stressed specimens. In relation to the SHM of timber-bridges, this examination needs to be carried out on in-service bridge girders. If a measureable effect can be identified, then further research can lead to the creation of a non-destructive measurement technique. Possible techniques could involve microwaves, ultrasound or vibration to examine cellular damage in the outer stressed regions of a girder. The comparison of DS-3 with DS-5 is thus one first step.

A comparison of DS-3 with DS-5 by seven point box plots is made in Figures 3-17 and 3-18; in the former figure MoE data are reported and in the latter MoR data. DS-3 MoE has both a wider interquartile range and a wider 99 percentile range than DS-5 but a similar median. The

interquartile ranges of both DS-3 MoR and DS-5 MoR are similar, but the DS-3 mean is significantly below the DS-5 means. The DS-5 MoR 99 percentile ranges are larger than the DS-3 MoR ranges. Thus, there are differences between the two datasets.

Degradation will cause change and it is not unexpected that firstly, the DS-3 MoE 99 percentile range is greater than the DS-5 MoE 99 percentile range and secondly, that the DS-3 MoR mean is less than the DS-5 MoR mean. What is unexpected is that the DS-3 MoE maximum values are greater than the DS-5 MoE maximum values and also that the DS-5 MoR 99 percentile range is greater than the DS-3 MoR 99 percentile range. The narrow DS-5 MoE interquartile ranges are what might be expected of clear samples, but the wide DS-5 MoR ranges are not what are expected of clear samples that have a narrow MoE range. Something unexpected occurred and examining data on a per girder basis provides further insight.

Figures 3-19 and 3-20 represent the same data as shown in Figures 3-17 and 3-18 respectively, but separated out and shown for each girder. It can be seen in Figure 3-19 that the DS-3 mid-span girder MoE data point (brown dot) is sometimes higher and sometimes lower than the DS-5 excised sample data (blue and green dots). This variation is in contrast to the DS-5 MoR data (refer Figure 3-20, brown dots) which, for all girders, is lower than the DS-3 MoR data from the lower stressed regions A and B (refer Figure 3-20, blue and green dots). Therefore, the mean effect represented by Figure 3-18 (girder MoR lower than excised clear MoR) is also true for each individual girder, as represented in Figure 3-20. What is happening is still unclear because the two parameters MoE and MoR are being examined individually. To obtain greater insight, they need to be examined together.

In Figure 3-21, DS-3 (brown dots) and DS-5 (green dots) are plotted. In each case MoR is plotted as ordinate and MoE as abscissa. Data are only plotted for girders that have a complete set of both MoR and MoE values. This is because if any one sample was not obtainable there was the possibility that the girder was partly degraded by biological or mechanical defects. Even though each data pair, one green and one brown dot, represents an individual girder, the two clusters are distinctly different.

The degree of difference can be seen by reference to Table 3-8. The average MoR of the DS-5 excised clears from each girder is about twice that of the girder DS-3 MoR from the same girder and the minimum about 1.3 times. Thus the clear MoR is at least 1.3 times the girder MoR. The

fact that the girder MoR is less than the excised clears is not surprising. As indicated in Section 2.2.20, the presence of defects in a material will cause a reduction of MoR such that the ultimate material strength will not be attained. The ultimate strength for bridge timber is above 10 GPa and the attained strength is only about 2% of that ultimate strength. As an example, Ironbark with MoR of 183 MPa is about 1.8% of 10 GPa.

What is surprising is that the range of DS-5 MoR data is as high as it is and this cannot be explained by examining DS-3 and DS-5 alone. As a particular example, data for one girder, girder #14, are shown in Figure 3-22. Although girder #14 is an Ironbark girder, its excised clear sample MoR-v-MoE values are lower than the mean Ironbark six sigma range. This girder is not necessarily representative of all the girders; it may be an extreme case. However, the fact that the excised clears have a range of MoE less than the complete girder is not explained by current literature. Further implications related to these DS-3 and DS-5 effects will be discussed in Determination 4 (Section 6.2.4).

Data obtained by comparing DS-3 with DS-5 is limited for three reasons. The first reason is that the sizes of the specimens are not the same. DS-3 girder data represents in-service girders with unknown diameters. They are from a set of bridges similar to the set from which DS-2 was derived; similar region, era and construction type. The DS-3 diameters will, therefore, be similar to that shown in Figures 3-11 and 3-12. DS-5 represents measurements from excised samples of undefined size, but these samples are likely to have cross-sectional areas 5% or less of the DS-3 samples. Although it is possible to compare the bending to failure data of an excised sample with the bending to failure data of the girder from which the sample was taken, the cross-sectional areas are significantly different. The clear cross-sectional area is about 5% of the girder cross-sectional area. Cellular damage, particularly at the girder surface may also be significantly different to the excised sample surface.

The second reason is that the condition states of the samples and girders were not recorded and the level of defects in these samples is no longer available. It is not known, therefore, if the measured value of MoE or MoR is low because of the intrinsic material parameters or because of material defects. There are two types of defects that are likely to affect the measured MoE and MoR. The first type is small defects at a cellular level. These are defects that might be caused by high stress and are the types that are of interest when comparing variously stressed samples. The

second type of defects is represented by examples of biological decay or gross mechanical damage. Biological decay can be caused by fungal activity and gross mechanical damage could be identified by evidence of splitting. Although these kinds of defects are of interest, they need to be evaluated independently and should not be part of an investigation into the primary effects of stress.

The third reason is that the sample age was not recorded. It is not possible, from DS-3 and DS-5, to determine the length of time that was required for any change of MoE or MoR to occur. It was apparent from DS-2 that girders had significantly degraded after 15 years in service but there was no MoR data for younger girders. It is, therefore, only possible to determine from DS-2 girders aged less than 15 years if a change in MoE or MoR has occurred, the magnitude of that change but not when it might have happened.

DS-4

The DS-4 set of QDMR girders is distinctive in that it contains data related to:

1. the condition state of the girders
2. the species of the girders
3. the mode of failure.

It contained neither details of the age of the girders nor accurate estimates of SMA. Because of the available recorded parameters it is possible to cluster these data, identify girders in different stages of degradation and identify an in-service degradation path. It is also possible to create regression models, predict MoR using MoE and condition state as prediction parameters.

As with analysis of DS-2, DS-3 and DS-5, the analysis of DS-4, using seven point box plot summaries and tabular methods, does not provide a clear understanding of the important relationships that affect in-service girder strength (refer Figures 3-23, 3-24, 3-25, and 3-26 and Table 3-10). Better understanding is gained by plotting the MoR-v-MoE vector as shown in Figure 3-27. Because DS-4 represents mainly girders removed from service, it is not surprising that only 25% have vector points above the S2 limit states (MoR 86 MPa, MoE 14 GPa). A regression model (Figure 3-27) explains about 70% of the variation in these data with a slope of about 3.9 $MPaGPa^{-1}$. This value of slope is not statistically significantly different from the slope

calculated for DS-1 of 3.4. Thus the two sets, one from Tasmania and one from Queensland, can be considered statistically similar.

Further understanding of how the MoR-v-MoE vector varies throughout the life of an in-service girder can be obtained by separating DS-4 into common clusters. To limit any confounding variation that may be caused by different species, only Ironbark girders are considered here. The first step is to cluster these data according to individual failure modes and condition states, as shown in Figure 3-28. As might be expected both DS-4-7 and DS-4-8, which were assessed as CS-1 and CS-2, appear in the upper right quadrant above the S2 limit states. DS-4-9, DS-4-10 and DS-4-11 which were assessed as CS-2 to CS-4 were below the 86 MPa limit state. However, the DS-4-10 and DS-4-11 clusters have significant variations and some of these data appear anomalous. This particularly applies to data representing girders #48 and #49. To minimise the effect of these apparently anomalous girders, the MoR-v-MoE data for each cluster were then averaged.

The clustering and averaging are shown in Table 3-12, together with the characterisation mean value for Ironbark. Data in Figure 3-29 show the path of a hypothetical in-service girder as it degrades. The major features of this path are that both MoR and MoE decline as the hypothetical girder degrades. Further features of this behaviour will be discussed in relation to Determination 5 (Section 6.2.5).

Data were also clustered according to both Ironbark and condition state. The mean value of each cluster is presented in Figure 3-30. The regression of MoR on MoE achieves a coefficient of determination of 0.98. There is, therefore, on average a very low level of unexplained variation; less than 2%. The inference from this interpretation is that, generally, experienced visual assessors are very good at evaluating the condition state of a timber-bridge girder. However, with regard to an individual girder, the assessment may not be of such a high quality. It may be for this reason that girders #48 and #49 appear to be anomalous; they may have appeared visually more degraded than they actually were. Therefore, to improve such assessment, it is important they are supported by measurements.

The regression models calculated for DS-4 enabled MoR prediction equations to be created (refer Table 3-15). By regressing MoR on MoE a coefficient of determination of 0.71 was obtained. By including condition state as a prediction parameter, this coefficient was increased

by about 15% to 0.86. This increase was almost twice that achieved with DS-2 when age was included as a prediction parameter. Inclusion of the average condition state of the cluster, rather than the condition state of the individual girder, reduced the unexplained variation further to about 2%. It is likely, therefore, that the unexplained variation for an individual girder can be further reduced by more accurately quantifying girder condition state by measurement. Consequentially, the unexplained variation for an individual girder can be reduced by temporally measuring the mechanical parameters of that girder. Thus, the regression of MoR on MoE of temporal data for an individual girder is likely to contain much less variation than data as shown in Figure 3-27, which are for all girders and all represented species. How this is to be achieved will require further research, beyond the scope of this thesis.

To ensure that the data presented in Figure 3-28 and 3-30 were representative, they were compared graphically with the data in Figure 3-27, by overlaying the data as shown in Figures 3-31 and 3-32. In both cases, the data appear evenly distributed about the DS-4-1 regression line and within the prediction bounds. Firstly, it is inferred that DS-6 Ironbark data reasonably represent DS-4-1. Secondly, since the average condition state data (solid orange line) lies close to the DS-4-1 regression line, it is inferred that it is generally a reasonable representation of DS-4-1.

DS-6

This dataset, from CSIRO, comprised data obtained by measuring the clear samples of over 100 Australian timbers. Even though the dataset represents both softwoods and hardwoods, it is remarkable that the set is consistent with a coefficient of determination of 0.74 for a linear regression model (refer Figure 3-33 and Table 3-16). The slope of the DS-6 regression model of MoR on MoE is about 7 MPa GPa^{-1}, which is significantly different from the MoR on MoE regression slopes of the previous data (DS-1 to DS-4) that have slopes of about 3 MPa GPa^{-1}. Further implications of DS-6 are discussed in Determination 2 (Section 6.2.2).

Summary of the complete data-set group, DS-1 to DS-6

This section has addressed DS-1 to DS-6 as individual datasets. However, it is already apparent that there are several significant features in bridge girder data which have not previously been identified by other authors. These features are:

1. The source (bridge location) and species of a girder does not necessarily cause anomalous values of girder MoR-v-MoE vector. All bridge girders appear to fit one consistent set.
2. Girder MoR can be statistically modelled and predicted with unexplained variations of less than 14% by using MoE, condition status and age as prediction parameters.
3. The MoR-v-MoE excised clear data are not similar to the MoR-v-MoE girder data but are characteristically different.
4. The effective value of MoE not only varies significantly within a set, but some girders have MoE well above the maximum mean values characteristic for any species of timber.

These features are examined in more detail and in combination in Determination 2 (Section 6.2.2).